Using Land Cover Changes to Mitigate the Impacts of Hot Temperatures in South African Cities

Timothy Chambers (CHMTIM004)

Dissertation Presented for the Degree of

Master of Science in Environmental and Geographical Science

University of Cape Town

Supervisor: Assoc Prof Babatunde Abiodun

April 2023

Plagiarism Declaration

---

1. I know that plagiarism is wrong. Plagiarism is to use another's work and pretend that it is one's own.
2. I have used the Harvard convention for citation and referencing. Each contribution and quotation in this dissertation from the works of other people has been attributed and has been cited and referenced.
3. This dissertation is my own work.
4. I have not allowed, and will not allow, anyone to copy this work with the intention of passing it off as his or her own.

Signature:

Signed by candidate

Abstract

South African cities are negatively impacted by hot temperatures, which have severe impacts on human health. Climate change and population growth are expected to exacerbate these impacts in the future, given that Southern Africa has been projected as a hotspot for future warming and growth. The added socio-economic factors leave a large proportion of South Africa's population vulnerable to these hot temperatures. Although several studies have identified strategies for adapting to, or mitigating, the impacts of these hot temperatures, these strategies require extensive resources. The effective implementation of the strategies in a local context would need to identify and prioritise areas with highest risk, and with greatest reward.

This thesis addresses these issues by examining the spatial distribution of temperatures in ten hot South African cities and investigating the impact of land cover changes on both the current distribution of temperatures, and in reducing future temperatures. The study analyses observation and simulation datasets, using Landsat 8 satellite observations to produce high-resolution land surface temperature (LST) maps over each city. The 2020 South African land cover (SANLC2020) dataset is then incorporated into the Urban Canopy model (UCM) and the Weather Research and Forecasting model (WRF) to simulate conditions over the cities. To investigate the effectiveness of using land cover changes as potential cooling strategies, two idealised but realistic scenarios were implemented into the model: (a) increasing tree coverage to 60% across the urban area and (b) increasing the albedo of all building roofs to 40%.

The results of the study reveal substantial temperature differences (up to 10°C) between neighbourhoods within the cities. These differences show strong correlations to observed variations in land cover, which itself shows links to socioeconomic status and historical policies. In all but one of the study areas, the cities are found to be cooler than the surrounding, less vegetated rural areas, illustrating an Urban Cool Island (UCI) effect. This is caused by the importation of trees, moisture, and reflective surfaces by people. The addition of the converted SANLC land cover dataset significantly enhances the performance of the WRF model. Using this, the model showed good skill in reproducing observed spatial

patterns and values of temperature. The model-based sensitivity tests showed that both scenarios could reduce the surface temperature in the cities by up to 3°C. The information gathered in the study highlights the significant potential there is for targeted land cover changes to mitigate the impacts of hot temperatures, reduce thermal inequality, and adapt South African cities into thermal refuges.

Acknowledgements

I would like to take this opportunity to express my sincere gratitude to my supervisor, Assoc Prof Babatunde Abiodun, for his guidance and support throughout my Master's degree. His patience and encouragement were invaluable in helping me complete this research. I am also extremely grateful to my family and friends for their unwavering support and understanding during the course of my studies, in particular my parents and grandparents.

I am grateful for the financial support of the University of Cape Town (UCT), as well as the American Red Cross and the Global Disaster Preparedness Center (GDPC).

Table of Contents

List of Acronyms

AWS	Automatic Weather Station
COPD	Chronic Obstructive Pulmonary Disease
Corine	Coordination of information on the environment
DEM	Digital Elevation Model
GIS	Geographical Information Systems
GCM	Global Climate Model
GDP	Gross Domestic Product
GFS	Global Forecast System
LST	Land Surface Temperature
NLCD	National Land Cover Database
NUDC	National Urban Dataset
OLI	Operational Land Imager
RCM	Regional Climate Model
RCP	Representative Concentration Pathway
RDP	Reconstruction and Development Program
RMSE	Root Mean Square Error
SANLC	South African National Land Cover Dataset
SAWS	South African Weather Services
SRTM	Shuttle Radar Topography Mission
SUCI	Surface Urban Cool Island
SUHI	Surface Urban Heat Island
TIR	Thermal infrared
MODIS	Moderate Resolution Imaging Spectroradiometer
UCI	Urban Cool Island
UCM	Urban Canopy Model
UHI	Urban Heat Island
WRF	Weather Research and Forecasting
WRF_MODIS	WRF simulations with MODIS land cover
WRF_ROOF	WRF simulation scenario with increase in roof reflectance
WRF_SANLC	WRF simulations with SANLC land cover
WRF_TREE	WRF simulation scenario with increased tree cover
WRF-UCM	WRF coupled with UCM

List of Figures

List of Tables

Chapter 1: Introduction

1.1 Background

South African cities play a crucial role in the socio-economic development of the country. The cities accommodate over 40 million people, which is about two-thirds of the country's population (Statistics South Africa, 2022). They provide amenities to employ the population, driving the economy and contributing significantly to the country’s GDP. Additionally, they also serve as major hubs for cultural and social activity, offering a place for people to come together and engage in activities that bring them closer together. This has an important role in promoting diversity and inclusivity, allowing for people of many diverse ethnic and cultural backgrounds to interact and develop greater understanding and respect for each other. Where people gather, there is also a convergence of thoughts and an exchange of ideas. This can drive positive social and political changes, and promote innovation and growth, leading to new ideas and opportunities for the country's development.

However, South African cities are also focal points for many of the challenges the country faces (Coalition for Urban Transitions, 2021). High levels of poverty, inequality, and unemployment are often more pronounced in the cities, partly due the stark contrasts between the wealthy and the poor, and partly due to the high concentration of people and the rapidly evolving urban landscape. A number of these issues are rooted in the country’s apartheid past. After the initial segregation, there was a rapid influx of predominantly poorer people into cities. Government planning was not equipped to deal with this, leading many people to live in often unsuitable locations and housing. This was most apparent in the formation of informal settlements where little to no government regulations, infrastructure or services were provided. The result was, and is still today, many people living in inadequate conditions and having limited access to resources. Along with the more obvious social vulnerability associated with this, people can also be particularly vulnerable to negative environmental factors. One such factor is the risk of heat-related illnesses and mortality from the exposure to high temperatures.

1.2 Health impacts of high temperatures

There is a strong relationship between high temperatures and human mortality. In recent times, heat has been shown to be responsible for approximately 350,000 global deaths per year (Burkart et al., 2021). This often occurs in the form of heat waves, with events such as the 2003 European and the 2010 Russian summer heat waves accounting for approximately 70,000 and 55,000 deaths on their own (Robine et al., 2008; Barriopedro et al., 2011).

When individuals are exposed to high temperatures for extended periods, their bodies respond to the stress by implementing two key mechanisms to maintain core temperature: vasodilation and sweating. Vasodilation increases blood flow to the skin, facilitating the transfer of heat from the body to the environment. Sweating, on the other hand, releases water onto the skin, which evaporates and cools the skin, further aiding in heat dissipation (Kenny & Jay, 2013). These physiological responses are crucial for preventing core temperatures from rising to dangerous levels. However, the body's efforts to regulate temperature through these methods come at a cost, as they place increased demands on individuals' cardiovascular and thermoregulatory systems and can also lead to dehydration. In populations that are already at risk of related illnesses due to factors like age or pre-existing conditions, this increased demand can lead to deaths, most commonly cardiovascular in nature, but also respiratory and other cause related (Ebi et al., 2021). In addition to these stress-response related deaths, the exceedance of the body's thermoregulatory capacity under extreme heat stress can lead to heat stroke, which in turn can cause fatalities.

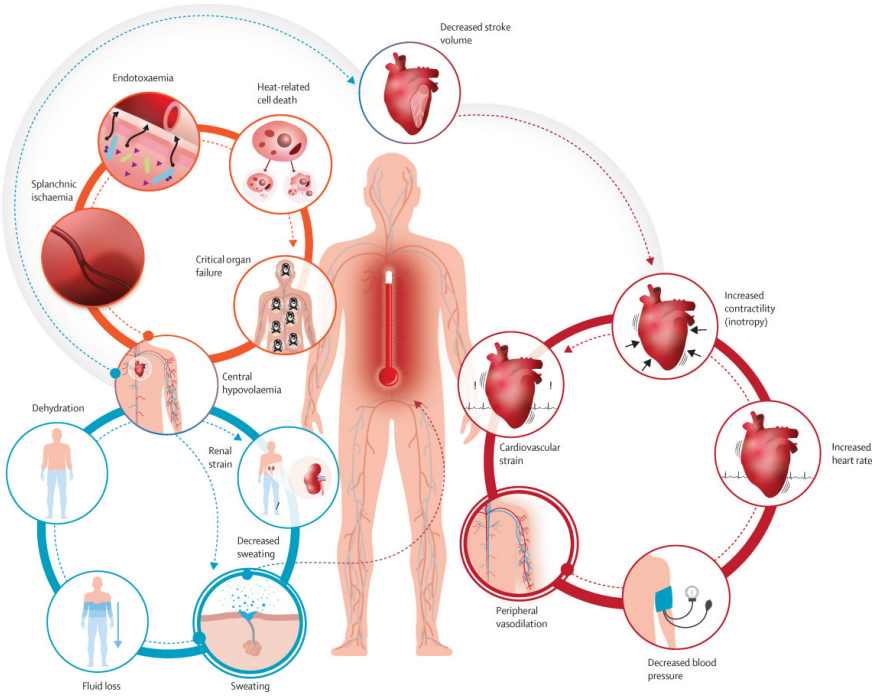

Figure 1.1 The physical pathways involved with human heat strain (Source: Ebi et al., 2021; https://www.thelancet.com/article/S0140-6736%2821%2901208-3/fulltext).

In South Africa, Scovronick et al. (2018) estimated that approximately 0.4% of all deaths can be attributed to hot temperatures (~2000 deaths per year). However, this varies significantly across the country and across different age groups. Certain districts of South Africa have rates as high as 3.5%, and the 0-4 years and 65+ years age groups have been shown to be at far greater risk of mortality than other groups (Scovronick et al. 2018, Fig 1.2).

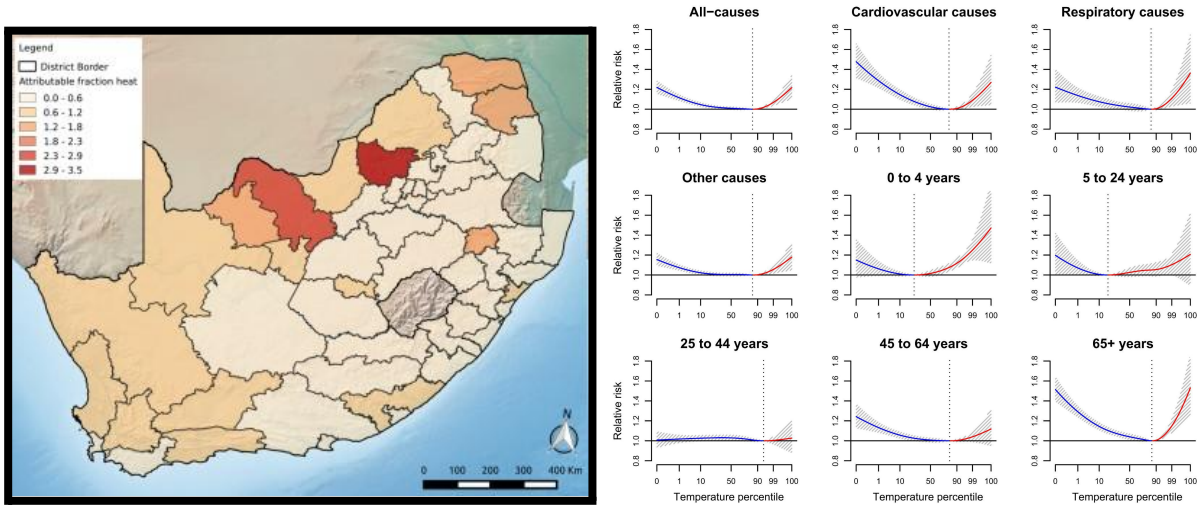

Figure 1.2. Temperature and health risk (Source: Scovronick et al., 2018). (i) Percentage of deaths attributed to hot temperatures in South African districts; (ii) risks of mortality associated with maximum daily temperature at various age groups.

In addition to mortality, hot temperatures have a number of other negative impacts on society. There is extra strain on the power grid because of increased need for air conditioning and refrigeration. This increases the risk of load shedding and blackouts, as well as increasing the burning of fossil fuels and release of greenhouse gases, further contributing to hotter temperatures and reduced air quality (Krayenhoff et al., 2021). Reduced air quality in turn causes increased cases of respiratory and cardiovascular diseases, including asthma, COPD and lung cancer. (Manisalidis et al., 2020; Bălă et al., 2021). With increased temperatures, both evaporation and water demand increase. This places extra strain on already overextended water resources and can lead to water shortages (Schilling et al., 2020). The productivity of workers has also been shown to decrease above certain temperature thresholds, with human error increasing, and along with it the time spent on breaks and the agitation levels of the workers (Ioannou et al., 2017, Ebi et al., 2021).

1.3 Approaches for studying the spatial distribution of high temperatures

The negative impacts of high temperatures have prompted numerous studies to focus on heat, with the goal of better understanding it and providing solutions for dealing with it. Traditionally, the use of station observations has been the primary source of temperature information in these studies. Stations can provide temporally continuous information about various climate variables regardless of weather conditions. However, the problem with this approach is that they cover a limited area and are few and far between. The values they provide may only be relevant to within a short distance of the station. Unless there is a very dense network of stations, the data can result in information that is not representative of the larger area.

In South Africa, most weather stations are located in larger cities and airports, with rural areas and smaller settlements generally under-represented. Even within these larger urban centres, the number of weather stations is often limited. While this is not a significant problem at larger scales and in homogenous climates, it becomes a major limitation when studying temperature in cities with marked variations.

More recently, satellite thermal imagery has provided another method of analysing temperatures, offering a potential solution to the spatial constraints of station observations. Remotely sensed data offers information across the entire globe and, unlike station data, is not dependent on the observation network of a specific location. This is particularly useful in low-income countries and remote areas where infrastructure is not available for ground-based measurements.

This imagery is captured by thermal sensors onboard satellites, which detect the amount of infrared radiation emitted from points on the earth's surface. This allows for the creation of thermal images of the surface, and extraction of land surface temperature (LST). Compared to traditional station measurements, this LST has vastly greater spatial coverage and is more evenly spread across the world, making it a powerful tool for studying the spatial variability of temperature. Consequently, it has found numerous applications, including in agriculture, disaster management, environmental monitoring, and surveillance/reconnaissance. However, one of its most promising applications is in urban planning and management, where it can be used to identify spatial patterns of land surface temperature at a city-level. This application allows for the better identification of hot areas within cities and helps to identify the causes of temperature variations across the urban landscape.

Landsat 8 imagery is one of the best sources for studying these urban temperature patterns. Its relatively high resolution (30m, downscaled from 100m) gives it an advantage over lower-resolution alternatives like the 1km MODIS thermal imagery, which is more frequently collected but may not provide the detail needed for urban applications.

However, while this thermal imagery is very useful, it too is still limited, particularly when it comes to temporal resolution. Imagery is typically collected at the same time of day, with several days between image captures, making it difficult to study diurnal temperature changes or specific days. Additionally, the data can be affected by cloud cover and atmospheric interference, impacting the accuracy and usefulness of the information, particularly in areas where cloud cover is a frequent occurrence.

A method of addressing both the spatial and temporal constraints of station observations and satellite thermal imagery is the use of atmospheric models. These models utilise data from observed climate, as well as earth and atmosphere characteristics, and combine them with complex dynamical equations to simulate and predict a wide range of variables.
One key advantage of atmospheric modelling is its ability to provide climate data that is both spatially and temporally continuous. By incorporating data from multiple sources and using sophisticated mathematical models, atmospheric modelling techniques can provide detailed information about the complex interactions between atmospheric, geological, and environmental factors that contribute to high temperatures.

1.4 Motivation for the present study

There is a need to understand and respond to hot temperatures in cities. This need becomes even more relevant when considering future changes. Climate change, characterised by increases in the global surface temperature, is accompanied by the enhanced frequency, severity, and duration of hot temperatures and heat waves (Ebi et al., 2018). In South Africa, warming over the interior of the country is predicted to increase by between 3°C and 7°C by the end of the century, depending on emission scenarios (Engelbrecht. 2019). In addition, human populations are also expanding. This is particularly true in less developed regions. In recent times, South Africa's population has been growing by ~750,000 people per year (Statistics South Africa., 2022). At this same rate, the population would double by the end of the century. Large percentages of this growth would likely be in cities, and specifically in low-income informal settlements. The combined increase in both temperature and population is expected to greatly increase the number of people exposed to hot

temperatures. Without addressing the issue, this would likely result in substantial increases in the related mortality. (Yang et al., 2021).

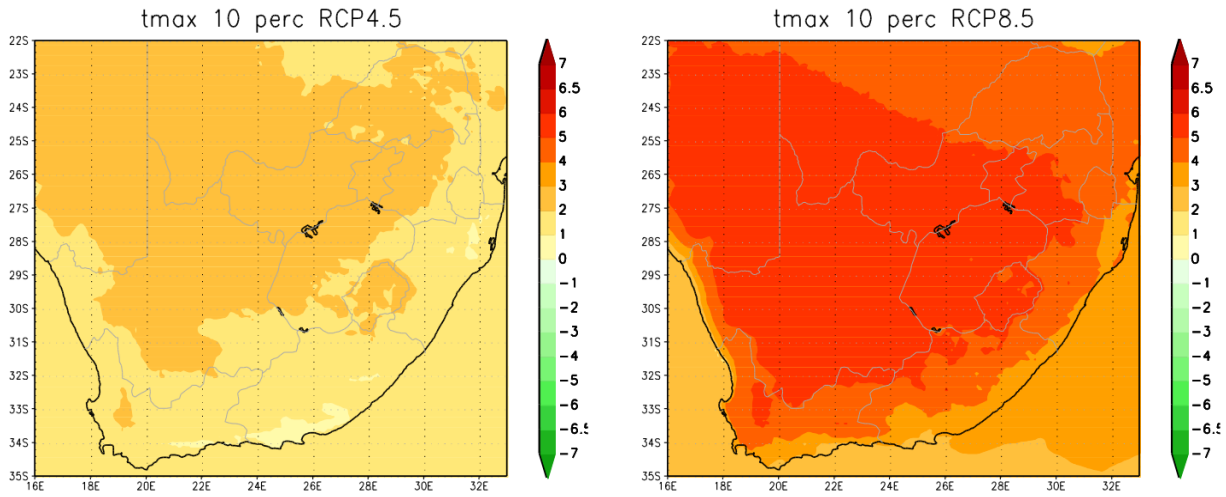

Figure 1.3 Projected changes in future air temperatures (2070-2099) under both low mitigation (RCP8.5) and medium-high mitigation (RCP4.5) scenarios (Source: Engelbrecht, 2019).

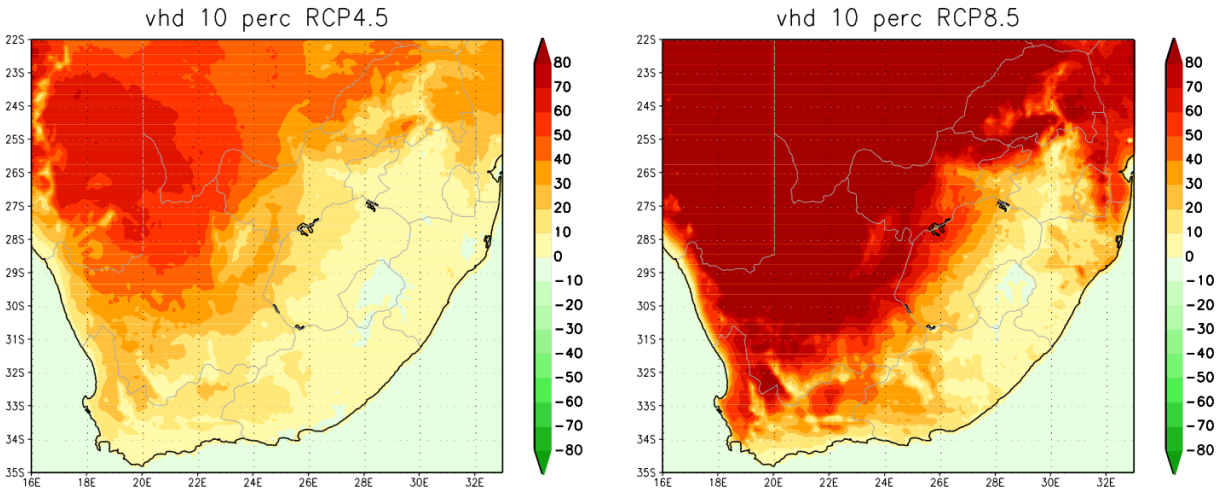

Figure 1.4 Projected change in the number of hot days (over 35 °C) experienced in the future (2070-2099) under both low mitigation (RCP8.5) and medium-high mitigation (RCP4.5) scenarios (Source: Engelbrecht, 2019).

Insufficient information on the spatial distribution of high temperatures in cities, particularly in less developed countries, remains a challenge. Despite numerous studies focusing on identifying the causes of heat, vulnerable populations, and strategies to reduce heat, the findings are not consistent across locations and are biassed towards wealthier, well-resourced countries.

The impact of high temperatures can vary significantly depending on physical characteristics, such as climate, vegetation, and city layout, as well as socio-economic factors such as the standard of living and capacity to respond. Therefore, it cannot be assumed that studying heat in one location provides accurate information that can be universally applied.

Ideally, there should be access to accurate information on heat for every location in the world, but this is not yet feasible. Currently, most of the available information is skewed towards more developed countries with greater research capacity. This leaves a significant research gap in less developed countries where physical and social factors can be vastly different. Hence, there is a pressing need for research in these areas to better understand the characteristics and impacts of high temperatures and develop context-specific mitigation and adaptation strategies.

Climate models have been used as a tool to better understand heat and test mitigation and adaptation strategies. However, the majority of this research has been conducted at relatively large scales (regional to global). This has left gaps in the knowledge at the local or city level, where heat characteristics can change significantly over short distances. Higher resolution simulations can help address this issue, but they require high-resolution data for the model to input. While topographical data is globally available at the necessary resolutions, high-resolution land cover data is limited to certain areas. Creating a South African-specific land cover dataset which can be used by the model would help to address this limitation.

Despite the need and value of temperature mitigation and adaptation projects, implementing and maintaining them in South African cities has often been overlooked in favour of providing more urgent basic services such as housing, transportation and education facilities (du Toit et al., 2018). In the context of the country, this is understandable. To change this and ensure that these projects actually go ahead, it is important to identify the populations who are in the greatest need of these measures and provide feasible location-based solutions that will not have significant financial and resource burdens. Past studies have looked at hot temperatures in the country and identified population groups and regions vulnerable to their negative impacts, but at too large or general a scale for mitigation and adaptation strategies to be implemented at. The use of satellite thermal imagery would provide a method that can help identify these vulnerable populations more precisely.

Numerous studies have also looked at ways to reduce temperatures, or at least reduce people's exposure to them. While cooling devices like air conditioning are highly effective in an indoor

space, they actually increase outdoor temperatures and have significant resource and environmental burdens (de Munck et al., 2012). This makes it necessary to identify and implement other solutions which are both sustainable and effective. In this regard, land cover changes have been shown to be effective ways of reducing temperatures, but how these would work in a South African context and how the effectiveness would change from one city to another remains unknown. Climate modelling, combined with high-resolution land cover data, could provide a useful means of testing this.

1.5 Aim and objectives

The main aim of this study is to investigate the effectiveness of land cover changes in reducing temperatures in hot spots across South African cities and assess their potential to reduce temperature disparities and mitigate the impacts of future warming.

The objectives of the study are to:

1. Identify temperature hot spots in each city
2. Identify the relationship between land cover types and temperature
3. Evaluate the performance of the WRF model in simulating temperatures in the cities
4. Evaluate the potential of trees and reflective roofs in reducing temperatures in the cities

1.6 Thesis outline

This thesis consists of six chapters. **This chapter** provides a background for the study, highlighting the impacts of hot temperatures on people and the need to address them. It then presents the motivation for the study, as well as its aims and objectives.

Chapter 2 is the literature review chapter. It consists of relevant past studies, providing an overview of the methods used to study temperature; disparities in temperatures across locations and what causes these; and potential methods of reducing temperature.

Chapter 3 is the methodology chapter that describes the datasets, climate model, simulation experiments, and data analysis methods used in the study.

Chapters 4 and 5 present and discuss the results of the study. While Chapter 4 focuses on the satellite-based LST results and discussion, Chapter 5 focuses on the model-based results and discussion, assessing the capabilities of the WRF model and the newly created land cover dataset, as well as the potential of two cooling strategies.

Chapter 6 provides concluding discussions, potential applications of the research and recommendations for future work.

Chapter 2: Literature Review

This chapter reviews the literature relating to hot temperatures in urban areas. It starts by looking at the current disparities in heat stress distribution across urban settlements (Section 2.1) and the inequality of future warming (Section 2.2). It then looks at how satellite imagery can be used to identify disparities in temperature (section 2.3), before reviewing potential cooling strategies (section 2.4) and looking at how atmospheric models can be used to simulate climate at a city scale (section 2.5).

2.1 Disparity in heat stress distribution across urban settlements

Several studies have attributed heat stress disparities within urban settlements to a combination of environmental, built environment, and social factors (e.g., Bindajam et al., 2020; Sun et al., 2019). These studies have also argued that the factors themselves are strongly linked. For instance, the physical characteristics of locations can determine the heat stress they experience. Topography can affect the amount of sun or shade an area receives; where hot and cool air collects; and how exposed an area is to wind (Bindajam et al., 2020). Water features such as oceans, dams and rivers can affect temperatures due to their high heat capacity and moisture content. The temperature within the built environment also varies with relation to urban form, surface reflectance, and the amount of green space (Sun et al., 2019).

Social factors often influence where people live in relation to these physical drivers (Mehrotra et al., 2018). In many cases these social factors can be directly correlated to heat stress and its associated health risks. Poorer populations are generally more limited in their choice of areas where they can live, the type of houses they can build, and the cooling infrastructure they can implement. This often leads to these communities living in more exposed locations with hotter temperatures. Mehrotra et al. (2018) found that areas of informal housing in Mumbai were on average 2°C hotter than areas with formal housing. Jagarnath et al. (2020) also noted a similar relationship in Durban, with neighbourhoods at highest risk of heat stress being lower-income informal, and traditional housing. Hsu et al. (2021) found a link between income level and heat stress, but also showed that race played a role as well. The average person of colour living in areas with higher heat island intensity than whites in all but 6 of the 175 largest urbanised areas in the continental United States.

2.2 Global warming and heat stress inequality

There is ample evidence that global warming is exacerbating heat stress inequality by widening the existing gap in vulnerability and resource access. This is supported by studies like Herold et al. (2017), Diffenbaugh & Burke (2019), and Alizadeh et al. (2022). These all demonstrate that the populations who are already at risk of heat stress will be disproportionately impacted as heat events become more frequent and intense. On a global scale, the heat stress impacts will be felt more acutely in regions that lack adequate infrastructure and resources to cope with extreme heat. Higher-income regions have greater institutional and individual capacity to rapidly adapt, which can buffer climate-induced increases in exposure. Lower-income regions, however, have reduced adaptive capacity and are slower to react, translating to escalating impacts and increasing inequality (Diffenbaugh & Burke, 2019; Alizadeh et al., 2022). On top of this, research has shown that lower-latitude regions, where most low-income countries are situated, are also expected to warm at greater rates than the higher latitudes. This further contributes to the current disparities (Herold et al., 2017; Alizadeh et al., 2022).

On the individual level, there is again a strong link to socio-economic factors (Zografos et al., 2016; He et al., 2022; Laue et al., 2022). Outdoor workers, who come from predominantly lower-income communities, will have greater exposure to increased heat and will likely be far more impacted by future warming than populations in higher-income, indoor jobs (He et al., 2022). The same is true for populations who are already exposed to heat risk through their living situations (location, access to air conditioning, poor insulation and ventilation) or health (pre-existing conditions, access to medical resources). These populations have a very limited “buffer”, and will feel any future warming far more than those with better access to resources.

2.3 Mapping global temperature inequality with satellite thermal imagery

A number of studies have used Landsat imagery to conduct research on these differences in temperature, with most focusing on urban areas (e.g. Stathopoulou & Cartalis 2007; Keeratikasikorn & Bonafoni, 2018; Alahmad et al., 2020). Of these, most were specifically interested in the surface urban heat island (SUHI) phenomenon and its relationship to the underlying land cover. A few have also focused on the temperature variations within cities themselves, and also the potential to estimate air temperature from land surface temperature.

2.3.1 Urban versus Rural

Stathopoulou & Cartalis (2007) and Keeratikasikorn & Bonafoni (2018) used Landsat 7 and 8 thermal imagery to evaluate the daytime SUHI effect in Thai and Greek cities. Both studies found that temperatures in the urban areas were significantly warmer than their rural surroundings (3-5°C on average). Zhang & Sun (2019) showed similar rural-urban differences in the two Canadian cities they studied. In a more arid context, Alahmad et al (2020) looked at LSTs in the country of Kuwait. They found that night-time LSTs in the urban areas were up to 3.5°C warmer than the rural surroundings, but daytime values actually showed the opposite effect. Urban daytime temperatures were approximately 1.1°C cooler on average.

2.3.2 Intra-city differences

On a more intra-city note, Mirzaei et al. (2020) looked at daytime LSTs in the hot, arid city of Isfahan over a three-year period. They noted large differences between different zones of the city. The coldest averaged 40.1 °C and the hottest 48.7 °C. Mentaschi et al. (2022) also observed large summer LST differences within the 14 megacities they studied. The largest of these differences were in Tokyo (up to 17°C) and New York (16°C). The smallest differences were in Paris and London (9-10°C). In Pietermaritzburg, Sithole & Odindi (2015) found a general trend of decreasing temperatures with distance away from the urban centre. Areas nearer the centre were up to 33°C, while more vegetated outskirts were down to 24°C.

2.3.3 Land cover variation

The differences in rural versus urban and intra-city temperatures have been closely linked to land cover. The Zhang & Sun (2019) study found more open, bare areas and industrial zones to be hot spots, while more forested green spaces had considerably cooler temperatures. The Alahmad et al. (2020) study showed that the imported green infrastructure was the main reason for the cooler daytime city temperatures in Kuwait; and Schwaab et al. (2021) extensively illustrated that urban areas covered in trees had lower temperatures than the rest of the urban fabric in the 293 European cities they studied. This averaged in the range of 0-4°C in southern European regions and 8-12°C in central Europe. In South Africa, this is no different, with Magidi & Ahmed (2022) showing well vegetated urban areas in Tshwane to be up to 5°C cooler than less vegetated areas.

2.3.4 Using LST for air temperature prediction

While thermal imagery has revolutionised the production of spatially continuous LST maps, its relatively infrequent capture of data and the fact that it only measures surface temperature, not air temperature, limits its scope. To overcome this, there have been many suggestions of relating surface temperatures to air temperatures. This would allow for one measure to be estimated by the other and vice versa. Kloog et al. (2012), Pelta et al. (2016), and Rosenfeld et al. (2017) all showed good correlations between the two measures, but the actual estimation of values still poses a difficult challenge (Zhou et al., 2019). In general, it has been found that simple equations cannot adequately quantify the relationship, and it has instead been suggested that reasonable estimations would need to be produced as part of more complex models (e.g., atmospheric models).

2.4 Land surface cooling strategies

To address the impacts of heat, there has been a drive to implement adaptation and mitigation strategies. Two cooling strategies have been widely suggested in literature (Santamouris et al., 2017; Turner‐Skoff & Cavender, 2019; Aram et al., 2019; Santamouris & Fiorito, 2021; Krayenhoff et al., 2021) : (1) urban greening through the addition of trees to city areas, and (2) increasing urban albedo through the implementation of reflective urban surfaces.

2.4.1 Urban greening with trees

Trees have the ability to cool temperatures through shading and evapotranspiration. Shade is produced by both the canopy and the trunk, reducing the amount of solar radiation that reaches the ground by approximately 60-90%. Evapotranspiration involves the movement of water from the roots of trees up to the leaves, stems and flowers, where it evaporates and takes energy away from the surroundings (Ng et al., 2012). The effectiveness of both of these cooling mechanisms is dependent on the physical properties of the trees (e.g., type of trees, tree height, canopy thickness), as well as their location in terms of climate and position in the urban space (Manoli et al., 2019). In some instances, the cooling properties of trees can be offset or even surpassed by their other properties (Chen and Jim., 2008). The darker colour of trees can result in a decreased albedo (or reflectivity), leading to increased absorption of sunlight. Moreover, the release of water vapour through evapotranspiration can increase humidity, and the presence of trees can also act as an air shield, stopping wind from moving

through, and trapping heat that is released from the surface at night (Heisler and Grant., 2000).

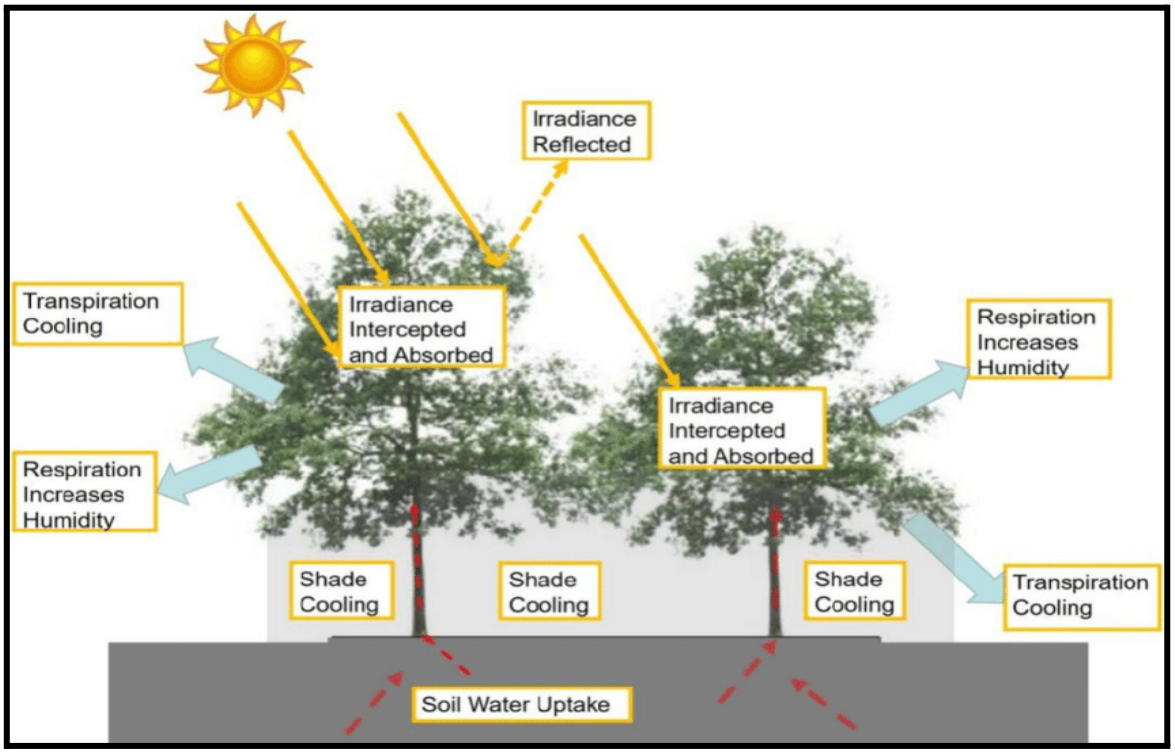

Figure 2.1 Cooling effect of trees (Source: Zhang et al., 2019).

The differences that can occur in a trees' cooling effectiveness makes it important to test tree impact on a case by case basis. Studies across the globe have done this using both model and observation based methods.

A review paper by Krayenhoff et al. (2021) used 47 higher quality studies to examine this effectiveness. These showed that on average for every 10% increase in canopy cover, there was a ~0.3°C decrease in air temperature. This value did however vary considerably, with another review by Santamouris et al. (2017) showing that overall cooling of air temperature varied between 0.1°C and 5°C depending on the study. Other research has been more location specific. Jonsson (2004) used station and satellite measurements to better understand the role of trees in Gaborone, finding more forested urban areas to be as much as 2°C cooler than their less forested surroundings. Rahman et al. (2017) looked at air temperatures within the tree canopy in Munich, measuring daytime values up to 3.5°C cooler than outside the canopy.

Ng et al. (2012) used model based methods to test the effectiveness of future tree cooling in Hong Kong, noting that for a 1°C decrease in street level air temperature, one third of the available land areas would need to be covered by trees. In a South African context, Souverijns et al. (2022) identified variations in air temperature in Gauteng. They found that the less vegetated Johannesburg CBD and the townships of Alexandra, Tembisa and Soweto were on average approximately 1°C hotter than the more vegetated urban surroundings.

While the majority of studies have used air temperature as a measure of cooling effectiveness, the introduction of thermal imagery has given rise to the measure of surface temperature being used as well. Abdulateef & A. S. Al-Alwan (2022) conducted a study in Baghdad to test the effect of urban greening on surface temperatures. They found that trees could reduce these LSTs by between 10°C and 20°C depending on the surface type. In South Africa, Magidi & Ahmed (2020) used thermal imagery to study LST variations in Tshwane, showing vegetated urban areas to be up to 5°C cooler than the less vegetated areas. In Manchester, Armson et al. (2012) also looked at surface temperatures, using ground based measurements to test the difference between surfaces shaded by trees and those which were not. They found shaded areas to be up to 19°C cooler than unshaded.

The large variations in the cooling effect of trees have led other studies to examine what causes these differences. Rahman et al. (2014) researched the cooling effectiveness of five common tree species in Manchester. Their ground-based measurements showed that evapotranspiration cooling was closely related to the growth and stress tolerance of the species. In general, the faster the tree grew, the greater the Leaf Area Index (LAI) and subsequent evapotranspiration. The growth rate differences meant that quicker-growing trees produced 3 to 4 times the cooling of the slow-growing trees. Potchter et al. (2008) researched the oasis effect in an arid settlement in Israel. They found that while the more vegetated settlement did show cooler conditions than the surroundings, this varied across tree types. Sub-tropical trees cooled their surrounding atmosphere by up to 4°C more than the desert species. This was due to adaptations of local desert tree types in reducing water loss. (i.e., less evapotranspiration). Other studies by Pataki et al. (2011) and Jiao et al. (2017) also found that species type was a major driver in the cooling effectiveness. Manoli et al. (2019) and Cheng et al. (2022) both considered the location of the trees in terms of climate. These studies showed that the cooling by trees was far greater in hot arid areas where humidity was lower, compared to hot tropical regions where high humidity reduces transpiration ability.

Cheng et al. (2022) did, however, note that this cooling effectiveness was only up to a certain temperature threshold, with temperatures over 34°C starting to reduce the trees' cooling ability and impact its health. Other research (e.g. Chen and Jim, 2009) has considered the physical characteristics of the cities in which urban trees are located. In the Chinese cities they studied, the shading effect by trees is negligible as most buildings and people are above the canopy. This is true for a number of larger, denser cities where high-rise buildings dominate the urban landscape.

All of these studies highlight the importance of accounting for the individual study area's circumstances when considering the use of trees as a cooling strategy.

2.4.2 Increasing albedo through reflective surfaces

When solar radiation reaches the surface it is either absorbed or reflected back into the atmosphere. By adding reflective coatings and using more reflective materials, one can increase the solar reflectance of building roofs and walls, sidewalks, and streets. This decreases the amount of energy that is absorbed, reducing surface and ambient temperatures (Fig 2.2. Krayenhoff & Voogt, 2010; Global Cool Cities Alliance, 2012).

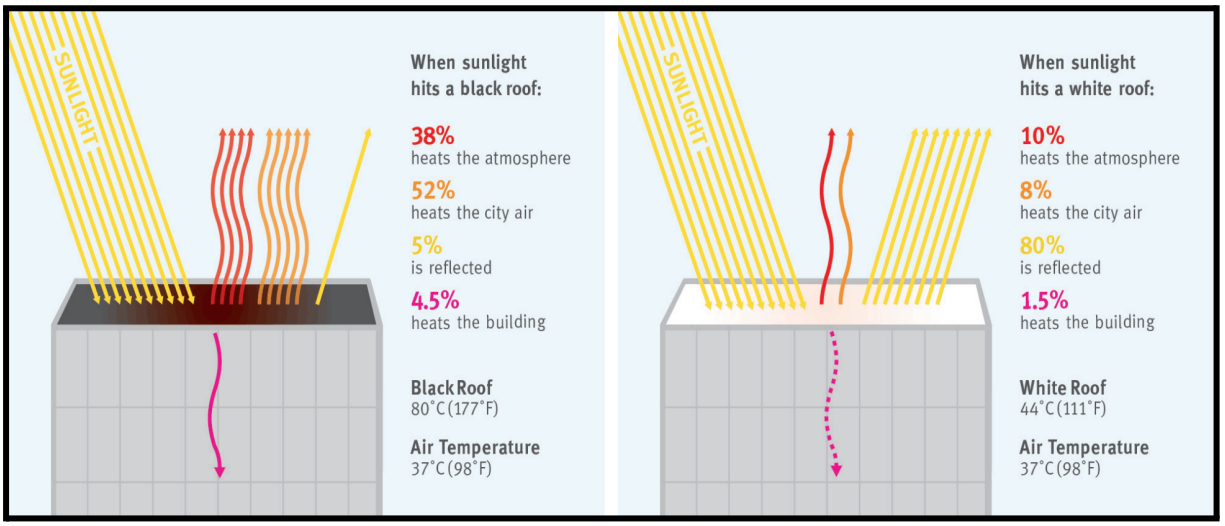

Figure 2.2 The difference in solar absorption and reflection between a black roof and a white roof, and the subsequent temperature contrasts (Source: Global Cool Cities Alliance, 2012).

In light of climate change and warming cities, there has been much focus on using albedo changes to improve the thermal environments of cities. This is because it is a fairly simple

and cost-effective method that does not drastically alter the urban landscape and can easily be implemented during maintenance or construction of new infrastructure (Akbari et al., 2012). While increasing the reflectance of walls, roads and pavements has shown some potential for cooling, the most effective cooling surface is usually roofs. This is partly because they cover a large (and unused) surface area within urban spaces, and partly because of their position above the street level. Solar radiation reflected by roofs mostly escapes the urban canopy without being absorbed by other urban surfaces. Contrastingly, pavements, roads and walls can result in reflection of radiation onto other buildings and people (Mohegh et al., 2018).

Studies on roof albedos in cities have been conducted across many locations and at many scales. At a global scale, Oleson et al. (2010) modelled the effects of universally installing white roofs, using an urban canyon model coupled with a global climate model. Averaged over all urban areas, daily maximum temperature decreased by 0.6°C and daily minimum temperature by 0.3°C. In a review of model-based urban cooling studies, Krayenhoff et al. (2021) found that high-reflectivity coatings or materials offer approximately 0.2 °C to 0.6 °C air temperature cooling per 10% increase in albedo. Mohammed et al. (2021) found similar overall changes in Dubai, but noted that cooling was far greater in the denser parts of the city than in the more spread out parts. At the smallest scale, a review study by Santamouris (2014) found that indoor temperatures in moderately insulated buildings typically decreased by approximately 2°C with reflective roofs.

However, in South Africa, a large percentage of low-income housing is not well insulated, leading to roof reflectivity having even greater impacts on indoor temperatures. Kimemia et al. (2020) tested the effectiveness of a cool paint coating on a shack-like structure in Johannesburg. Over a year-long period, they found an average reduction in inside maximum air temperature of 4.3°C compared to the inside of the equivalent uncoated structure. Studies by Sanedi (2019) found similar values of cooling in the Northern Cape, while GIZ (2021) found cooling of up to 7°C in buildings in KwaZulu-Natal.

The colour and materials of roofing directly impacts how much radiation it will absorb, reflect and transmit. Simpson & McPherson (1997) tested the impacts of varying colours (i.e., albedo) of composite shingle roofs on their respective surface temperatures. They found that white roofs (albedo of ~ 0.75) were up to 20°C cooler than grey (~0.30 albedo) or silver (~0.50 albedo), and up to 30°C cooler than brown roofs (~0.10 albedo). Synnefa et al. (2006)

found similar results while testing 14 different types of reflective coatings. They also noted the effect of weathering, with the thermal performance of coatings degrading over time. This degradation has led to the development of coatings which self-clean so as to reduce the loss of reflectance and subsequent cooling effectiveness (Cheng et al., 2021).

2.5 Application of atmospheric models for city-scale studies

Several studies have employed atmospheric models to study city-scale atmospheric characteristics and test hypothetical changes in variables (e.g., Bhati & Mohan, 2015; Li et al., 2017; Berardi et al., 2020). These atmospheric models are powerful tools that can simulate the behaviour of the earth's atmosphere with varying levels of detail and accuracy. They do this by dividing the earth into a 3-dimensional grid, noting the physical properties and solar input of each grid point, and then solving the complex mathematical equations, which are used to represent the physical atmospheric processes occurring (Karlický., 2013). They are commonly divided into two categories, Global climate models (GCMs) and Regional climate models (RCMs). The GCMs (Fig 2.3) simulate the atmosphere on a global scale and at lower resolutions. These models are designed to capture the long-term behaviour of the earth's climate system, including large-scale patterns such as the global circulation of air and ocean currents and the distribution of heat and moisture across the planet. They are also used to study the long-term impacts of greenhouse gas emissions and other human activities on the global climate system.

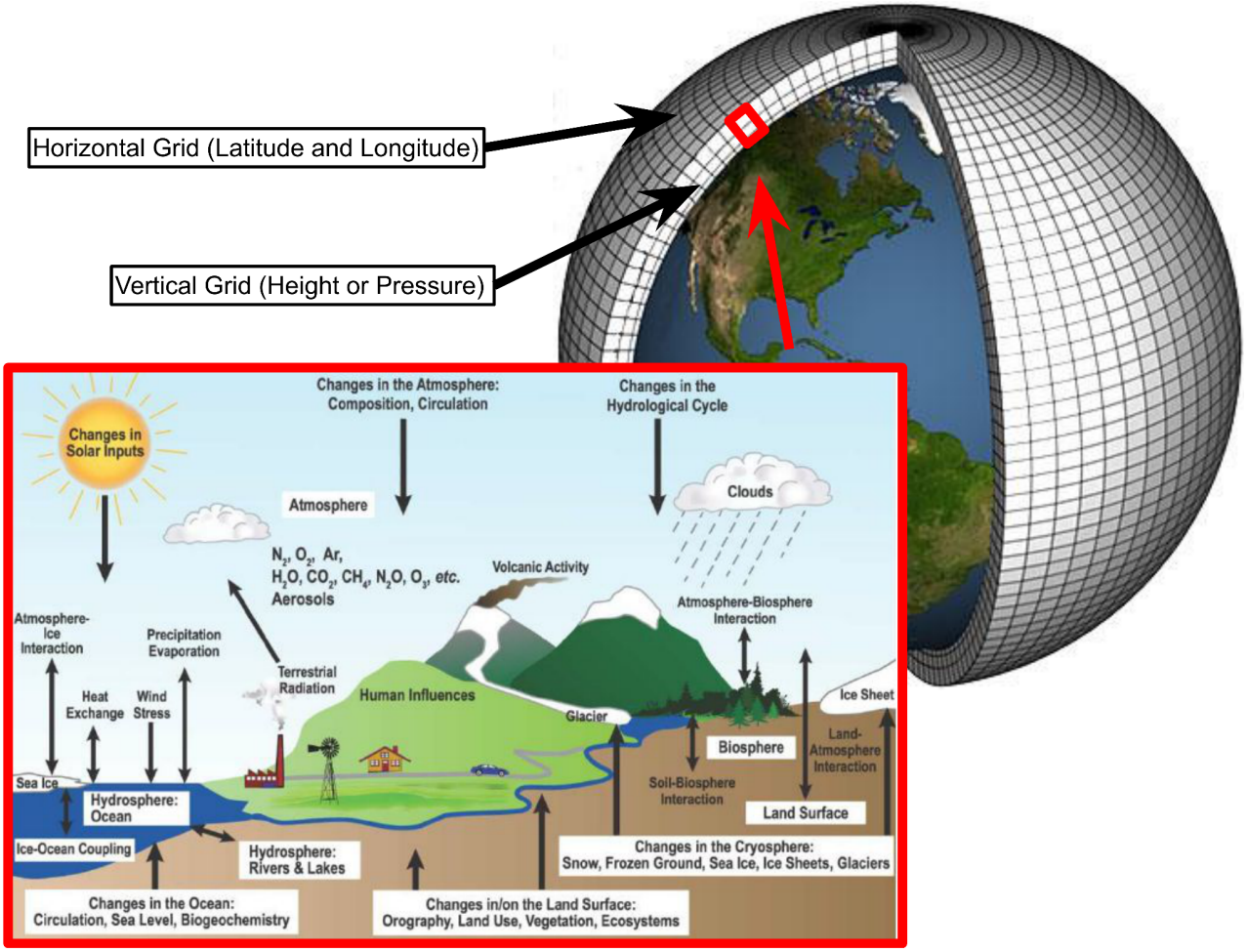

Figure 2.3 Example of a global climate model (GCM) grid and its input (Source: Lawrence Livermore National Laboratory; https://celebrating200years.noaa.gov/breakthroughs/climate_model/welcome.html)

On the other hand, RCMs provide simulations over smaller regions but at higher resolutions. These models are designed to capture the regional variations in climate that can occur within a country or a city. RCMs make use of the information from GCMs or global reanalysis products and downscale it using dynamical methods to include smaller scale processes and features which the GCMs miss, helping to improve the accuracy of the simulations (Lynch, 2008; El-Samra et al., 2018).

In this study, the need for high-resolution information necessitates the use of a RCM. The RCM chosen here was the Weather Research Forecasting Model (WRF). This was combined with an Urban Canopy Model (UCM) to aid urban specific simulations. Both of these are described in more detail in the methodology section, but are introduced here to give context to the research which has previously been conducted with these models.

2.5.1 Quantifying and mapping UHIs

Li et al. (2019) used WRF-UCM to quantify the urban heat island (UHI) in Berlin by running high-resolution temperature simulations. Results were well-correlated with observational data (coefficient of 0.95) and had a root mean square error (RMSE) of 1.76℃. Bhati & Mohan (2015) observed similar accuracy when studying the UHI in Delhi, also testing the simulations with and without the UCM. Non-UCM simulations had RMSE values of 1.63℃ and the UCM of 1.13℃. Giannaros et al. (2013) used WRF to look at the Athens UHI, finding that urban air temperatures were up to 4℃ hotter at night, but had negligible differences during the day.

2.5.2 Improving model

The skill of the WRF-UCM model in reproducing climate is directly dependent on the accuracy of the information fed into it. At a city scale, land cover types and values are one of the most impactful sources of error, making it important to use datasets that reflect what is on the ground (Masson et al., 2020). In Europe and the United States, high-resolution urban datasets have more recently been created in the form of the 100m Corine land cover in Europe (Li et al., 2018) and the 30m NLCD in the United States (Wickham et al., 2014). These have been shown to improve simulations when compared with older, lower-resolution datasets (Li et al., 2017). However, in other parts of the world, urban datasets are very limited. To address this, multiple studies have created their own. In China, Li et al. (2022) recently created a 100m national urban dataset (NUDC) to improve and simplify urban modelling across the country. Vahmani & Ban-Weiss (2016) used remote sensing values of albedo and vegetation cover to improve on already existing datasets, reducing RMSE between simulations and observations from 3.8°C to 1.9°C. Li et al. (2014) similarly used satellite data to extract more realistic values of land cover type, green vegetation fraction, and leaf area index to feed into the WRF model. This resulted in improved simulation of near-surface meteorological elements when compared to ground observations.

2.5.3 Testing solutions

The proven performance of the WRF-UCM has allowed for a number of cooling strategies to be tested using the model. Vahmani & Ban-Weiss (2016) used WRF-UCM and satellite imagery and found that up to 58% of the variation in temperature in Los Angeles was due to the vegetation fraction. Berardi et al. (2020) used WRF-UCM to test the effectiveness of

greening scenarios in Toronto Canada, finding a decrease in daily maximum air temperatures of approximately 2℃.

Contrastingly, Mughal et al. (2020) used the model to test the effect of cool roofs on air temperatures in Singapore, finding a decrease of approximately 1.3℃ across the city. Morini et al. (2016) looked to mitigate the UHI in Terni, Italy by increasing the albedo of roofs, walls and roads- showing potential air temperature decreases of approximately 2℃, and Jacobs et al. (2018) used WRF-UCM to test the effectiveness of increasing albedo and vegetation in Melbourne during a heat wave, showing small decreases (up to 1℃) in air temperatures across the city.

Chapter 3: Methodology

This chapter describes the methodology used in the study. The study areas and their characteristics are highlighted in Section 3.1. The datasets and their sources are then presented in Section 3.2. The final part, Section 3.3, contains the methods that were employed. This includes how the thermal imagery and the WRF model were used, and how the information produced from these was analysed.

3.1 Study area

The study area is South Africa, but with a focus on 10 cities located in hot areas across the country (Fig 4.1). The cities were chosen for the following reasons: (i) they are in the districts that have witnessed high percentages of deaths attributed to hot temperatures (Scovronick et al. 2018); (ii) they are in areas vulnerable to future warming (Engelbrecht. 2019); (iii) they currently experience hot temperatures; (iv) they have a large population (more than 50,000 people).

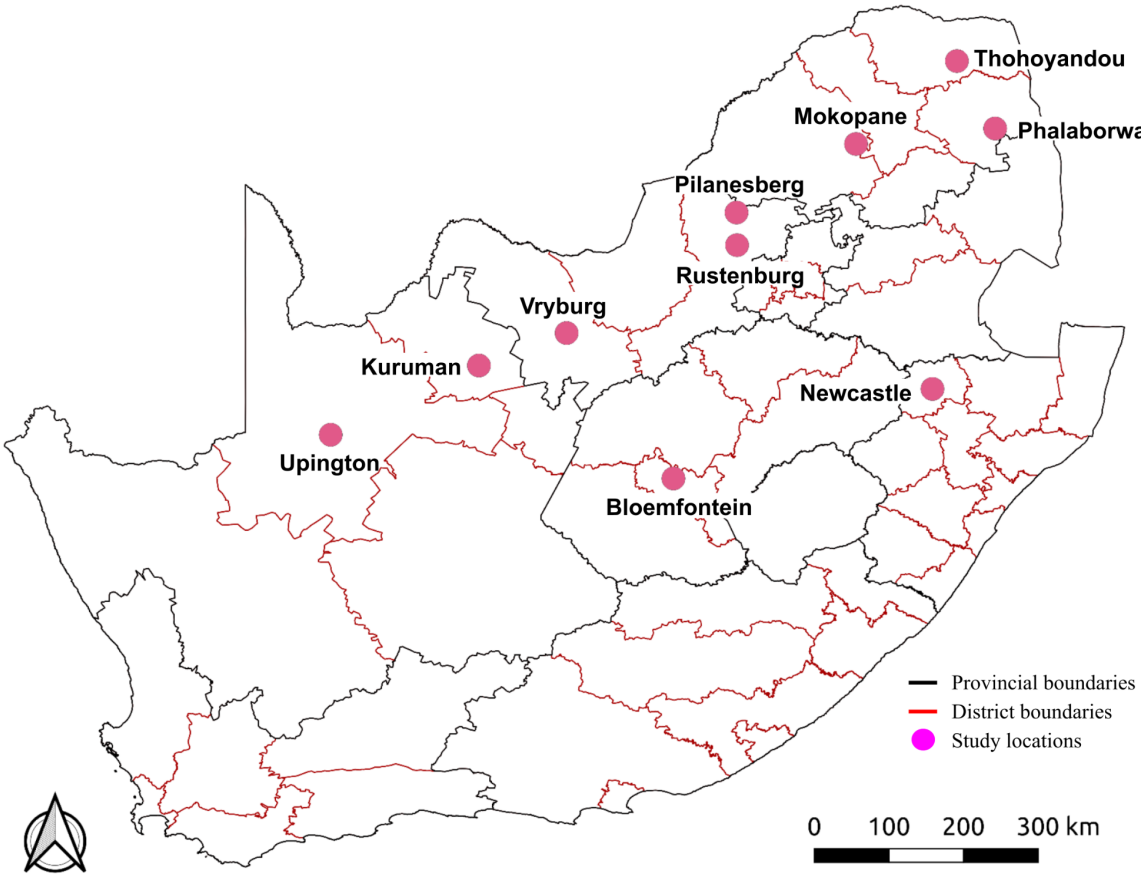

Figure 3.1 Locations of the 10 selected cities used in the study.

Table 3.1 Information about the 10 cities used in the study. The temperature information was extracted from the CSAG Climate Information Platform (CIP) and mortality information from Scovronick et al. (2018).

Study Area (coordinates)	Population (people)	Elevation (masl)	Biome	Climate classification (Koppen)	December average max (℃)	Hot days (number of days)			Number of heat related deaths in district (1997-2013)	Heat related deaths in district (% of total deaths)
						≥ 32℃	≥ 36℃	≥ 95th percentile		
Bloemfontein (29.11ºS, 26.22ºE)	600,000	1400	Grassland	BSk (arid, steppe, cold)	30	40	5	18	1404	0.8
Kuruman (27.36ºS, 23.39ºE)	80,000	1350	Savanna	BSh (arid, step, hot)	33	75	15	19	565	1.5
Mokopane* (29.11ºS, 26.22ºE)	200,000	1400	Savanna	BSh (arid, steppe, hot)	28	17	1	19	530	0.7
Newcastle (27.75ºS, 30.09ºE)	300,000	1200	Grassland	CWb (temperate, dry winter, hot summer)	29	30	13	18	1448	1.5
Phalaborwa (23.92ºS, 31.08ºE)	100,000	400	Savanna	BSh (arid, steppe, hot)	32	82	18	14	2000	1.3
Pilanesberg** (25.29ºS, 27.20ºE)	100,000	1050-1150	Savanna	BSh (arid, steppe, hot)	32	98	24	N/A	7522	3.5
Rustenburg (25.65ºS, 27.25ºE)	550,000	1050-1300	Savanna	BSh (arid, steppe, hot)	31	52	5	17	7522	3.5
Thohoyandou (23.06ºS, 30.59ºE)	250,000	500-800	Savanna	BSh (arid, steppe, hot)	29	38	5	17	1849	1.4
Upington (28.45ºS, 21.24ºE)	70,000	800	Nama Karoo	BWh (arid, desert, hot	36	130	55	17	509	1.1
Vryburg** (26.96ºS, 24.73ºE)	50,000	1200	Savanna	BSk (arid, steppe, cold)	36	123	36	N/A	2086	2.5

** information is only available for Polokwane ~50km away **Hot day information from SAWS observations 2014-2018*

3.2 Datasets

The study makes use of three dataset types: (1) Station data, (2) Satellite data, and (3) simulation data.

3.2.1 Station data

The station data used in this study was obtained from the South African Weather service (SAWS) and from the Weather Underground station network. The 2m air temperature from SAWS was used both in the validation of the WRF simulations and in calculating the number of hot days in some of the study areas. This dataset is in the form of hourly values and covers the period from January 2014 to December 2018, but with missing data in some locations for certain days/periods. The Weather Underground network combines AWS airport station data and quality controlled personal weather station data. Observed air temperatures and wind speed data for our study areas were obtained through its online platform at https://www.wunderground.com/. This information allowed for hot and low wind days to be identified, aiding the selection of Landsat imagery days and WRF simulation days.

3.2.2 Satellite data

The satellite datasets used in the study can be divided into Geographical Information Systems (GIS) data, which show physical location characteristics, and Landsat 8 data, which shows temperature information. These were both analysed using the QGIS platform.

3.2.2.1 GIS data

GIS data consisted of Digital Elevation Models (DEMs), satellite imagery, population density data, and land cover data. DEMs were from the 2000 Shuttle Radar Topography Mission (SRTM., 2013). They were accessed through the USGS EarthExplorer portal and are at 30m resolution. The DEMs were used to analyse topographical elevation, aspect and shading in relation to the temperatures in each study area. Google satellite images were used to visually observe the landscape of each study area. These images were obtained through the Google Earth platform, with the imagery taken between 2016 and 2018. Most images were below 1m resolution and produced by Maxar technologies Airbus.

The 2019 South African population density data was obtained from Africa data hub. This data is produced by Meta in partnership with the Center for International Earth Science

Information Network (CIESIN) at Columbia University. It is produced by using satellite imagery to identify buildings and then correlating this information to existing census data. This gives an estimate of the number of people per 30m square tile, which was used to identify where most of the population lived within the study areas.

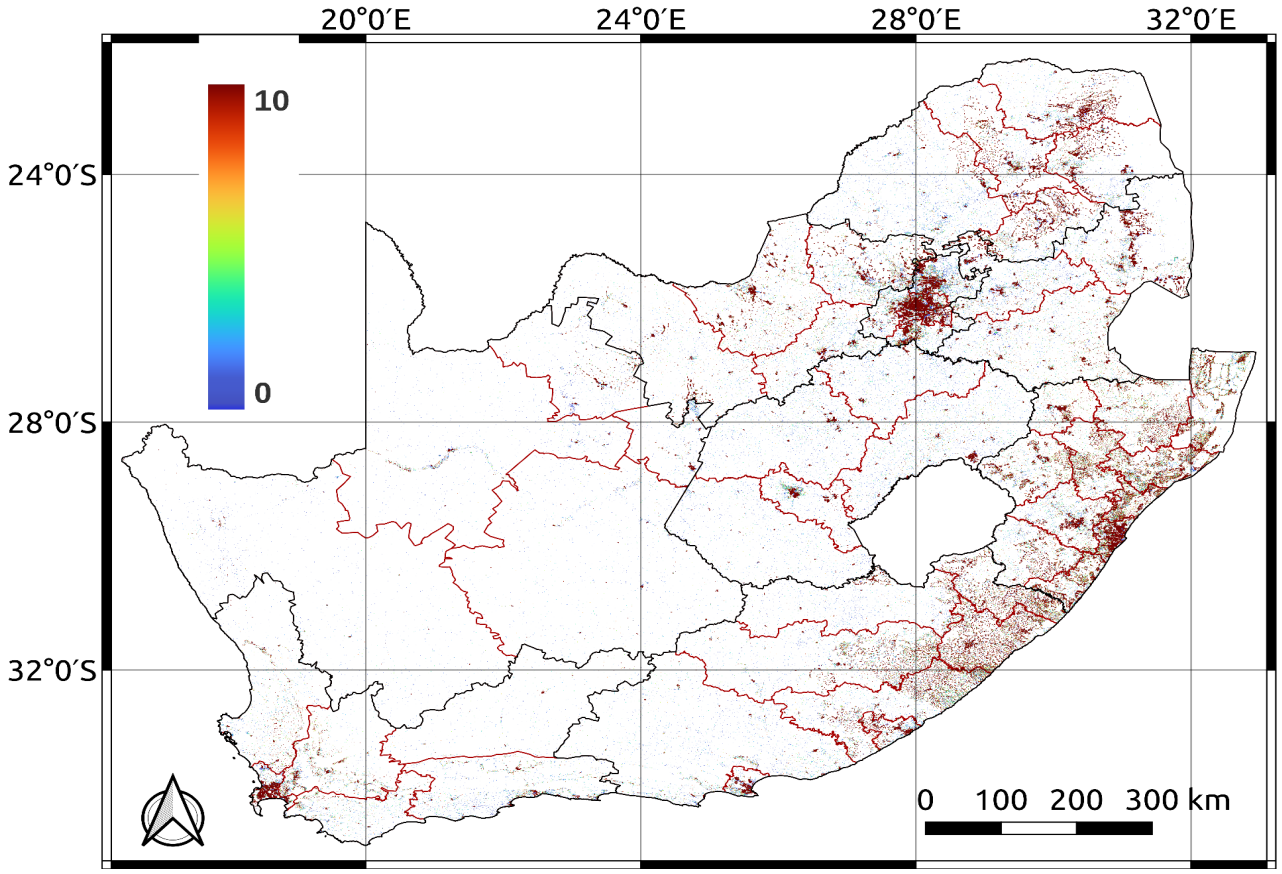

Figure 3.2 Population density map of South Africa (number of people per 30m square). Information sourced from Africa data hub (2019).

The South African National Land Cover Dataset (SANLC) is a GIS based land cover map produced for the Department of Forestry, Fisheries and the environment. It aims to "inform a wide variety of activities ranging from environmental planning and protection, economic development, compliance monitoring, enforcement, and strategic decision making" (DFFE, 2021). In this study, the 73 class, 30m resolution 2020 dataset is used for identifying land cover types in the respective study areas, as well as for improving WRF model simulations through the creation of a new land cover input.

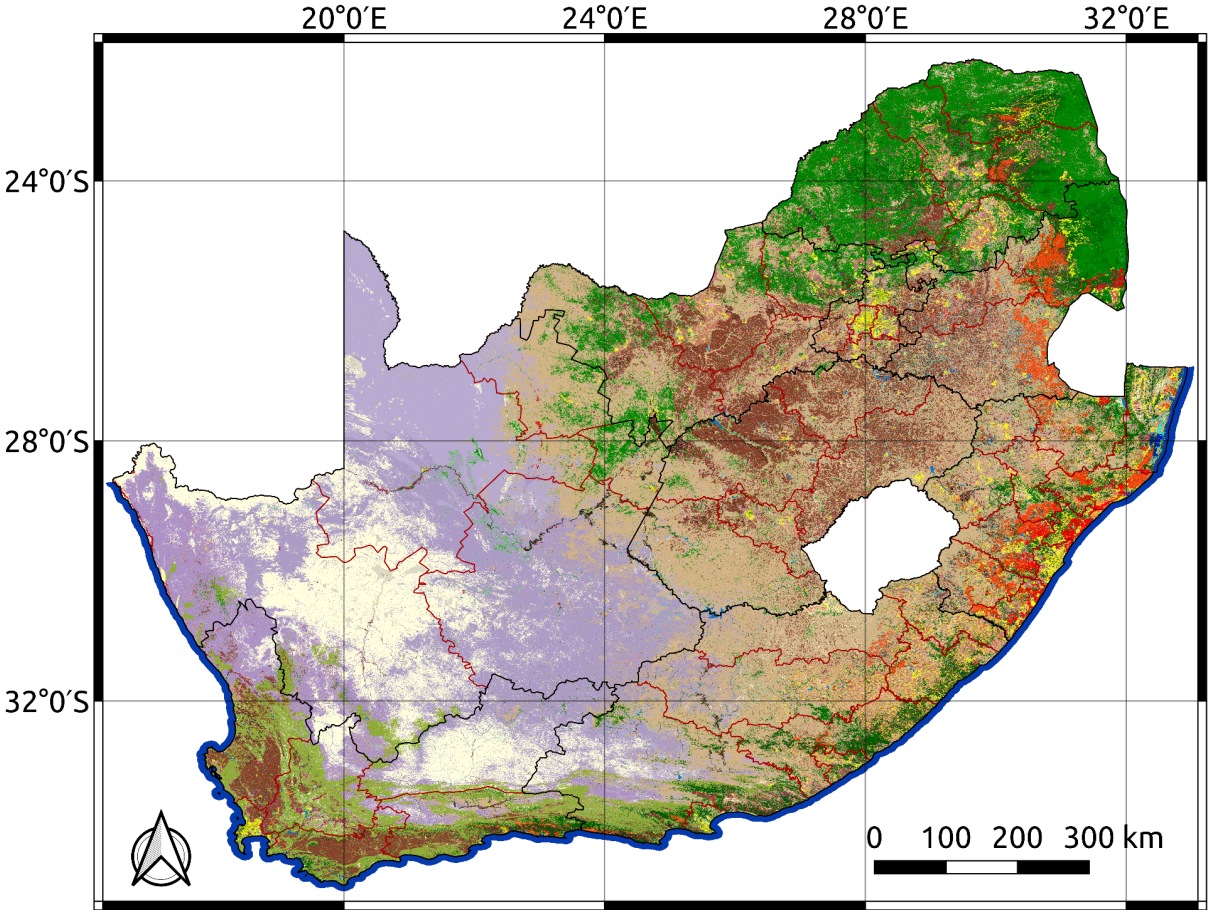

1		Contiguous (Indigenous) Forest (*combined* very high, high, medium)	38		Commercial Annuals Pivot Irrigated
2		Contiguous Low Forest & Thicket (*combined classes*)	39		Commercial Annuals Non-Pivot Irrigated
3		Dense Forest & Woodland (35 - 75% cc)	40		Commercial Annuals Crops Rain-Fed / Dryland / Non-Irrigated
4		Open Woodland (10 - 35% cc)	41		Subsistence / Small-Scale Annual Crops
5		Contiguous & Dense Planted Forest (*combined classes*)	42		Fallow Land & Old Fields (Trees)
6		Open & Sparse Planted Forest	43		Fallow Land & Old Fields (Bush)
7		Temporary Unplanted Forest	44		Fallow Land & Old Fields (Grass)
8		Low Shrubland (other regions)	45		Fallow Land & Old Fields (Bare)
9		Low Shrubland (Fynbos)	46		Fallow Land & Old Fields (Low Shrub)
10		Low Shrubland (Succulent Karoo)	47		Residential Formal (Tree)
11		Low Shrubland (Nama Karoo)	48		Residential Formal (Bush)
12		Sparsely Wooded Grassland (5 - 10% cc)	49		Residential Formal (low veg / grass)
13		Natural Grassland	50		Residential Formal (Bare)
14		Natural Rivers	51		Residential Informal (Tree)
15		Natural Estuaries & Lagoons	52		Residential Informal (Bush)
16		Natural Ocean, Coastal	53		Residential Informal (low veg / grass)
17		Natural Lakes	54		Residential Informal (Bare)
18		Natural Pans (flooded @ obsv time)	55		Village Scattered (bare only)
19		Artificial Dams (incl. canals)	56		Village Dense (bare only)
20		Artificial Sewage Ponds	57		Smallholdings (Tree)
21		Artificial Flooded Mine Pits	58		Smallholdings (Bush)
22		Herbaceous Wetlands (currently mapped)	59		Smallholdings (low veg / grass)
23		Herbaceous Wetlands (previous mapped extent)	60		Smallholdings (Bare)
24		Mangrove Wetlands	61		Urban Recreational Fields (Tree)
25		Natural Rock Surfaces	62		Urban Recreational Fields (Bush)
26		Dry Pans	63		Urban Recreational Fields (Grass)
27		Eroded Lands	64		Urban Recreational Fields (Bare)
28		Sand Dunes (terrestrial)	65		Commercial
29		Coastal Sand Dunes & Beach Sand	66		Industrial
30		Bare Riverbed Material	67		Roads & Rail (Major Linear)
31		Other Bare	68		Mines: Surface Infrastructure
32		Cultivated Commercial Permanent Orchards	69		Mines: Extraction Sites: Open Cast & Quarries *combined*
33		Cultivated Commercial Permanent Vines	70		Mines: Extraction Sites: Salt Mines
34		Cultivated Commercial Sugarcane Pivot Irrigated	71		Mines: Waste (Tailings) & Resource Dumps
35		Commercial Permanent Pineapples	72		Land-fills
36		Cultivated Commercial Sugarcane Non-Pivot (all other)	73		Fallow Land & Old Fields (wetlands)
37		Cultivated Emerging Farmer Sugarcane Non-Pivot (all other)			

Figure 3.3 The 2020 South African National Land cover Dataset with a 73 class land cover legend (Source: DFFE, 2021).

3.2.2.2 Landsat 8 thermal imagery

Landsat 8 (Collection 2 level 1) imagery was obtained through the Earth Explorer interface, courtesy of the U.S. Geological Survey (USGS). It was captured by a satellite launched in 2013 which carries an Operational Land Imager (OLI) sensor and a Thermal infrared (TIR) sensor. The TIR sensor provides the thermal information used in the study (Band 10), while the OLI sensor (Bands 4 and 5) provides information about vegetation, water and clouds which was used to correct the thermal images and select those with no cloud interference. The thermal band 10 has a spatial resolution of 100m, which is then resampled to 30m, and a temporal resolution of 16 days. The data was used for studying the distribution of temperatures across each study area.

3.2.3 Simulation data

Simulation data was obtained through the Weather Research and Forecasting (WRF) model. This will be expanded upon in the methods section.

3.3 Methods

Methods are divided into two main parts: Those related to thermal imagery (section 3.3.1 to 3.3.3) and those related to the WRF model (3.3.4 to 3.3.9).

3.3.1 Thermal imagery conversion

In order to use Landsat thermal information properly, the land surface temperatures (LSTs) first needed to be calculated from the raw digital numbers obtained from the satellite. For this study, the QGIS based RS & GIS plugin by Barane and Dwarakish (2017) was used. Following the calculations in the Landsat 8 users handbook (Vaughn Ihlen, 2019) the images were first atmospherically corrected to account for the sun elevation and angle - turning the thermal band 10 digital numbers into Top of Atmosphere Radiance (TOA), Reflection (TOR) and then Brightness temperature (BT). From here, the land surface emissivity (e) was calculated using a Normalized Difference Vegetation Index (NDVI) image based method from Sobrino et al. (2004). This made use of bands 4 and 5 to calculate NDVI and proportion vegetation (pv). The final LST calculation was based on an equation from Artis and Carnahan (1982) and Weng et al. (2004):

$$LST = \frac{T\lambda}{1+(\frac{\lambda * T\lambda}{\rho})lne}$$ (Equation 3.1)

Where LST is land surface temperature (in °C), T is at satellite brightness temperature (°C), λ is the wavelength of radiation emitted (11.5 μm), ρ is 1.438x 10^-2 mK and e is land surface emissivity.

3.3.2 Creation of representative images

Images for each of the cities were collected from the period January 2014 to December 2018. These were manually filtered to choose images which: (i) had no clouds or shadow over the study areas; and (ii) were from days which reached maximum air temperatures of at least 30°C (checked using station data from Weather underground and SAWS). All of these images were captured between 09:55 AM and 10:28 AM local time, with the imagery for each individual location captured at roughly the same time (within 1-2 minutes) across all years. Once appropriate images had been selected, these were all processed to extract LST according to the method above. Each area's image collection (9-18 images) was then combined into one image using the QGIS raster calculator. This gave the final representative image for each location.

Table 3.2 Landsat 8 thermal images used in each location and their time of capture.

City	Number of images used	Time of day for imagery (UTC+2)
Bloemfontein	18	10:09
Kuruman	15	10:21
Mokopane	10	10:01
Newcastle	9	09:56
Phalaborwa	9	09:55
Pilanesberg	9	10:08
Rustenburg	13	10:08
Thohoyandou	11	09:55
Upington	11	10:28
Vryburg	9	10:15

3.3.3 Identification of hot and cool spots and their relation to physical characteristics

To highlight differences in LSTs across the study areas, hot and cold anomalies were identified. This was based on the average urban temperature in each study area. QGIS was used to calculate these average temperatures and then identify the areas that were significantly hotter (i.e., ≥ 2°C) than the average (highlighted in red), and the areas that were significantly cooler (i.e., ≥ 2°C) than average (highlighted in blue). To better understand what was influencing these differences in LSTs, the representative images for each study area were overlaid with the DEM and contour data, land cover data, population density data and satellite imagery. The relationship between LST and these physical characteristics was then visually analysed to identify the strength of their relationships.

3.3.4 WRF model description

A regional climate model called the Weather Research Forecasting model (WRF) was used in the study. The WRF model is a mesoscale numerical weather prediction system developed by the National Center for Environmental Prediction (NCEP) and the National Center for Atmospheric Research (NCAR) (Skamarock et al., 2019; NCAR). It can be used for both atmospheric research (as a RCM) and operational forecasting at scales ranging from tens of metres to thousands of kilometres. It can produce simulations based on actual atmospheric conditions, as well as idealised conditions. The WRF model has two alternative dynamical cores: Nonhydrostatic Mesoscale Model (NMM) and Advanced Research (ARW). For our study the ARW core (version 4.2.1) was used

The WRF model is one of the most useful RCMs available and has been widely tested around the world, making it an attractive choice for this research. WRF's versatility and proven skill means it can be applied to many fields and topics across the globe, but it does have its limitations, In order to better represent city characteristics more accurately, it is necessary to combine WRF with an Urban Canopy Model (UCM) (Kusaka and Kimura., 2004). The UCM allows for greater differentiation between urban classes, better representing the large heterogeneity of urban landscapes and improving the outputs of simulations.

3.3.5 WRF land cover input

While the WRF model itself can be used at very high resolution, the simulations are only as good as the data entered into them. The land cover datasets available over South Africa are very limited in both resolution (500m) and spatial accuracy, which at a country-wide or regional level is not an issue, but down at a city scale, this becomes a major limitation. A higher resolution and more accurate land cover dataset therefore becomes very important to show smaller-scale differences.

3.3.5.1 SANLC

While the SANLC dataset is not made with climate modelling in mind, its separation of land cover types at a resolution of 30m and into an extensive 73 class dataset, means that it has the potential to be converted into a very useful input for climate models. Additionally, the creation of the dataset has now been moved to an automated CALC system, which means that it will be updated far more timeously (biennially) than most other land cover datasets, eliminating errors that could occur with quickly changing classes. The version used in this study is SANLC2020.

3.3.5.2 Conversion

To be able to use the dataset in the WRF model, it had to be converted into a format the model could read. To do this, the modified 20 class IGBP MODIS Noah dataset used in WRF was chosen as a template to convert the 73 class dataset onto, combining classes that would be expected to have similar thermal properties. The method of conversion was based upon:

- The physical descriptions of each land cover class in the SANLC2020 dataset and the MODIS dataset.
- Satellite observed similarities between the classes in the two datasets.
- Thermal similarities between classes. For example in areas which consistently showed homogenous temperature, but covered multiple SANLC2020 land covers, the land cover classes were combined.

Once it had been decided which MODIS land cover class each SANLC2020 class would be converted to (Table 3.3), FORTRAN code was developed and used to read in each pixel of the SANLC dataset (Fig 3.4b, for example) and replace it with the chosen MODIS class, producing a final SANLC_converted dataset as seen in Figure 3.4d, for example.

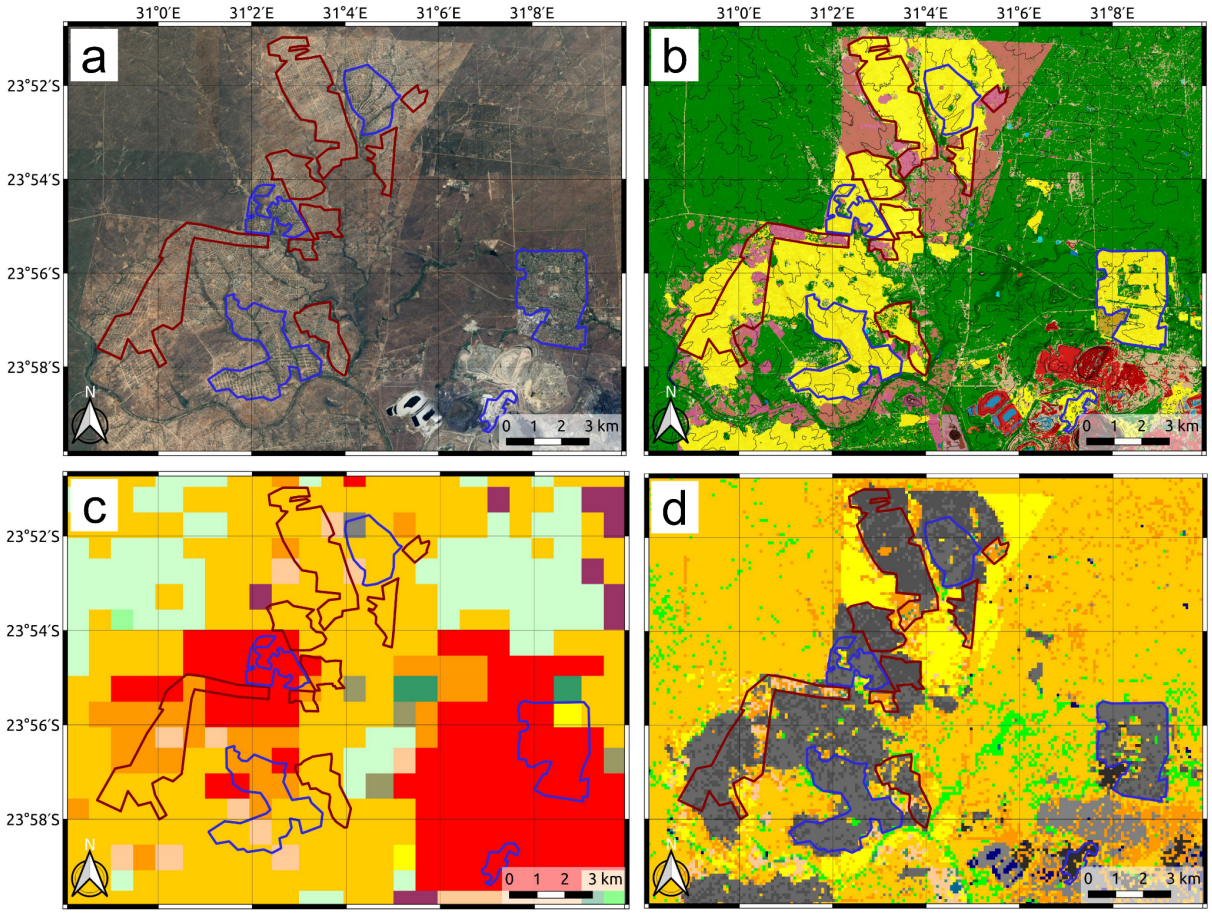

Figure 3.4 Spatial maps of the Phalaborwa study area: (a) Google satellite; (b) SANLC2020 land cover; (c) MODIS land cover; (d) SANLC_converted land cover.

As Figure 3.4c and 3.4d illustrate, the MODIS and SANLC converted datasets have significant differences between them. These land cover differences can directly influence the surface temperatures simulated using these datasets. It is therefore very important to understand how and where the datasets differ. Using Figure 3.4c as an example, one can see how the lower-resolution MODIS land cover does not identify the spatial extent of Phalaborwa's urban areas (red) very well. It roughly identifies the larger, more established areas, but with little precision, often being skewed a few kilometres away from the actual expanse. Meanwhile, the smaller, newer and less established settlements are not recognised at all. Conversely, the higher-resolution SANLC_converted land cover (Fig. 3.4d) identifies the spatial extent of the urban areas extremely well and also splits these areas into three categories, high density (medium grey), low density (light grey) and industrial (dark grey).

Urban areas are not the only parts affected by this. The majority of smaller scale land cover features are not present in the MODIS dataset. This includes water features like dams and rivers; smaller patches of cultivated land; changes in tree density within classes; bare land between classes; and much more. While many of these under-represented features are small, they can have significant impacts on local climate, especially those with very strong thermal signals (e.g., water, trees and bare land). The SANLC_converted dataset is far superior in identifying these, showing far more accurate spatial representations of the patterns that are seen on the ground (Fig. 3.4a).

Table 3.3 Land cover categories for MODIS and SANLC2020 datasets, highlighting which SANLC2020 categories were converted to which MODIS category to form the new SANLC_converted

MODIS category	SANLC categories converted to MODIS	SANLC2020 categories
Evergreen Needleleaf Forest (1)	5	1. Contiguous (indigenous) Forest 2. Contiguous Low Forest & Thicket 3. Dense Forest & Woodland (35 - 75% cc) 4. Open Woodland (10 - 35% cc) 5. Contiguous & Dense Planted Forest 6. Open & Sparse Planted Forest 7. Temporary Unplanted Forest 8. Low Shrubland (other regions) 9. Low Shrubland (Fynbos) 10. Low Shrubland (Succulent Karoo) 11. Low Shrubland (Nama Karoo) 12. Sparsely Wooded Grassland (5 - 10% cc) 13. Natural Grassland 14. Natural Rivers 15. Natural Estuaries & Lagoons 16. Natural Ocean, Coastal 17. Natural Lakes 18. Natural Pans (flooded @ obsv time) 19. Artificial Dams (incl. canals) 20. Artificial Sewage Ponds 21. Artificial Flooded Mine Pits 22. Herbaceous Wetlands (currently mapped) 23. Herbaceous Wetlands (previously mapped) 24. Mangrove Wetlands 25. Natural Rock Surfaces 26. Dry Pans 27. Eroded Lands 28. Sand Dunes (Terrestrial) 29. Coastal Sand Dunes & Beach Sand 30. Bare Riverbed Material 31. Other Bare 32. Cultivated Commercial Permanent Orchards 33. Cultivated Commercial Permanent Vines 34. Cultivated Commercial Sugarcane Pivot Irrigated 35. Commercial Permanent Pineapples 36. Cultivated Commercial Sugarcane Non-Pivot 37. Cultivated Emerging Farmer Sugarcane Non-Pivot 38. Commercial Annuals Pivot Irrigated 39. Commercial Annuals Non-Pivot Irrigated 40. Commercial Annuals Crops Rain-Fed / Dryland 41. Subsistence / Small-Scale Annual Crops 42. Fallow Land & Old Fields (Trees) 43. Fallow Land & Old Fields (Bush) 44. Fallow Land & Old Fields (Grass) 45. Fallow Land & Old Fields (Bare) 46. Fallow Land & Old Fields (Low Shrub) 47. Residential Formal (Tree) 48. Residential Formal (Bush) 49. Residential Formal (Low veg / grass) 50. Residential Formal (Bare) 51. Residential Informal (Tree) 52. Residential Informal (Bush) 53. Residential Informal (low veg / grass) 54. Residential Informal (Bare) 55. Village Scattered (Bare only) 56. Village Dense (bare only) 57. Smallholdings (Tree) 58. Smallholdings (Bush) 59. Smallholdings (Low veg / grass) 60. Smallholdings (Bare) 61. Urban Recreational Fields (Tree) 62. Urban Recreational Fields (Bush) 63. Urban Recreational Fields (Grass) 64. Urban Recreational Fields (Bare) 65. Commercial 66. Industrial 67. Roads & Rail (Major Linear) 68. Mines: Surface Infrastructure 69. Mines: Extraction Sites: Open Cast & Quarries 70. Mines: Extraction Sites: Salt Mines 71. Mines: Waste (Tailings) & Resource Dumps 72. Land-fills 73. Fallow Land & Old Fields (wetlands)
Evergreen Broadleaf Forest (2)	1, 2, 3	
Mixed Forest (5)	42, 57, 61	
Closed Shrubland (6)	9	
Open Shrubland (7)	8, 10, 11, 43, 46, 58, 62	
Savannas (9)	4, 6	
Grasslands (10)	7, 12, 13, 59, 63	
Permanent Wetlands (11)	22, 23, 24, 33, 34, 38, 39, 73	
Croplands (12)	32, 35, 36, 37, 40, 41	
Barren or sparsely vegetated (16)	25, 26, 27, 28, 29, 30, 31, 45, 55, 60, 64, 69, 70, 71, 72	
Water (17)	14, 15, 16, 17, 18, 19, 20, 21	
Low density residential (31)	47, 48, 51, 52, 53, 56	
High density residential (32)	49, 50, 53, 54	
High intensity industrial (33)	65, 66, 67, 68	

3.3.6 WRF-Coupled Urban Canopy Model (WRF-UCM)

The creation of the new SANLC dataset divides urban land cover classes into three categories (low-density residential, high-density residential, and high-intensity industrial), where the original MODIS dataset had only one urban class. This separation of classes meant that it was now possible to assign different physical characteristics to the urban classes to make them more representative of what is on the ground. This is done by coupling the WRF model with the single layer Urban canopy model (UCM) (Kusaka and Kimura, 2004). The UCM consists of two-dimensional, symmetrical street canyons with simplified buildings. It estimates the surface temperature of roof, wall and road surfaces, as well as the fluxes from these surfaces (Tewari et al. 2004). Being able to edit values of building height and width, street width, vegetation cover, and thermal properties of surfaces provides studies with far more scope to test sensitivities and improve simulations.

3.3.7 Experimental design

This study requires the model to be run at high resolution in order to pick up city scale changes in variables. To do so while limiting computational power and still picking up larger scale atmospheric forcings, nesting was used. This involved creating a model domain with an outer “parent” domain at 1800m resolution, a middle “daughter” domain at 600m resolution and then the final inner study area domain at 200m resolution (Fig 3.5).

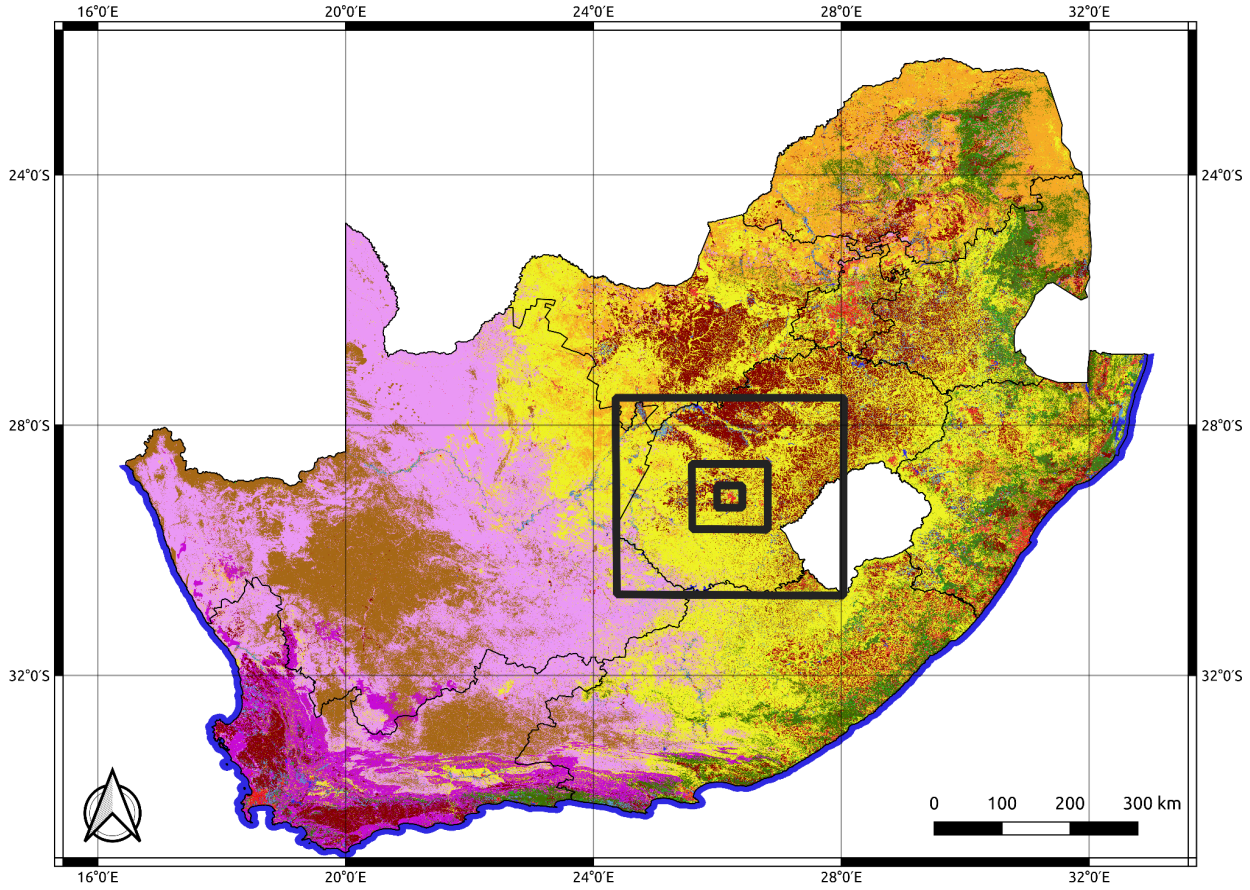

Figure 3.5 The WRF nesting setup over the Bloemfontein study area. The outer nest at 1800m resolution, the middle at 600m and the inner at 200m.

Apart from defining the model domains and resolutions, it was also necessary to specify the length of the simulation, the source of the initial conditions, and the time-step between the solving of model equations (Table 3.4). The length was chosen based on a full day of study plus an initial 21 hour "spin up" time, which would allow the model to stabilise before its outputs were used. Initial conditions were obtained from the Global Forecasting System (GFS), and the time-step was chosen in accordance with the resolution of the simulations. In addition to these, the model also has several physics schemes, or parameterisations, that need to be specified according to the scopes of the study. The ones used in this research were based on the WRF user guide's suggested high-resolution setup, which are summarised in Table 3.5.

Table 3.4 Basic simulation set-up for all 4 simulation scenarios.

Length (hours)	Spin-up (hours)	Nests	Initial conditions	Feedback	Time-step (seconds)	Resolution (nest 1, 2, 3)
45	21	3	GFS data	One directional	7, 7/3, 7/9	1800m, 600m, 200m

Table 3.5 Physics options used in WRF simulations.

Physics Scheme	Option used
Microphysics (mp_physics)	Thompson
Longwave radiation (ra_lw_physics)	RRTMG scheme
Shortwave radiation (ra_sw_physics)	RRTMG scheme
Land Surface (sf_surface_physics)	Unified Noah LSM
Surface layer (sf_sfclay_physics)	Eta similarity method
Planetary Boundary Layer (bl_pbl_physics)	Mellor Yamada Janjic

3.3.7.1 Control simulations

To test the influence and usefulness of the newly created SANLC_converted dataset, simulations for each of the study areas were run using both the SANLC_converted and the MODIS land cover datasets. MODIS was chosen as a reference because it is the highest resolution WRF dataset available over South Africa. The dates of these simulations were chosen from days within the group of Landsat thermal images that was processed earlier in the study. These were cross-referenced with observational weather data (SAWS and Weather Underground) to choose the hottest day with weak synoptic conditions (winds below 20 km/h) for each study area (Table 3.6). The simulations themselves were then run using the CHPC-Lengau computer cluster, being run with Parallel NetCDF and OpenMP.

Table 3.6 Chosen simulation days for each location (with the days maximum temperature).

City	Simulation date	Maximum temperature (°C)
Bloemfontein	2015-11-10	35
Kuruman	2018-11-16	38
Mokopane	2016-01-06	34
Newcastle	2015-12-30	30
Phalaborwa	2016-10-29	38
Pilanesberg	2015-11-10	36
Rustenberg	2015-11-10	36
Thohoyandou	2016-10-29	34
Upington	2016-12-03	42
Vryburg	2017-11-06	37

3.3.7.2 Sensitivity (cooling scenario) experiments

Once the WRF model had been validated against the observational data, we were able to manipulate the characteristics of the land cover dataset to represent feasible adaptation and mitigation scenarios. The review study by Santamouris and Fiorito (2021) provided examples of reasonable values of albedo for an increased coverage of reflective white roofs, while the tree coverage present in the more vegetated parts of our study areas provided a good benchmark to work towards for urban fraction. For the two scenarios, the urban fraction and roof albedos were adjusted in separate simulations to represent (1) an increase in tree cover to 60% of the urban area in the high-density residential and high-intensity industrial classes; and (2) an increase in the albedo of roofs from 0.2 to 0.4 (20% to 40%) across all urban classes. These adjustments were performed in the urban parameters table (URBPARM.TBL) before running each simulation. Table (3.7) summarises the differences in these, as well as the characteristics of the initial WRF_MODIS and WRF_SANLC control simulations.

Table 3.7 Summary of, and differences between, the four WRF simulation scenarios used in the study.

Experiment Name	Type	Land cover Dataset	Urban Climate Model (UCM)	
			Urban fraction (nests)	Roof albedo (nests)
WRF_MODIS	Control	MODIS	UCM not used	
WRF_SANLC	Control	SANLC	0.4, 0.9, 0.9	0.2, 0.2, 0.2
WRF_TREE	Sensitivity	SANLC	0.4, 0.4, 0.4	0.2, 0.2, 0.2
WRF_ROOF	Sensitivity	SANLC	0.4, 0.9, 0.9	0.4, 0.4, 0.4

3.3.8 Model evaluation

To assess the skill of the model in simulating the temperature conditions and test the influence of the new land cover dataset, it was necessary to compare the model outputs with observational data. This was done for both surface temperature and air temperature. The surface temperatures produced by WRF were compared with the Landsat imagery from that day and time.

First the WRF_MODIS and WRF_SANLC simulations for each study area were spatially visualised in QGIS and overlaid with the relevant Landsat image (scaled to the same 200m resolution). From this, one could visually determine how well the model identified the spatial patterns of the LSTs.

To compare the actual values of LSTs, the QGIS raster calculator was used to calculate the differences (or bias) between the modelled and observed values (Observed LSTs - Modelled LSTs). These were also spatially visualised, showing the bias in each pixel across all study areas.

To statistically evaluate the performance of the simulations, three different metrics were used: (1) Absolute Error, (2) Root Mean Square Error (RMSE), and (3) Correlation. These were calculated using the Climate Data Operators (CDO) command line suite from the Max Planck Institute for Meteorologie. The metrics were all applied across the entire study domains for a single time step.

Absolute error measures the overall difference in value (°C) between the simulated and observed data:

$$AE = \frac{\sum_{i=1}^{N} (Xi - Yi)}{N} \quad \text{(Equation 3.2)}$$

Where $\sum_{i=1}^{N}$ = sum of grid point values starting from 1 to N, N = number of grid points, Xi = simulated values, and Yi= observed values

RMSE measures the overall deviation (whether positive or negative) of the simulated values from the observed (in °C):

$$RMSE = \frac{\sqrt{\sum_{i=1}^{N} (Xi - Yi)^2}}{N} \quad \text{(Equation 3.3)}$$

Where $\sum_{i=1}^{N}$ = sum of grid point values starting from 1 to N, N = number of grid points, Xi = simulated values, and Yi= observed values

Correlation measures both the strength and the direction of the relationship between the simulated and observed data:

$$R = \frac{\Sigma(Xi - \overline{X})(Yi - \overline{Y})}{\sqrt{(Xi - \overline{X})^2 (Yi - \overline{Y})^2}} \quad \text{(Equation 3.4)}$$

Where r= Pearson Correlation Coefficient, $\sum$ = sum of, Xi= simulated value, Yi= observed value, $\overline{x}$ = mean of simulated values, $\overline{y}$ = mean of observed values

For air temperature, the WRF simulated 2m temperature was compared with South African Weather Service (SAWS) observational air temperature for each study areas' chosen day. Since the station air temperatures for Phalaborwa and Thohoyandou were missing on these days, the comparison was limited to the other 8 study areas.

To visually analyse their relationships, the SAWS hourly station data was plotted against the WRF_SANLC hourly values for that same location (using Microsoft Excel). The two datasets were then also statistically analysed, calculating both the RMSE and Correlation between them. The equations for these are the same as Equations (3.3) and (3.4) above.

3.3.9 Sensitivity experiments evaluation

The results of the two sensitivity experiments were compared with the WRF_SANLC control simulation to see the impact the changes had on LST and air temperature. This analysis was performed using the Ferret data visualisation and analysis environment from NOAA.

First, the WRF_SANLC control scenarios were subtracted from the two cooling scenarios (WRF_TREE and WRF_ROOF) across each study area for the period 10 AM to 5 PM. From this, spatial plots of the average differences in both LST and air temperature were produced.

Using the LST spatial plots, locations where there was significant cooling were then chosen for each study area. Temporal plots of these locations could then be produced (using Microsoft Excel) to show the variations in cooling effectiveness of the two scenarios over time.

This sensitivity experiment evaluation represents the final methodological aspect of this study, with the remaining sections now dedicated to presenting the results, discussions, and conclusions.

Chapter 4. Drivers of Temperature Hot Spots in South African Cities

This chapter presents the results of the thermal imagery analysis and uses them to discuss the spatial distribution of land surface temperatures (LSTs) within the cities. It first shows the distribution of land surface temperatures and the physical properties for each study area, and identifies hot and cool parts within each (Section 4.1). It then discusses the drivers of the disparities in LSTs (Section 4.2), before summarising the hot and cool spots and their causes and circumstances (Section 4.3). It concludes by noting the most important findings and discussing the limitations (Section 4.4).

4.1 Spatial distribution of LST over the cities

All the cities are characterised by significant spatial variation in LST (Fig 4.1; Table 4.1). However, the magnitude of the variability differs among the cities. Seven of these show differences of at least 8°C between the coolest and hottest settlements within them, with the remaining cities of Bloemfontein, Newcastle and Vryburg showing differences between 4°C and 6°C. These differences are closely related to both the local climate and vegetation, but also appear to be heavily influenced by socio-economic factors.

To investigate the relationship between the spatial distribution of LST and the underlying land surface characteristics, Figures 4.2 - 4.11 compare the LST maps with physical features, population density, and land cover types. Essential information on the features and the LSTs are highlighted in Tables 4.2 - 4.11.

Table 4.1 Characteristics (spatial mean, maximum, minimum and range) of land surface temperature (LST) in the 10 selected study areas.

City	LST (ºC)			
	Mean	**Maximum**	**Minimum**	**Range**
Bloemfontein	34	36	31	5
Kuruman	40	44	35	9
Mokopane	37	42	33	9
Newcastle	34	36	32	4
Phalaborwa	37	41	33	8
Pilanesberg	37	41	31	10
Rustenburg	36	40	30	10
Thohoyandou	38	42	33	9
Upington	41	46	36	10
Vryburg	36	39	33	6

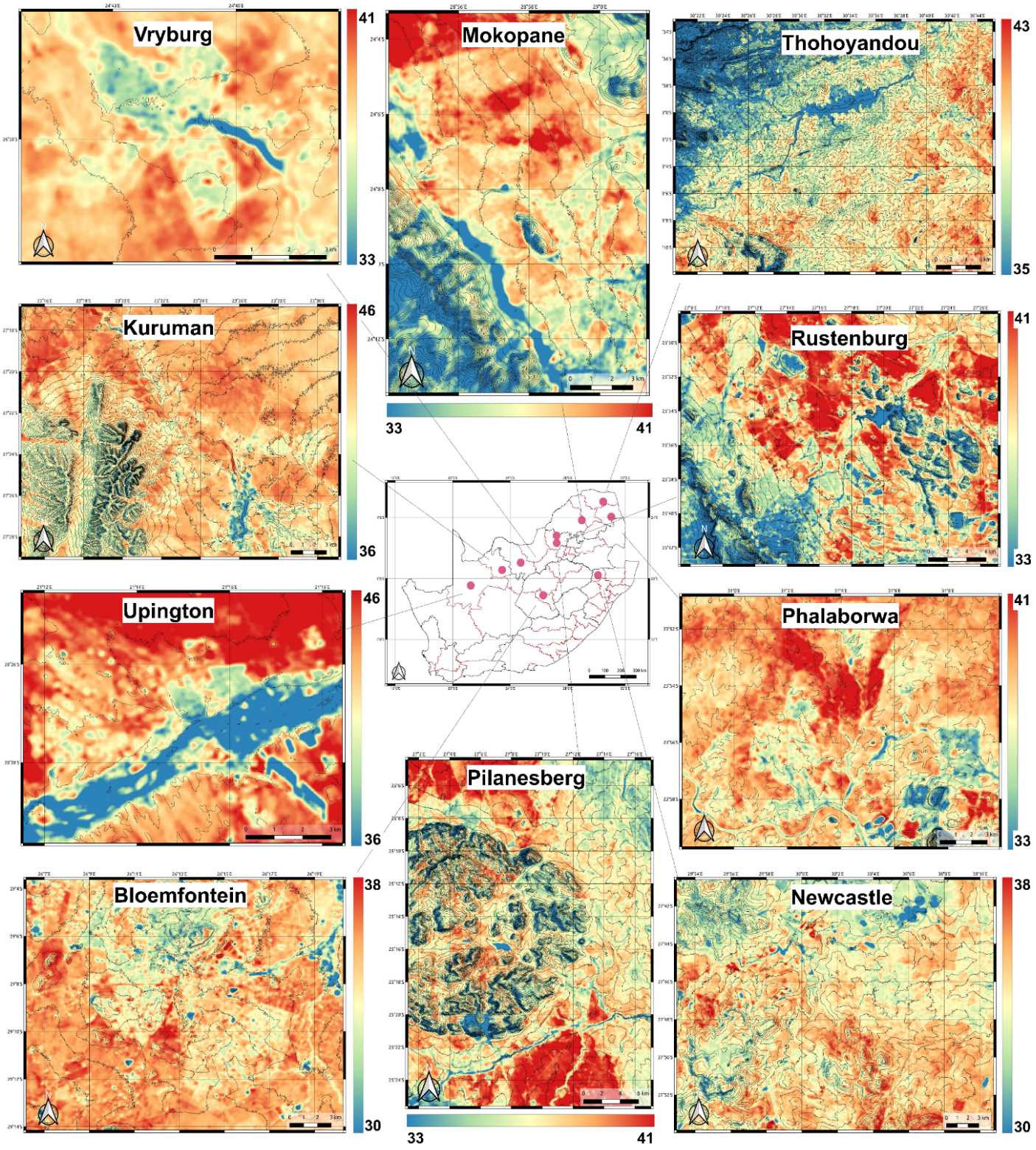

Figure 4.1 Land Surface Temperature (LST) maps of the 10 study areas (in °C). Note that the temperature scales are not the same for all maps. Scales were chosen to better highlight temperature distributions for each study area.

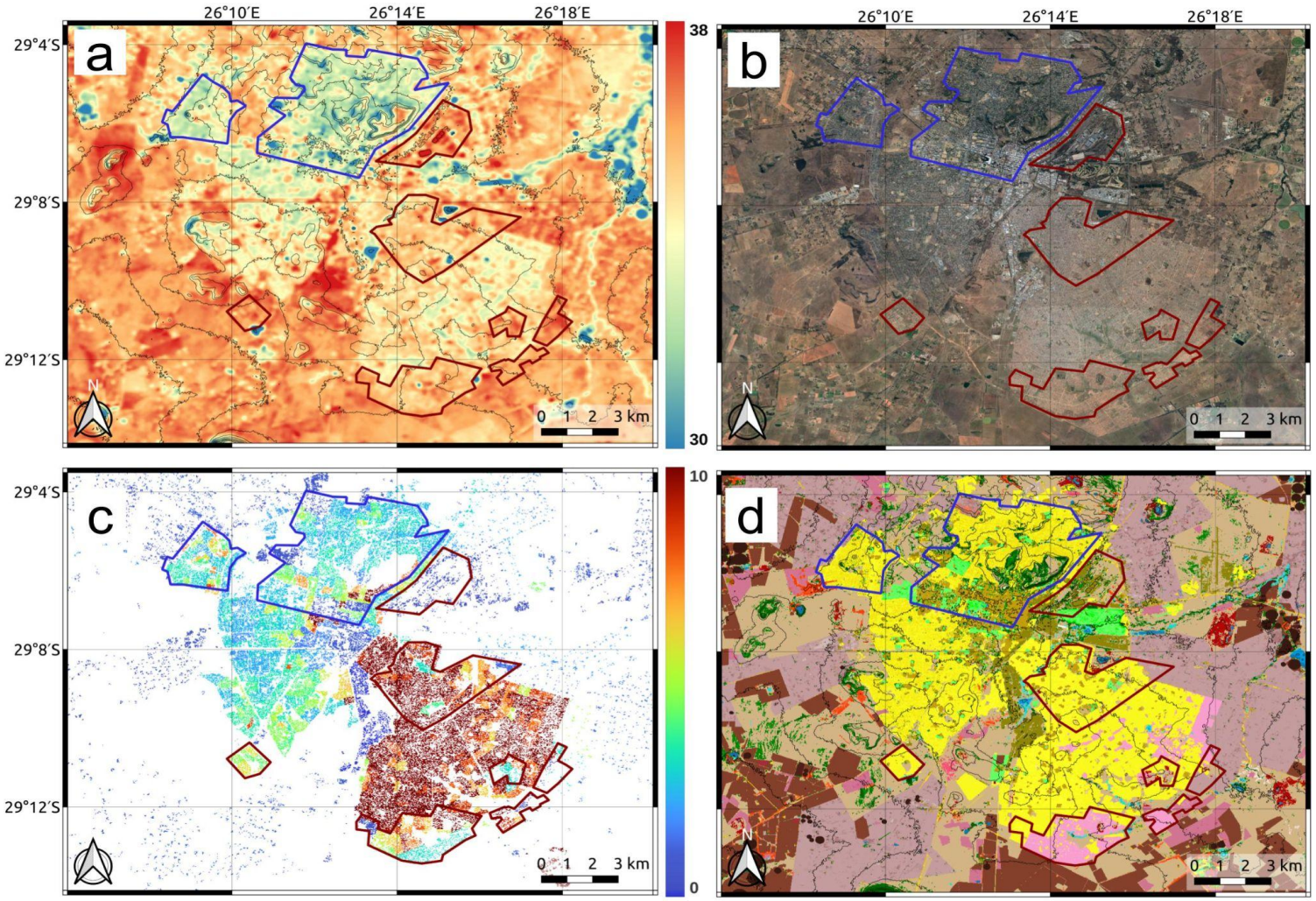

Figure 4.2: Land surface temperature (panel a) and physical features in Bloemfontein. Panel (b) shows the physical features as depicted by a Google satellite image. Panel (c) shows the population density in people/pixel; Panel (d) shows the SANLC2020 land cover (see Figure 3.1 for this dataset's legend).

Table 4.2: Highlights of physical features and LST distribution in Bloemfontein (Fig 4.2).

Feature	Attributes	Temperature
City Centre	• Located in the middle of the study area. • Contains a dense commercial and industrial zone, interspersed with recreational grounds. • Tree cover ranges from low to medium.	• Mostly lower than average temperature (30 - 34°C) depending on roof reflectivity and vegetation. • Warmer temperatures (36 - 41°C) over the large dark roofs of the Transnet train yard in the eastern part.
High-income areas	• Located to the north, NW and SW of the centre. • Features well-forested residential and recreational areas with large houses of medium to high density.	• Ranges between 31°C and 33°C for the residential areas. • Warmer (34 - 37°C) temperatures for open recreational grounds and the patches of natural vegetation.
Low-middle income areas	• Located SE of the centre, covering an expansive area. • Features low to middle-income residential housing (medium houses, high density). • Tree cover is low across the area. • Along the southern edges of the settlement, houses are smaller, less formal, and more scattered.	• Temperature is ~35°C across most parts. • Small valleys and more densely built-up areas are slightly cooler (32-34°C). • The less vegetated settlement edges are slightly warmer, reaching over 36°C and showing more similar values to the surrounding grassland (5°C warmer than the vegetated northern areas).
Non-built-up areas	• Dominated by grassland (often grazed) and crops (irrigated and rainfed).	• Grassland and rainfed crops are warm (36-37°C), while irrigated croplands (centre pivots especially) are much cooler (28-30°C).
Hot spots	• Transnet train yard; crops and grassland; the southern fringes of the S and SE settlement which are predominantly informal settlements.	
Cool spots	• Buildings with large reflective roofs (e.g., twin city mall); vegetated northern residential areas; water features.	

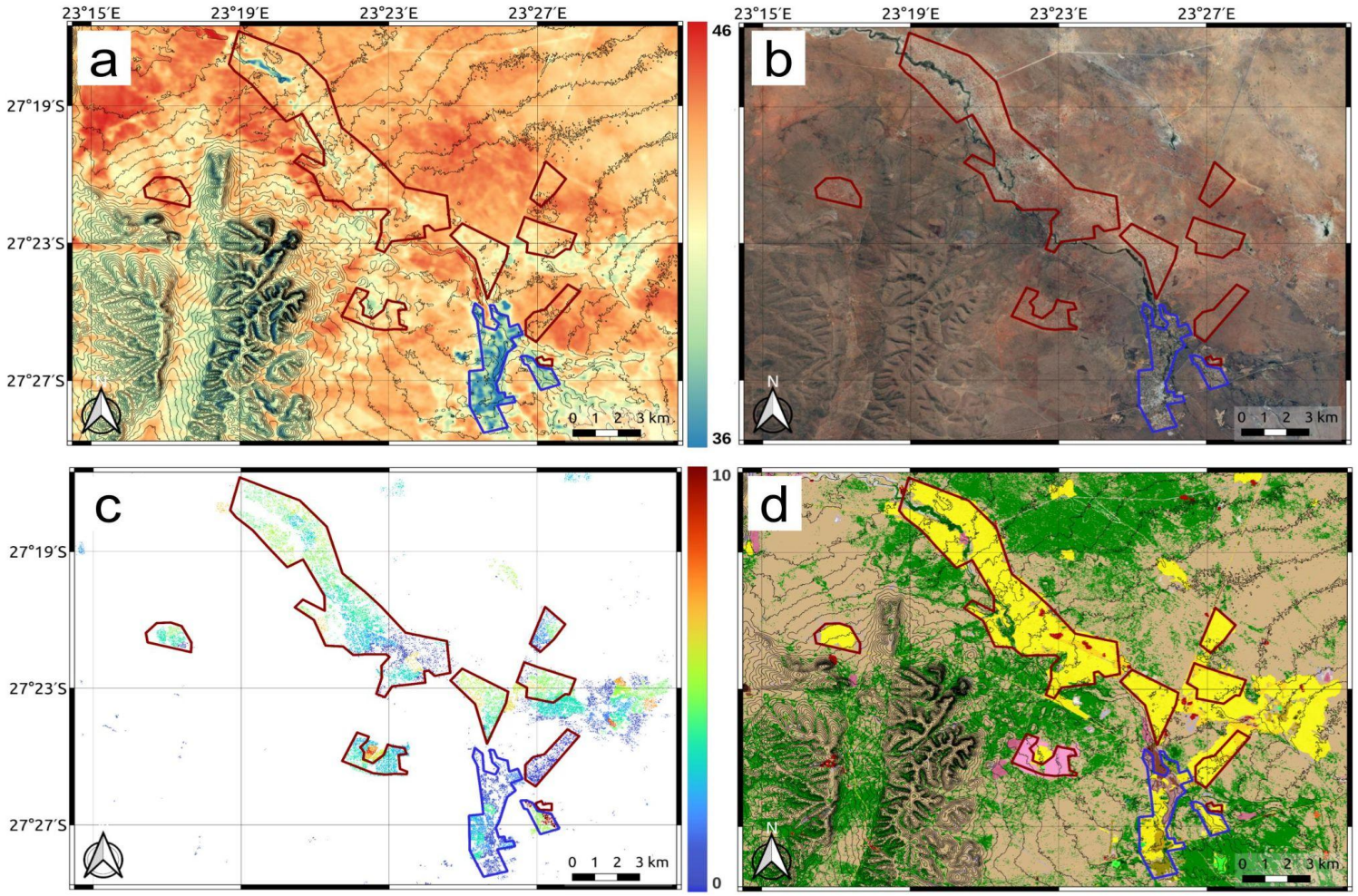

Figure 4.3 Same as Figure 4.2 but for Kuruman.

Table 4.3 Highlights of physical features and LST distribution in Kuruman (Fig 4.3).

Feature	Attributes	Temperature
City Centre	• Located in the south of the study area. • Small commercial centre in the middle and small industrial area further south.	• Temperatures range between 36°C and 38°C.
High-income areas	• Well-forested, medium density residential areas immediately to the east and north of the centre.	• Relatively cool temperatures, mostly between 35°C (closer to the river) and 38°C (further from river).
Low-income areas	• Located northwards of the centre. • Featuring the middle to lower-income settlements of Bankhara (NW), Maruping (N and far NW), and Mothibistad (NE). • These are generally quite spread out and have significant bare ground and low vegetation between houses, Maruping in particular. • Between Kuruman town and Mothibistand is an informal settlement with very few trees.	• Bankhara has temperatures of between 41°C and 43°C. • The denser central part of Mothibistad is ~ 39-41°C with the more dispersed edges up to 43°C. • Maruping has fewer cooler spots and temperatures range between 41°C and 43°C with small sections reaching up to 44°C. • The informal settlement has an average temperature of ~44°C (9°C warmer than the more forested, wealthier parts of Kuruman).
Non-built-up areas	• Mostly grassland and savanna.	• Ranges from 42°C to 45 °C. • Range depends on vegetation cover and reflectivity of underlying soils. • The more vegetated sections of savanna and the more reflective sections of grassland are often slightly cooler (42-43°C).
Hot spots	• Most settlements outside of Kuruman town, particularly the more spread out ones; the informal settlement between Kuruman and Mothibistad; grassland.	
Cool spots	• The more vegetated, higher-income areas in Kuruman town, particularly closer to the river.	

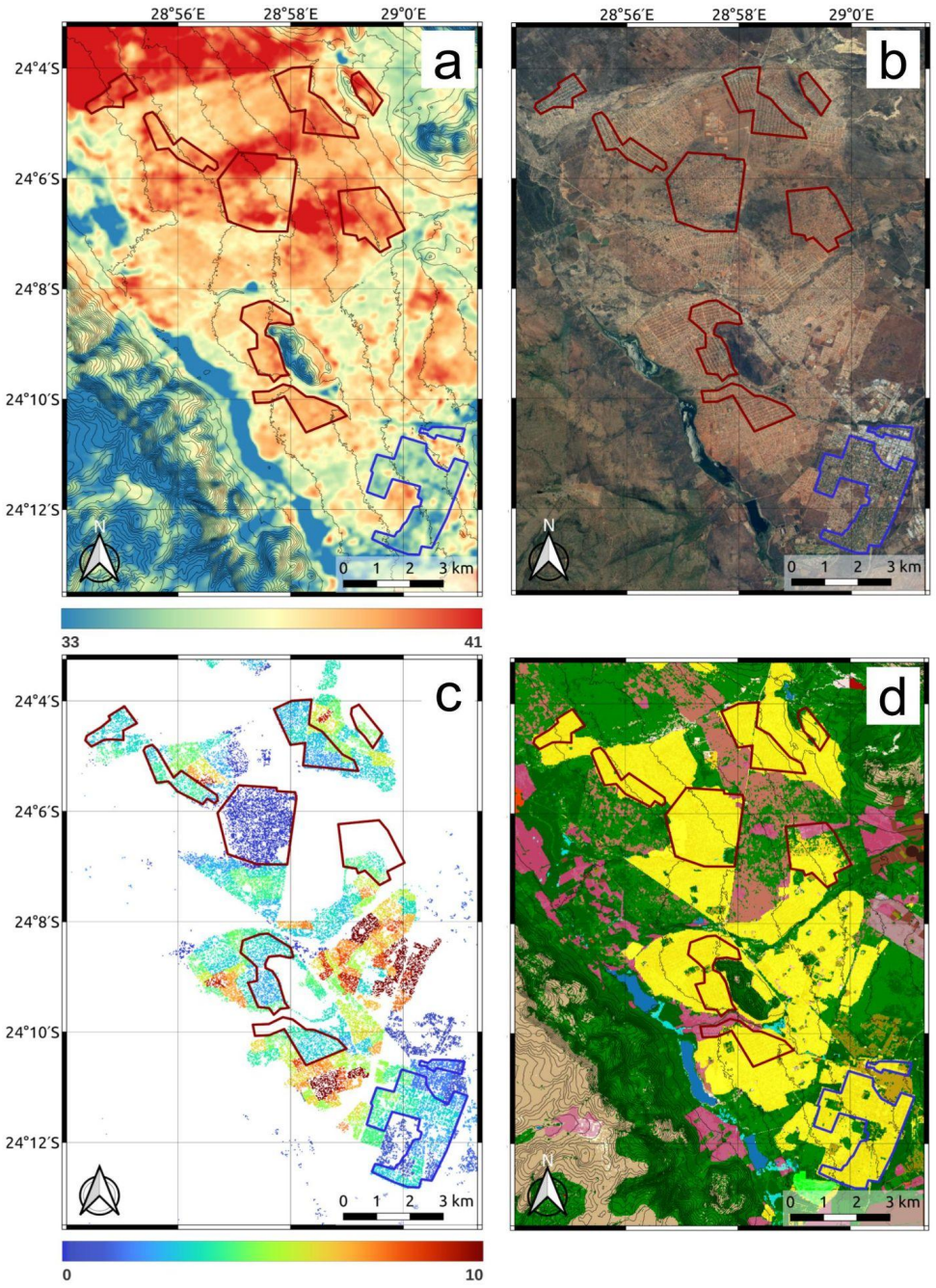

Figure 4.4: Same as Figure 4.2 but for Mokopane.

Table 4.4: Highlights of physical features and LST distribution in Mokopane (Fig 4.4).

Feature	Attributes	Temperature
City Centre	• In the south of the study area. • Consists of a relatively large commercial and industrial zone. • Middle section with tree cover and the remainder fairly bare.	• The vegetated middle part is ~35°C. • The remainder is ~38°C.
High-income areas	• Well-forested residential area south-adjacent to the centre. • Mostly medium density housing with some open land between.	• The forested parts have temperatures between 33°C and 36°C. • Open land is ~38°C.
Low-middle income areas	• To the NW of the centre. • Consists of multiple isolated settlements. • A general trend of decreasing density and formality of infrastructure with increased distance away from the southern city centre. • This correlates to an increase in bare ground and low vegetation between housing. • Trees are present across the majority of the settlements, but are sparsely distributed and related to the density of housing.	• The denser, more formal built-up areas range from 36-37°C. • The more spread out areas are generally warmer (38-40°C). • Small parts of these with darker soils and increased bare ground rise even higher (up to 42°C).
Non-built-up areas	• The non-built-up valley areas consist of mostly savanna, rainfed crops, and grazing land. • There are small sections of cooler woodland (~35°C). • The soil and vegetation colour impact the temperatures. • Some areas of darker soil and low vegetation reach up to 42°C. • Lighter vegetation/soils temperatures are ~38°C. • Vegetation cover is affected by controlled burns.	
Hot spots	• Less dense settlements across the area; the more exposed, darker soil savanna, crops and grassland.	
Cool spots	• High-income, well-forested areas in the southern settlement.	

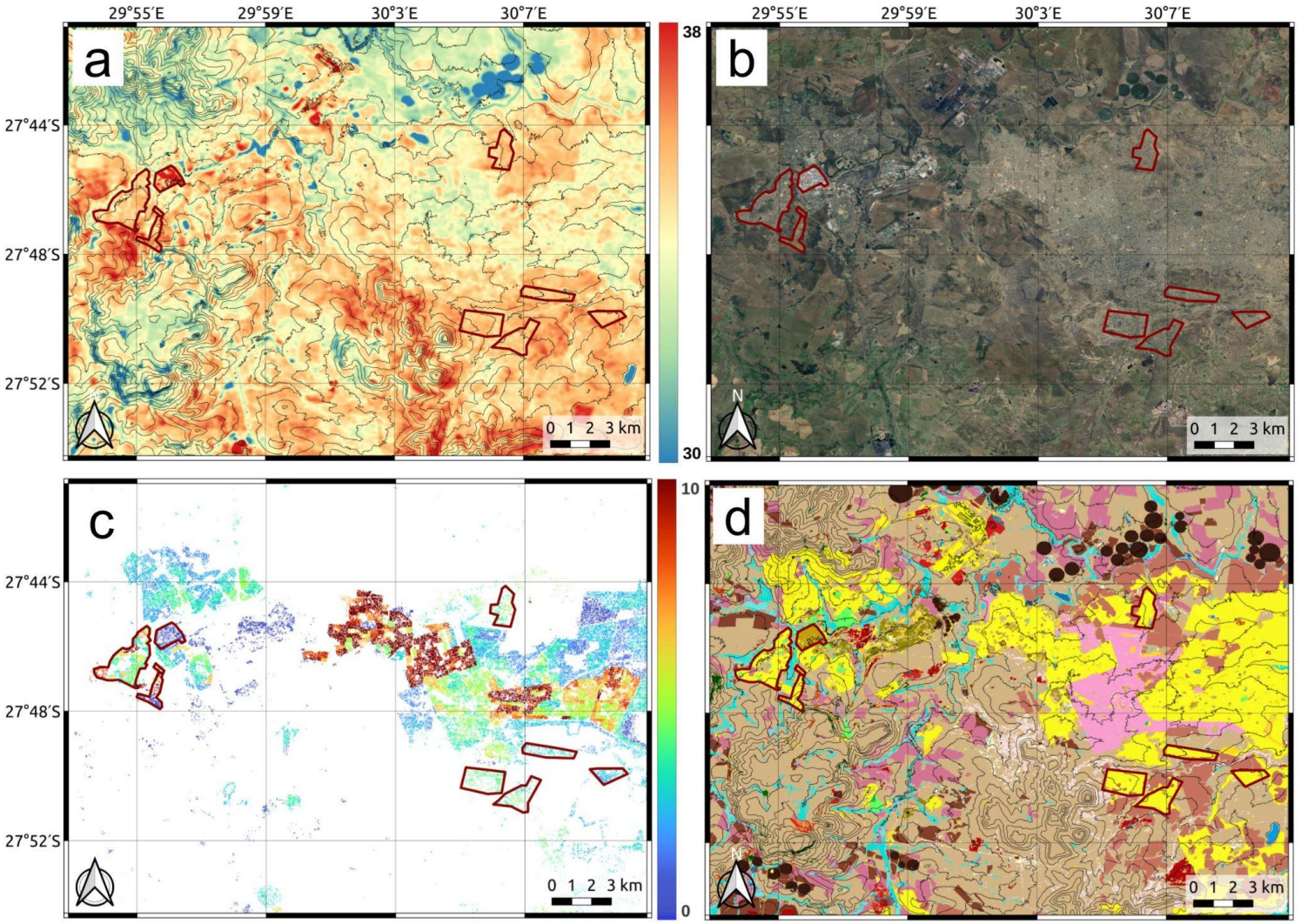

Figure 4.5 Same as Figure 4.2 but for Newcastle.

Table 4.5: Highlights of physical features and LST distribution in Newcastle (Fig 4.5).

Feature	Attributes	Temperature
City Centre	• Located in the western part of the study area. • Commercial area in the centre. • Large industrial areas ~2 km and ~10km east.	• Averages between 36°C and 39°C. • This varies with the reflectivity of roofs. • Reflective buildings drop down to 32°-33°C.
High-income areas	• Moderate to well-forested residential areas surround the commercial centre. • More forested to the north, less forested to the south.	• Temperatures across the residential areas vary little. • Almost all of the areas are around 33-34°C. • Some small sections of more forested areas north of the centre drop down to 32°C. • Some small areas of more open and less-established housing rise up to 35°C (a 3°C difference to more forested sections).
Low-income areas	• Situated ~5 km east of the centre. • Expansive, mostly middle-lower-income residential areas. • Made up of several settlements varying in density and establishment. • A general trend of decreasing density as one moves towards the outskirts of these settlements. • Tree cover across the areas is generally very sparse, but the vegetation and open spaces (mostly grass) between buildings is much greener than in other study areas.	
Non-built-up areas	• Non-built-up areas are mostly grassland and crops (irrigated and rainfed). • The natural grassland and rainfed crops are generally warmer than the residential areas (~35-36°C). • Irrigated crops are considerably cooler (down to below 30°C in centre pivots areas).	
Hot spots	• Commercial and industrial areas; the more spread out residential edges; recently constructed low-cost housing.	

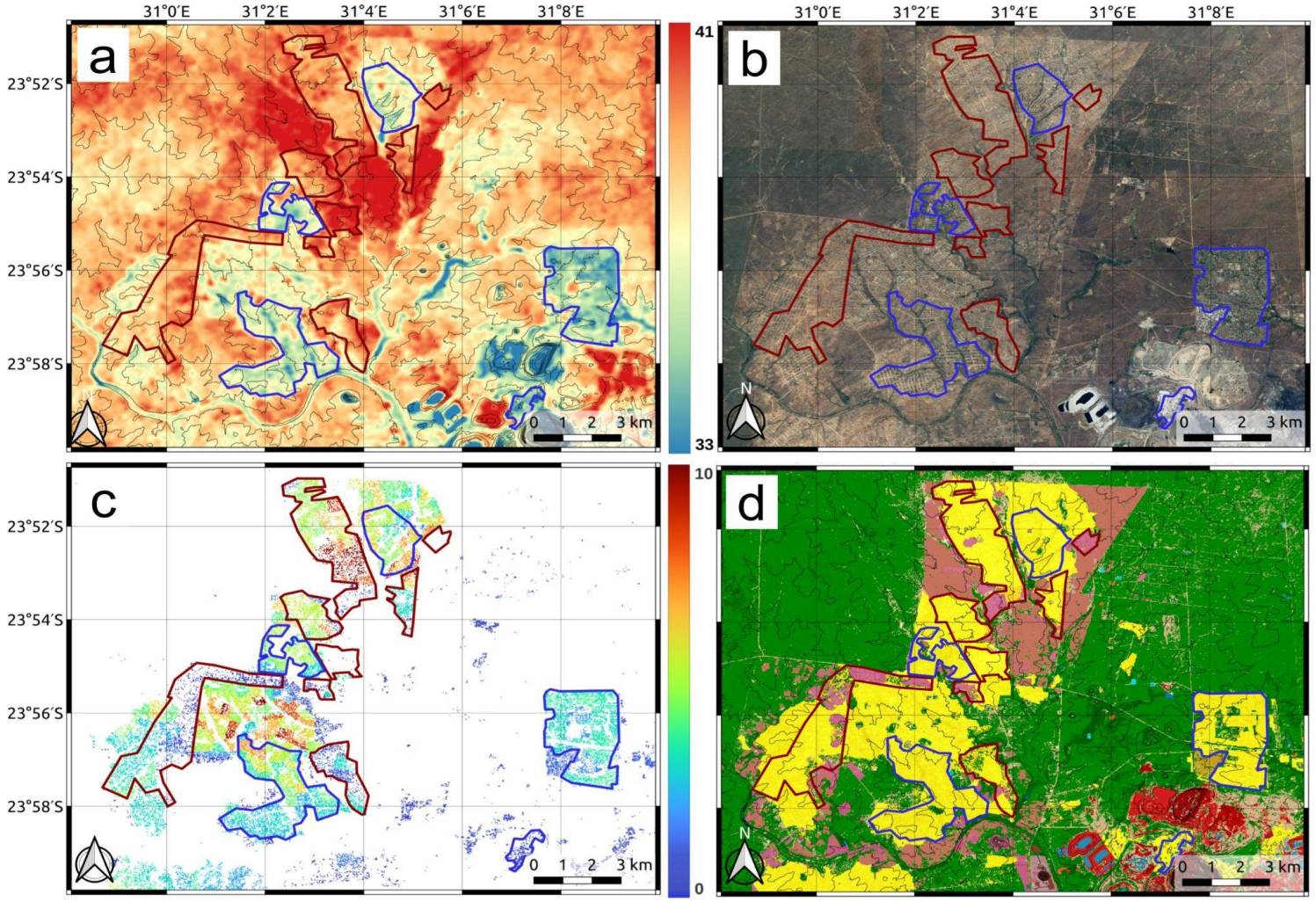

Figure 4.6 Same as Figure 4.2 but for Phalaborwa.

Table 4.6: Highlights of physical features and LST distribution in Phalaborwa (Fig 4.6).

Location	Features	Temperature
City Centre	• Located to the eastern half of the study area. • Consists of mostly commercial activity.	• Generally has temperatures around 36°C. • Darker surfaced areas of this reach up to 38°C.
High-income areas	• Medium density and well-forested residential areas surround the commercial centre. • They are interspersed with some recreational and open land.	• Temperatures of ~33-35°C in residential areas. • Recreational land and open areas warm up to 36°C and 39°C respectively.
Low-middle income areas	• To the western side of the study area. • Consists of Lulekani (far north), Ben (central) and Namakgale (south). • These all follow similar settlement patterns. • Denser central areas congregated around rivers and streams. These are fairly well-forested and more established. • Moving outwards in each settlement, there is a general trend of more scattered trees and housing, more open land between houses and less established infrastructure.	• The temperatures in the settlements are closely related to the layout. • Denser areas nearer to the rivers and streams have lower temperatures (34-36°C). • The less forested, dispersed outskirts are generally far warmer (~40°C), particularly those with more exposed soils (up to 41°C). • Aspect also plays a role in Lulekani. The east facing section is ~2°C warmer than the adjacent, flatter section.
Non-built-up areas	• Dominated by savanna (~38°C). • Significant areas of non-irrigated cropland and grazed grassland around the edges of the settlements (over 40°C and reaching up to 42°C). • South-Eastern mining area with hot (~42°C) and cold (~30°C) extremes (bare ground vs water).	
Hot spots	• Outskirts of all the more western settlements; exposed areas of the mining operation ; croplands and grazed grasslands.	
Cool spots	• Forested sections of Phalaborwa town and of the western settlements, particularly nearer the rivers.	

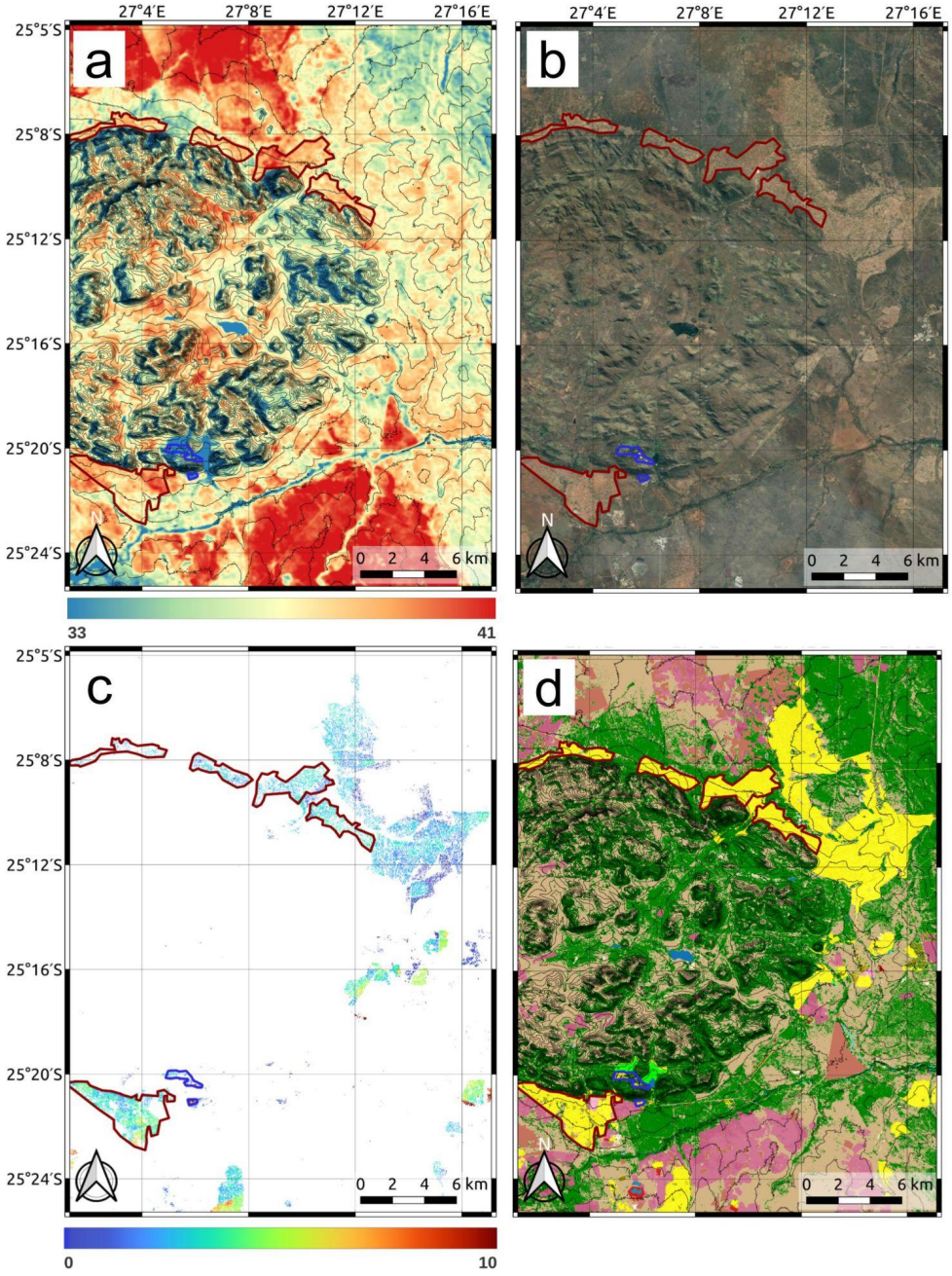

Figure 4.7 Same as Figure 4.2 but for Pilanesberg.

Table 4.7: Highlights of physical features and LST distribution in Pilanesberg (Fig 4.7).

Location	Features	Temperature
City centre	• There is no clear centre.	
High-income areas	• The Sun city resort (in the southern section of the crater) and the residential area just south of it. • These are heavily forested and well irrigated.	• The resort averages ~30°C • The more built-up parts of it are ~31-33°C. • The residential area to the south averages ~32-33°C
Low-middle income areas	• Make up most of the populated area. • Consist of a number of isolated settlements along the borders of the Pilanesberg national park. • The biggest settlements are to the south (Ledig), east (Mogwase) and north (Saulspoort). • These have predominantly low to medium density housing, interspersed with bare ground, grassland and some trees. • Trees are fairly consistent across the settlements, being low in density, but present in some form.	• Temperatures are similar across most of the settlements, averaging between 36°C and 39°C. • The eastern settlements are in the lower part of this range (~36°C). • There is a trend of gradual increase in settlement temperatures as one moves north and south from Mogwase. • These reach a maximum of ~38°C in Ledig and ~39°C in Saulspoort. • Some more spread out sections reach up to 41°C. • Vegetation cover and ground reflectivity impact temperatures.
Non-built-up areas	• Non-built-up land in the east and NE is mostly grassland and savanna averaging ~36-38°C. • Some sections of more vegetated savanna/woodland are cooler (~34°C). • Further south and NW the land is more degraded and fallow fields dominate. These are far hotter, averaging between 40°C and 42°C.	
Hot spots	• Fallow fields and degraded grassland in the south and NW; more scattered settlements in Saulspoort and Ledig.	
Cool spots	• Well-forested Sun city resort and residential areas.	

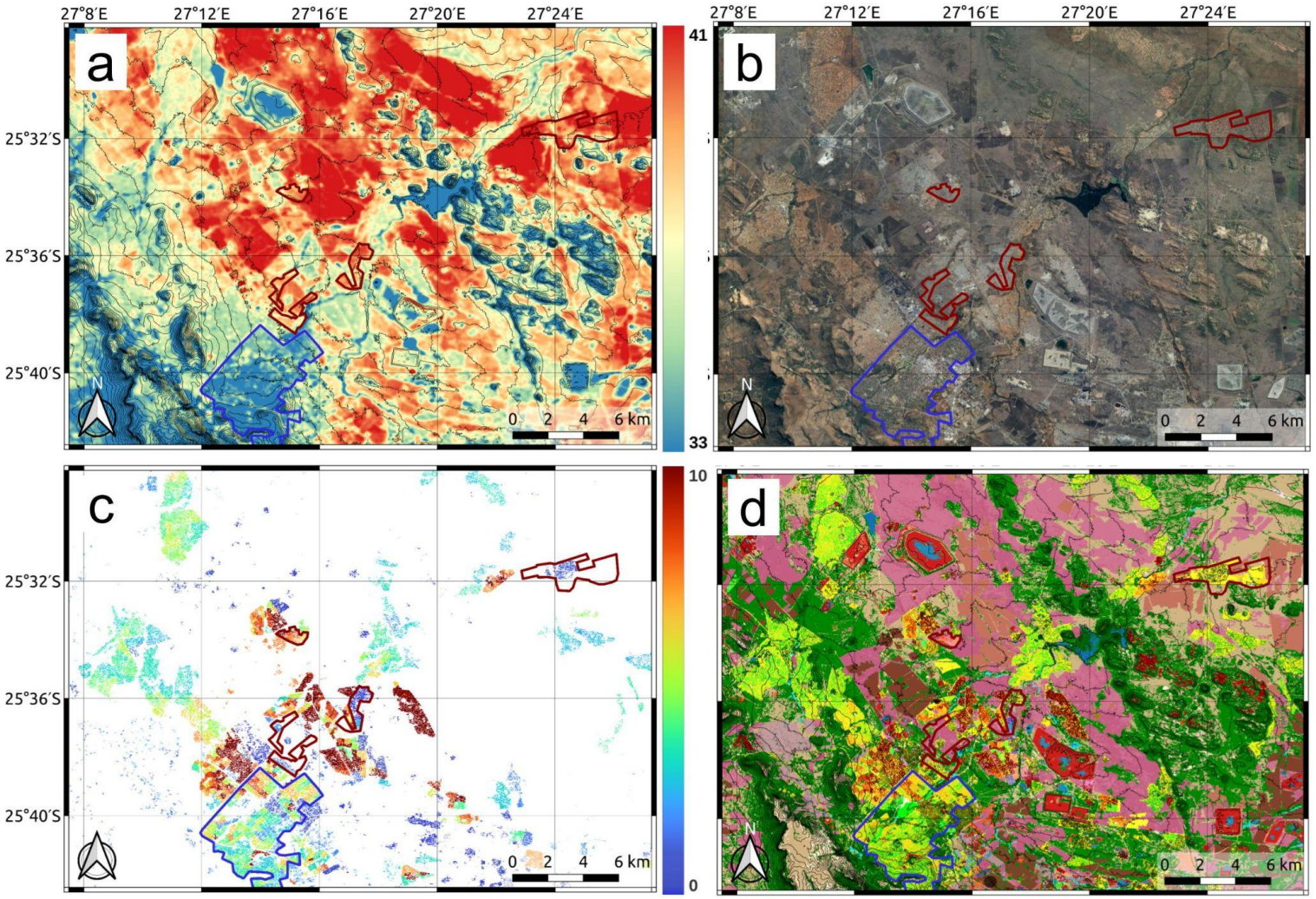

Figure 4.8 Same as Figure 4.2 but for Rustenburg.

Table 4.8: Highlights of physical features and LST distribution in Rustenburg (Fig 4.8).

Location	Features	Temperature
City Centre	• Located in the south of the study area. • Consists of a commercial sector with industrial zones to the north (~3km) and east (~1km).	• Temperatures across these areas vary significantly depending on roof reflectivity (30-37°C).
High-income areas	• Surround the city centre. • Well-forested and fairly dense residential areas. • Interspersed with irrigated recreational grounds.	• Residential areas average around 32°C. • More forested parts are down to 30°C. • More open recreational areas are up to 34°C.
Low-middle income areas	• Mostly middle-income residential areas to the NW. • These are first of higher building density and more formal grid layout (Tlhabane) and then become more spread out further NW (Phokeng). • Tree cover is moderate across these areas. • To the NE are a combination of lower and middle-income residential settlements. • These are interspersed with mining areas and fallow land. • Settlements range from very exposed and relatively spread out informal, to denser, more established informal, and then formally constructed, larger housing. • Tree cover is minimal across the informal areas and scattered in others.	• The denser, more established areas (both formal and informal) are slightly cooler (~35-36°C). • The sparser and less established areas are warmer (38°C and above). • Some of the more recently created informal settlements which are built on degraded, darker bare ground get even hotter (up to 40°C).
Non-built-up areas	• Dominated by grassy fallow land. • Savanna, grassland and rainfed cropland make up most of the remaining area (all ~40-42°C). • Other land covers include irrigated crops (~30°C) and small areas of indigenous forests (27°C- 32°C).	
Hot spots	• The less established informal settlements; fallow land and mining areas.	
Cool spots	• The forested southern settlement; indigenous forests; irrigated crops.	

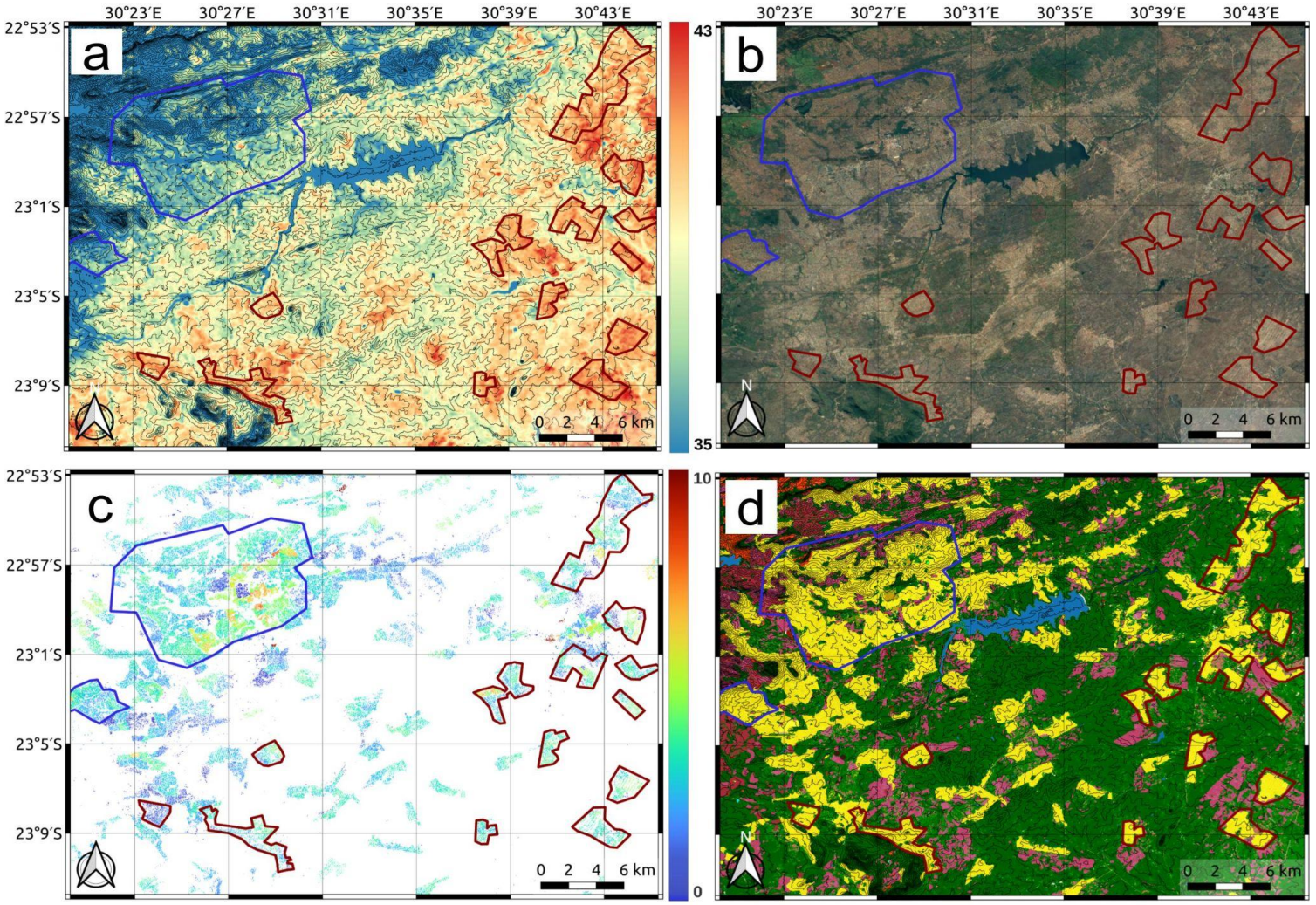

Figure 4.9 Same as Figure 4.2 but for Thohoyandou.

Table 4.9: Highlights of physical features and LST distribution in Thohoyandou (Fig 4.9).

Location	Features	Temperature
City Centre	• Located in the rolling hills to the NW of the study area. • Consists of a small commercial/industrial centre with relatively dark roofs. • Another industrial area is located ~2 km SW of this.	• Commercial / Industrial centre shows warm temperatures (~40°C). • The other industrial area is slightly cooler (~37-38°C).
High-income areas	• Residential areas are spread out around the city centre. • Denser, more vegetated housing in the northern parts of the area. • Less dense, less vegetated housing to the south.	• Lower temperatures in the northern areas, averaging ~35-36°C. • More heavily vegetated sections down to 33°C. • Southern parts average ~37°C.
Low-middle income areas	• Located across the southern and eastern part of the study area. • Consist of numerous isolated settlements. • Major settlements are Xigalo, Malamulele, Jimmy Jones, Phapazela and Ramukhuba. • Settlements are generally of low density and sparse vegetation.	• Temperatures follow a general pattern of increasing value as one moves further south and east. • Most areas average ~38-40°C. • Sparser settlements reach up to 42°C.
Non-built-up areas	• Non-built-up land is predominantly wooded savanna (35-37°C). • There are also large areas of more open savanna (37-39°C), some cropland/savanna mosaic (38-42°C) and some plantation and indigenous forest (27-28°C).	
Hot spots	• Most of the settlements in the southern and eastern parts of the study area ; the commercial/industrial centre.	
Cool spots	• Well-forested residential areas to the north; plantations and forests in the hilly NW.	

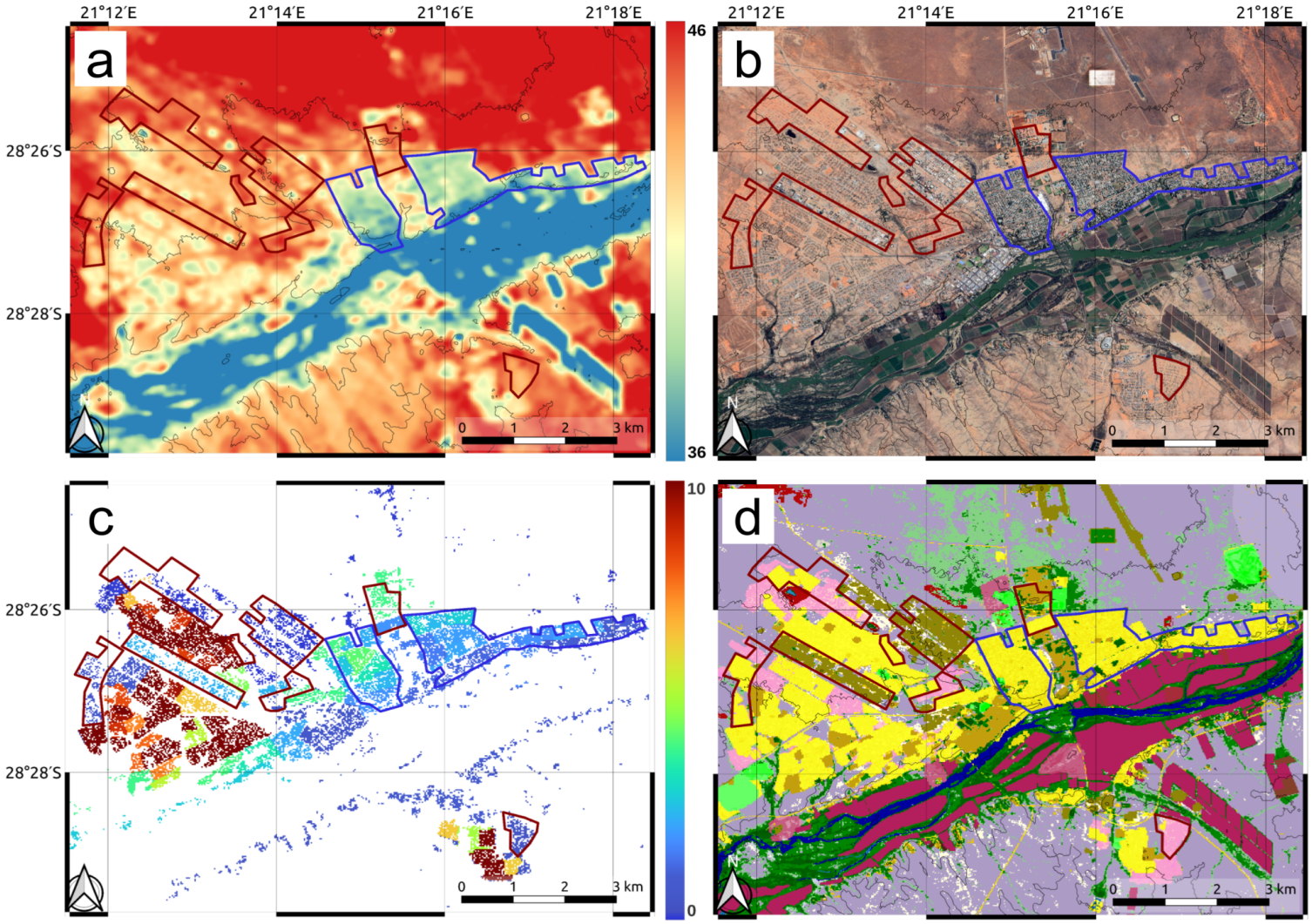

Figure 4.10 Same as Figure 4.2 but for Upington.

Table 4.10: Highlights of physical features and LST distribution in Upington (Fig 4.10).

Location	Features	Temperature
City Centre	• Located In the middle of the study area (against the banks of the Orange river). • Consists of a commercial sector with 2 main industrial areas to the north (~2km) and NW (~2km).	• The commercial centre averages ~41°C. • The two industrial areas average ~43°C. • Roof reflectivity plays a large role here. Reflective white roofs are cooler and darker surfaces warmer.
High-income areas	• Situated to the east of the centre. • Medium density, forested residential areas. • Located on the banks of the river and adjacent irrigated farmland.	• Temperatures are low relative to the surroundings (~36-39°C). • A general trend of closer to the river = cooler, further away = warmer.
Low-middle income areas	• Middle-income housing. to the SW and SE of the river. • Lower-middle-income residential areas to the NW. • These are medium density and sparsely vegetated, but with most houses having some trees. • On the outskirts of these settlements are lower-income, smaller and less established housing with very little vegetation.	• The SW and SE settlements average between 40°C and 42°C, dependent on tree density. • The more established settlements in the NW have similar temperatures. • The less established settlement edges show significantly warmer temperatures, rising to around 44-45°C and even going up to 46°C in parts.
Non-built-up areas	• Non-built-up land is predominantly open shrubland, (low, sparse grass and bare ground interspersed with infrequent small bushes). • This vegetation shows very hot temperatures (~44°C nearer to the Orange river and ~47°C further away). • Adjacent to the Orange river, there are well irrigated croplands where temperatures range between 32°C and 38°C depending on crop type and irrigation.	
Hot spots	• Sparser, less vegetated settlement edges; informal settlements; shrubland away from the Orange river.	
Cool spots	• Well-forested residential areas; croplands and natural vegetation adjacent to the Orange river.	

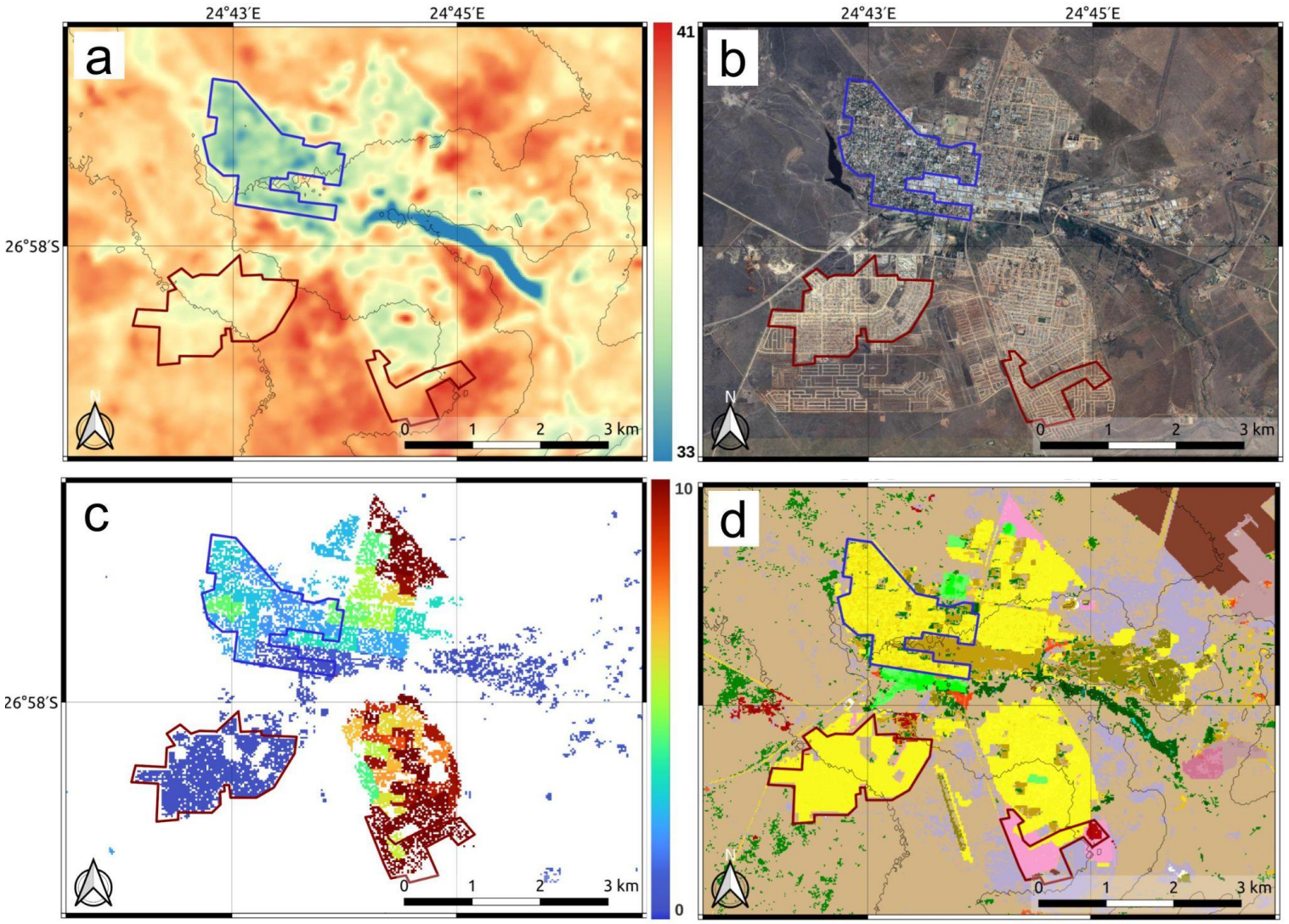

Figure 4.11 Same as Figure 4.2 but for Vryburg.

Table 4.11: Highlights of physical features and LST distribution in Vryburg (Fig 4.11).

Location	Features	Temperature
City Centre	• Located in the middle of the study area. • Commercial centre with an industrial area east-adjacent.	• Temperatures across both areas vary significantly depending on roof reflectivity (33-39°C).
High-income areas	• Fairly dense and well-forested residential area to the NW of the centre.	• Cooler temperatures (33-36°C). • Dependent on tree cover and roof reflectivity.
Low-middle income areas	• Middle-income NE sector. • This has a mix of smaller and larger residential houses and scattered trees. • SW sector with a mix of smaller, lower-income, and larger, middle-income housing and few trees. • SE, more recently constructed residential area with few trees and lots of bare ground between houses.	• The NE and SE areas average ~36-37°C. • The SW settlement is a bit warmer at ~37-38°C. • The newly constructed SE is the hottest (~39°C). • Variation in temperature depends on the density of housing and open spaces.
Non-built-up areas	• The natural vegetation is predominantly grassland, with sections of cropland, open shrubland and savanna between. • These all have warm temperatures, between 37 and 40°C (varies with levels of degradation and reflectivity of the vegetation and ground). • Small areas of river valleys (33-35°C) and centre pivot fields (30-31°C) have far cooler temperatures .	
Hot spots	• Sparser, less vegetated sections of the southern settlements; natural sparse vegetation.	
Cool spots	• Well-forested residential areas.	

4.2 Drivers of disparity in LST within the cities

The disparity in LST within the cities is driven by the cities underlying characteristics. This section explores some of the key drivers that consistently contribute to this disparity.

4.2.1 Built-up versus non-built-up land

In all the selected cities (except Thohoyandou), the LSTs of built-up areas are lower than the surrounding natural vegetation, croplands, and open recreational land. For instance, in Phalaborwa (Fig 4.12), the naturally occurring sparse savanna was about 5°C hotter than the more vegetated housing areas in between. These LST differences are most apparent in drier, more barren, and more degraded areas, with fallow land and non-irrigated croplands and mining areas often measuring at least 5°C higher than the nearby built-up land. The Pilanesberg and Rustenburg study areas also have good examples of this (Fig 4.7 and 4.8). In both areas, the temperature of fallow land and more exposed darker soils is ~42°C, while that of the built-up areas is less than 37°C. The Upington study area (Fig 4.10) also shows extreme differences, with its natural sparse shrubland reaching in excess of 47°C, while most of the built-up areas measure around 40°C, and even go down to 36°C in parts. Thohoyandou is the only area where this is not the case (Fig 4.9). The natural vegetation here is greener and more abundant, while the built-up areas are generally less vegetated and have more exposed soils and grass between housing, particularly in the southern sections of the study area. This results in built-up areas here being slightly warmer than non-built-up areas (by ~1-2℃).

The consistently cooler built-up areas found in this research are the reverse of the urban heat island reported in most studies (e.g., Stathopoulou & Cartalis., 2007; Keeratikasikorn & Bonafoni., 2018; Zhang & Sun., 2019). There are, however, a few examples of similar results under specific conditions (e.g., Rasul et al., 2015; Alahmad et al., 2020). The reversal can be explained by the climate and vegetation of the study areas, as well as the time of day of the image capture. The hot and relatively arid nature of the study areas means green vegetation is limited naturally, but can thrive in cities where it is brought in and irrigated. This is in contrast to most temperate cities where trees are naturally abundant and are generally removed to make space for urban areas. The late morning (~10 AM) capture time of the imagery can also contribute, with man-made surfaces having higher heat capacities than the surrounding land, and therefore taking longer to warm up, giving them lower temperatures earlier in the day.

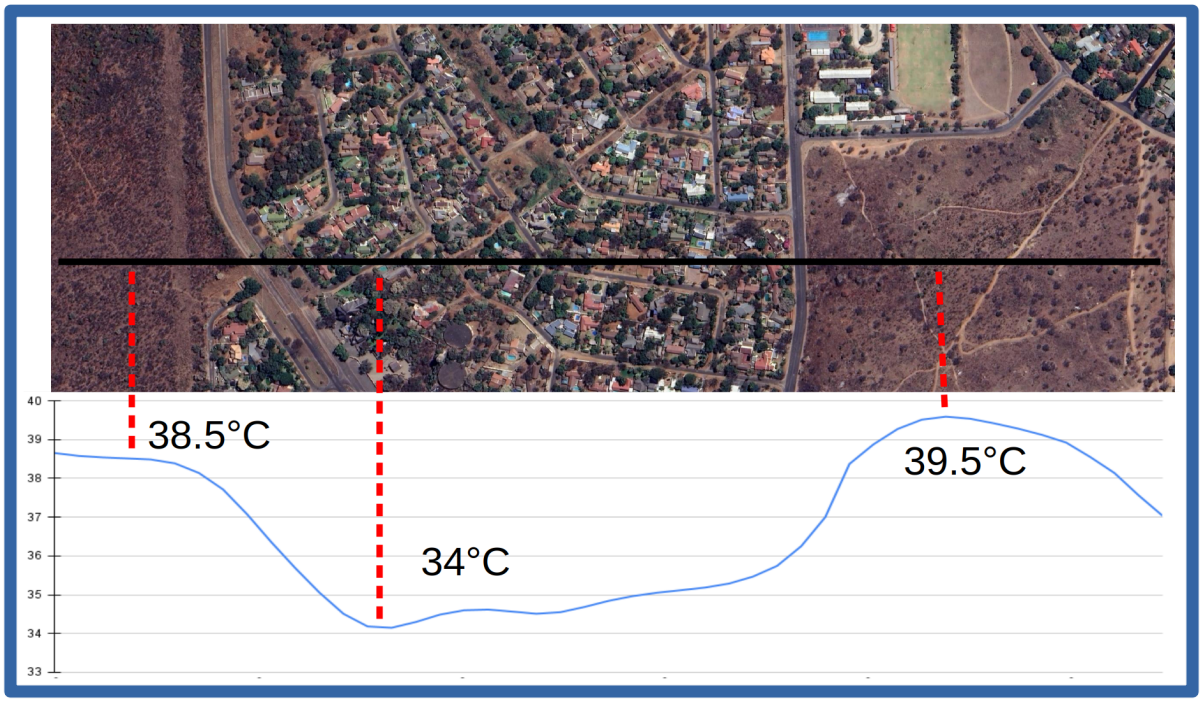

Figure 4.12 Cross section of LST in an area of Phalaborwa city, highlighting the difference in temperature between the natural vegetation and the built-up area.

4.2.2 Sparsely versus densely constructed settlements

All of the cities show examples of large temperature differences between settlements which are sparsely constructed versus those which are densely constructed. Denser settlements, which are dominated by man-made materials in these examples, tend to be cooler than sparser settlements, which have large sections of open or bare land between houses. This is most apparent where the natural vegetation is less dense and less green, and more barren land occurs (i.e., the more space between houses, the more barren, hot land there is in the urban area). In Rustenburg (Fig 4.13), two settlements that have similarly low tree cover also have significant differences in temperature. The temperature of the more densely constructed area is ~35.5°C, while the temperature of the more sparsely constructed areas is ~38.5°C. Similar examples can be seen in the other study areas. Upington (40°C vs 45°C; Fig 4.10), Phalaborwa (36°C vs 40°C; Fig 4.2), Vryburg (35°C vs 39°C; Fig 4.11) and Mokopane (36°C vs 39°C; Fig 4.4) all show this particularly strongly. These results imply that the man-made building materials are actually cooler than the surrounding land cover at this time of day.

While these results are again in contrast to most literature (e.g., Estoque et al., 2017; Nurwanda & Honjo, 2018), the characteristics of the surfaces and the image capture time can

explain this. The denser settlements consist of predominantly man-made surfaces. These have higher heat capacities than the bare ground and low vegetation found in the sparser settlements, and they also tend to have greater reflectance or albedo. This means there is generally a slower warming of surfaces in these denser areas (i.e., man-made surfaces retain their cooler night-time temperatures for longer), and there is also an increased amount of energy being reflected.

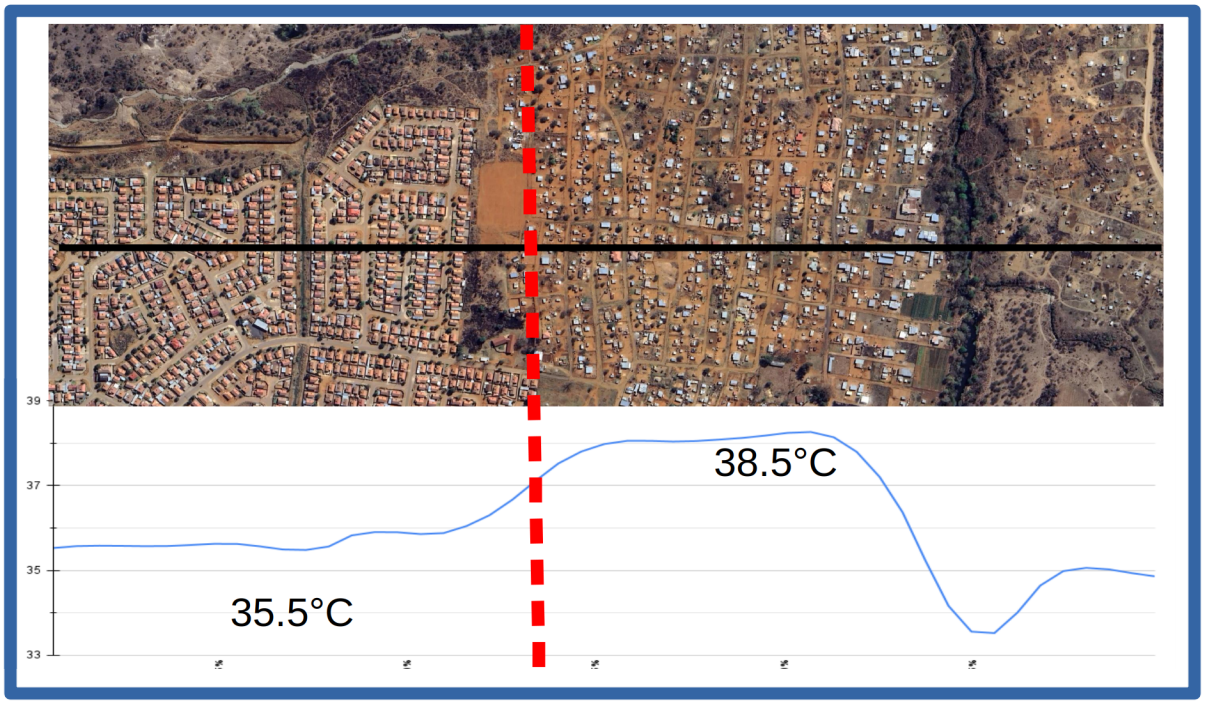

Figure 4.13 Cross section of LST in a section of the Rustenburg study area, highlighting the differences in temperature between densely constructed and sparsely constructed settlements.

4.2.3 Vegetation characteristics within cities.

The vegetation patterns in all study areas (except Newcastle) vary greatly from one part of the area to the next. For example, Kuruman, Thohoyandou and Upington all show large differences (~8-9°C) between the coolest and hottest residential areas, with the example from Kuruman in Figure 4.14 illustrating how these temperatures can differ dramatically over very short distances. This variation generally follows socio-economic patterns, with higher-income, well-established areas having a higher density and coverage of trees, while lower-income areas have fewer trees and more barren land with sparse vegetation. The temperatures follow this pattern very closely, with the most forested parts being on average at

least 5°C cooler than the least forested. Pilanesberg and Rustenburg again show the largest differences here, with the higher-income, well-forested sections being as low as 30°C, while informal settlements constructed on barren, degraded land with little to no vegetation rise up over 40°C. In Upington, this change is closely tied to proximity to the Orange river. Wealthier, forested parts (with temperatures as low as 36°C) are located very close to its banks and have ample water to irrigate and support tree growth, while areas further away from the river (up to 45°C) are far less vegetated, suggesting less access to irrigation.

These results are very similar to those reported in the numerous studies that investigated the cooling effect of trees (e.g., Santamouris et al., 2017; Krayenhoff et al., 2021) and the large differences between more vegetated and less vegetated areas of cities (e.g., Jonsson., 2004). Studies like Barrera et al. (2019) and Venter et al. (2020) have also shown strong links between these vegetation differences and socio-economic factors.

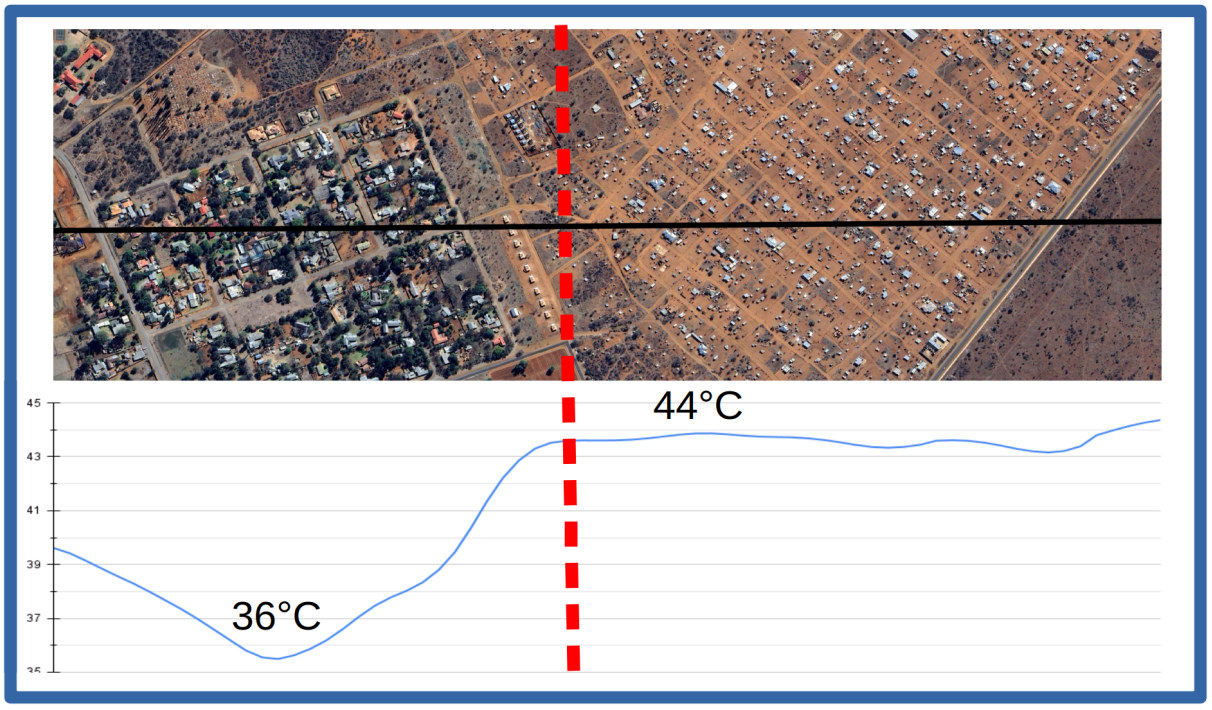

Figure 4.14 Cross section of LST in a section of the Kuruman study area, highlighting the temperature differences between settlements with extensive tree cover and those with very little tree cover.

4.2.4 Reflectivity of roofs

This driver is most apparent in larger industrial and commercial areas and in residential areas with dense housing. Buildings or areas with highly reflective roofs can have LSTs as much as

10°C cooler than those with darker, absorbent roofs. For instance, in Bloemfontein (Fig 4.15), the reflective white roofs can have LSTs as low as 29°C, while the LSTs of the dark metallic roofs, such as that of the transnet industrial area, rise up to over 40°C. This significant variation in roof temperatures can be observed in most of our study areas, particularly in the areas with larger industrial and commercial zones and their associated large buildings. This is related to the surface area of the roofs, with smaller buildings not having sufficient roof area to produce a thermal signal that can be detected by the satellite sensor. The exception to this is in very dense residential areas with relatively uniform roof characteristics (i.e., together they act as one large roof).

Results similar to these have been noted in numerous studies (e.g. Simpson & McPherson, 1997; Synnefa et al., 2006; Mohammed et al., 2021), providing strong evidence to support albedo-related cooling strategies.

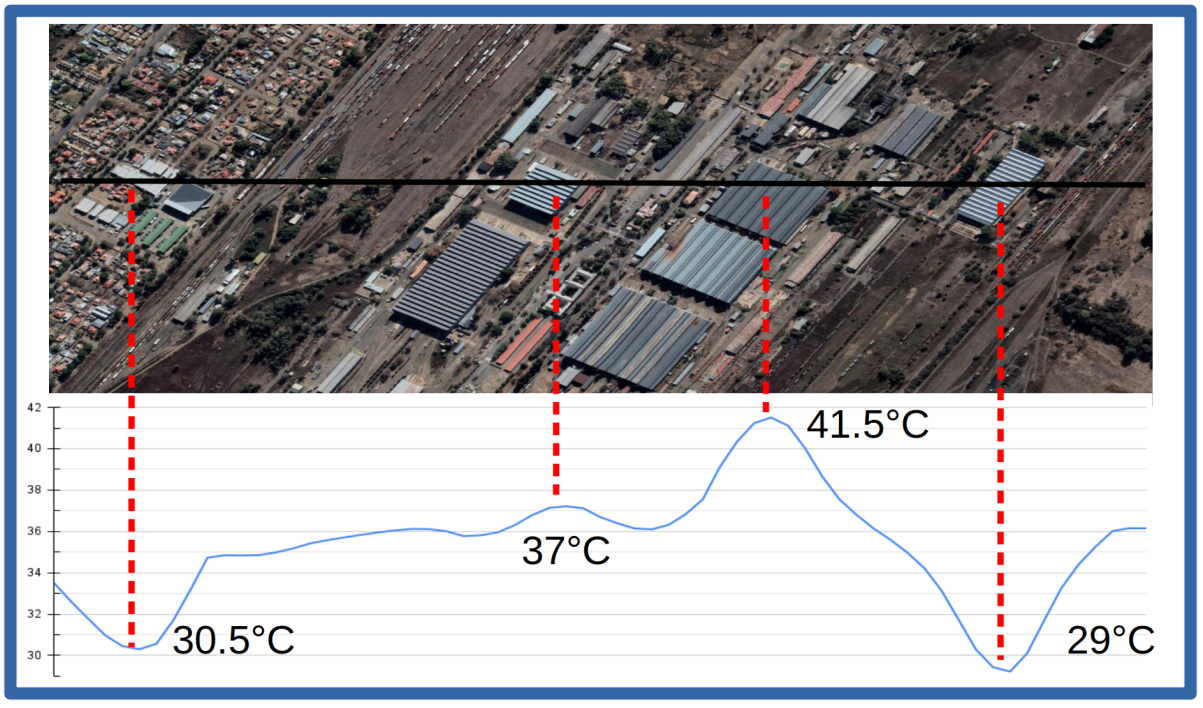

Figure 4.15 Cross section of LST in a section of the Bloemfontein study area, highlighting the difference in temperature between reflective roofs and darker, more absorbent roofs.

The aforementioned drivers, either individually or in combination, provide the foundation for explaining the occurrence of hot spots in the cities. In general, the results suggest that the greater the area of natural vegetation within the urban area, the hotter the city will be. This is

because the natural sparse vegetation is hotter than the other parts of the urban areas (***built-up versus non-built-up land)***. This also agrees with the results of the ***Sparsely versus densely constructed settlements*** section. Sparse settlements tend to have more natural vegetation within them and are therefore hotter than dense settlements.

Another aspect of this is that often where the housing is denser, the imported tree cover present is also denser. This is mostly due to the planting of trees in streets and gardens (***vegetation characteristics within cities***). In dense settlements, the combination of many garden and street trees close together results in significant overall tree cover, benefitting both those who have their own trees and those who do not. In more spread out areas, even if an individual house has significant tree cover, it does not benefit the surrounding houses. In the settlements that do not have extensive tree cover, the density can also impact the variations in roof-reflectivity-related temperatures. Dense settlement areas with reflective roofs will show far stronger thermal signals than more spread out settlements with the same roofs ***(Reflectivity of roofs).***

4.3 Hot spots and cool spots

This section summarises the specific urban hot and cool spots and directly identifies what causes their formation (Table 4.12). Although each settlement may differ slightly, these spots and factors consistently appear, either individually or in combination.

Table 4.12 Summary of urban hot spots and their causes.

Hot Spots	**Cause of heat:**	**Circumstances:**
● Informal settlements ● Houses on settlement edges ● Spread out houses ● RDP housing ● Industrial/Commercial areas ● Non-irrigated cropland	● Bare ground ● Few trees ● Lots of hot natural vegetation ● Dark roofs ● Limited moisture	● Socioeconomic (poor) ● Recently constructed ● Bad planning ● Coincidence

Starting with informal settlements as an example. These almost always have very few to no trees, they tend to have lots of bare land and exposed ground around houses, and natural hot vegetation dominates any open space. The circumstances for these land cover characteristics are almost always socio-economic (e.g., limited resources to plant trees and gardens; forced

to live in undesirable, exposed locations), but often combine with being more recently constructed. Informal settlements are often of the newer settlement types and as such can have more exposed soils from recent construction activities, more natural vegetation from being less developed, and less tree cover because of the time needed to establish larger trees. This same circumstance can also be true for other hot spots. Settlement edges tend to be where settlements expand from and where newer growth occurs, and RDP housing tends to be a more recent growth mechanism. What RDP housing can also illustrate though, is bad planning. Many RDP developments do not appear to have considered climate variables. Housing is often constructed in very exposed areas, reflective roof materials are not always used, and houses are often constructed too close together to plant trees between (Venter et al., 2020). Some industrial and commercial areas also demonstrate this poor planning, with very dark and absorbent roofing materials being used, resulting in far hotter temperatures than surrounding more reflective roofs.

Table 4.13 Summary of urban cool spots and their causes.

Cool Spots:	**Cause of coolness:**	**Circumstances:**
● Industrial/Commercial buildings ● Residential areas ● Recreational grounds ● Irrigated cropland	● Extensive tree cover ● Moisture ● Reflective roofs ● Proximity to water source	● Socioeconomic (wealthy) ● Well established ● Good planning ● Coincidence

Cool spots, as one would expect, tend to result from the reverse of what hot spots do. Industrial and commercial cool spots occur where roofs are very reflective, either through good planning or coincidence. Residential cool spots are normally a result of extensive tree cover and associated moisture, but can also result from proximity to features like rivers and dams. This itself is often a factor of socio-economic circumstance (resources to grow trees, ability to choose desirable places to live), establishment (older areas with a long history of greening), and good planning to go along with these. The other cool spots, recreational ground and irrigated croplands, generally appear because of their high moisture content and the subsequent cooling they experience through evaporation. In dry climates like our study areas, the level of moisture is often a function of socio-economics, with wealthier populations able to assign more resources to irrigation.

4.4 Summary and limitations

This chapter has analysed the spatial distribution of LSTs within 10 selected cities in South Africa, compared it with the associated physical features, and identified the causes of, and circumstances surrounding, hot spots and cool spots in the cities. The results of this section can be summarised as follows:

- The spatial variations of LSTs in urban areas are strongly influenced by the underlying land cover.
- The relatively arid nature of the study areas and the limited naturally occurring green vegetation leads to most urban areas being more vegetated, and subsequently cooler, than their natural surroundings during the day.
- Recently constructed settlements, particularly informal settlements, experience the hottest LSTs of urban areas, while older and more established settlements tend to be cooler.
- The locations of LST hot spots in the cities are closely linked to socio-economic factors, with poorer populations experiencing higher LSTs because of their living situations.

The use of Landsat thermal imagery to identify surface temperature distributions has been shown to be very effective. It is good at recognising the heterogeneous nature of settlement temperatures and is very helpful in identifying areas most susceptible to hot temperatures. However, the applications of the imagery are limited, and the robustness of the results can be improved in many ways.

The images used, as well as all other daytime images of the areas, are captured between 09:54 AM and 10:28 AM, depending on the study area. Meanwhile, the hottest surface temperatures occur between 12 PM and 1 PM. This means that the Landsat temperatures are not necessarily a true reflection of LST distribution or values during the time we are most interested in. Images are also only taken every 16 days, and their accuracy is sensitive to cloud cover. This often means that specific hot events are very difficult to study as one is limited to the available clear weather days.

Another limitation is when it comes to understanding heat distribution in relation to people. Surface temperature is only a true reflection of the temperature at the surface, and not the traditional air temperature or near-surface temperature, which is often a more crucial, or at least more used, factor when considering human health (Ho et al., 2016). Some of these limitations are addressed in the next chapter (Chapter 5), which reports the results of the Weather Research and Forecasting (WRF) simulations over the cities.

Chapter 5: Simulating the Influence of Land Cover Changes on Temperature Hot spots in South African cities

This chapter presents the findings of the model simulation part of the study. It first evaluates how well the WRF model simulates land surface temperatures and air temperatures (Section 5.1). Then it examines the sensitivity of these variables to increased tree cover and whitening of building rooftops (Section 5.2). It finishes by discussing the limitations of the WRF study (Section 5.3).

5.1 Evaluation of WRF simulations

This section evaluates the performance of WRF in simulating temperature over the cities by comparing the WRF simulations in two control experiments (WRF_MODIS and WRF_SANLC) with available observation datasets. The evaluation focuses on two temperature metrics: land surface temperature (LST) and 2m air temperature. The simulated LSTs are compared with Landsat observations, while the simulated air temperatures are compared with available meteorological station observations.

5.1.1 Land surface temperature

Figure 5.1 shows the comparison of the WRF simulated land surface data (WRF_MODIS and WRF_SANLC) with the equivalent Landsat observations. Figure 5.2 spatially represents the bias between these simulated and observed distributions, and Table A.1 (appendix) provides details of the findings from these Figures 5.1 and 5.2. The statistics of the model performance over the study domains is summarised in Table 5.1.

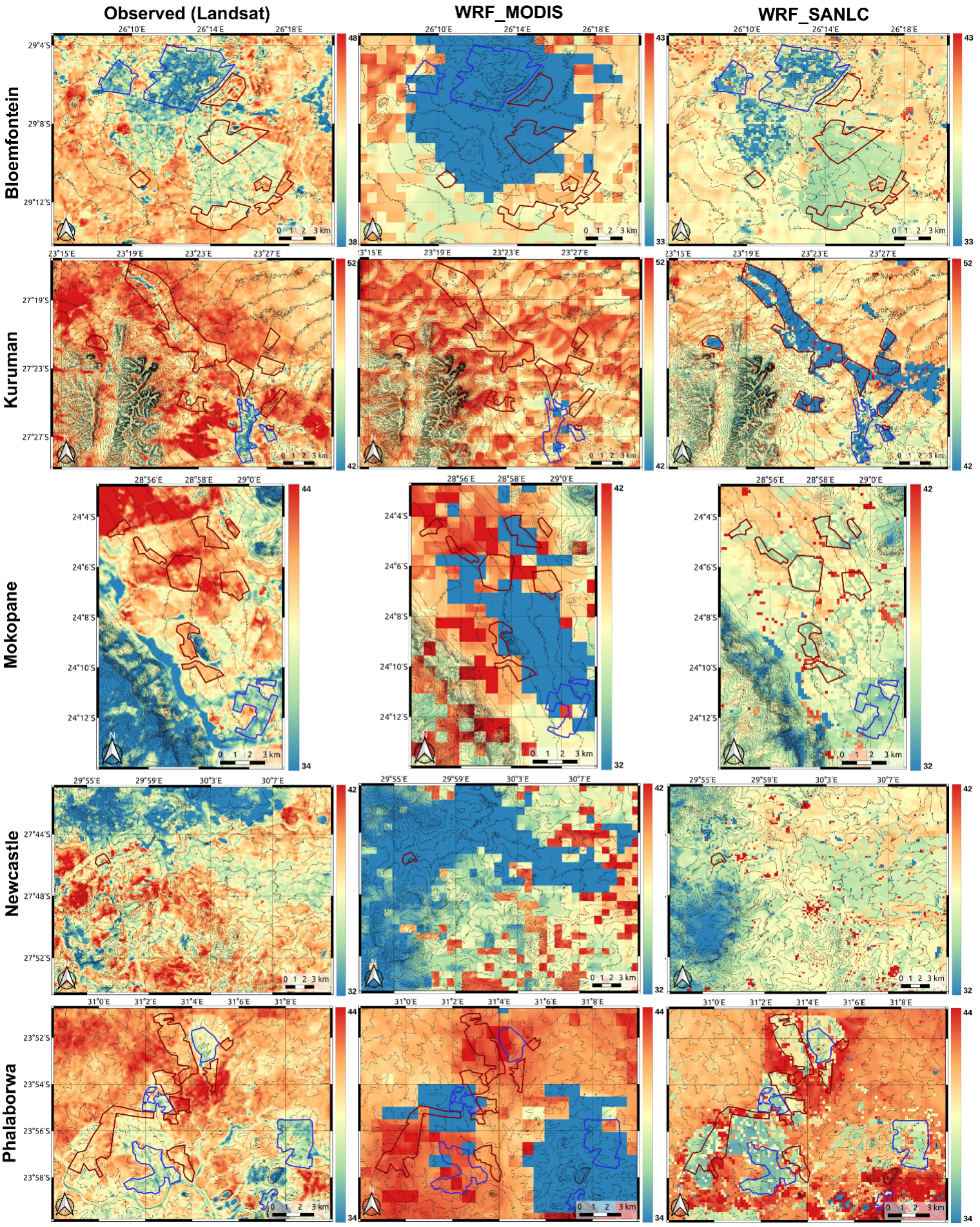

Figure 5.1 LST at 10 AM over the study areas (i) Observed Landsat thermal image, (ii) WRF_MODIS scenario, and (iii) WRF_SANLC scenario. Note that the temperature scales in Bloemfontein and Mokopane differ between Landsat and WRF images in order to better highlight spatial differences.

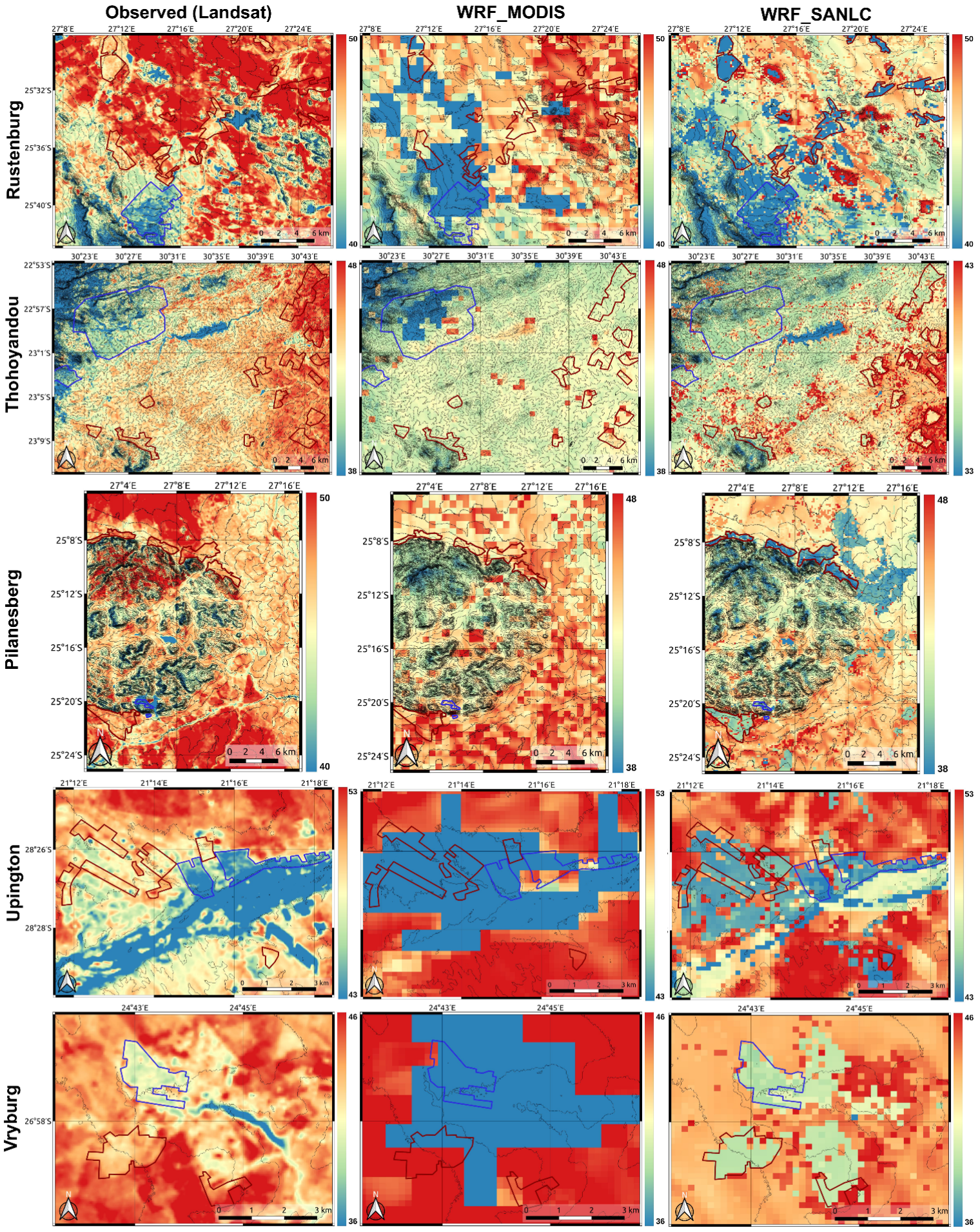

Figure 5.1 continued. Note that the temperature scales in Pilanesberg and Thohoyandou differ between Landsat and WRF images in order to better highlight spatial differences.

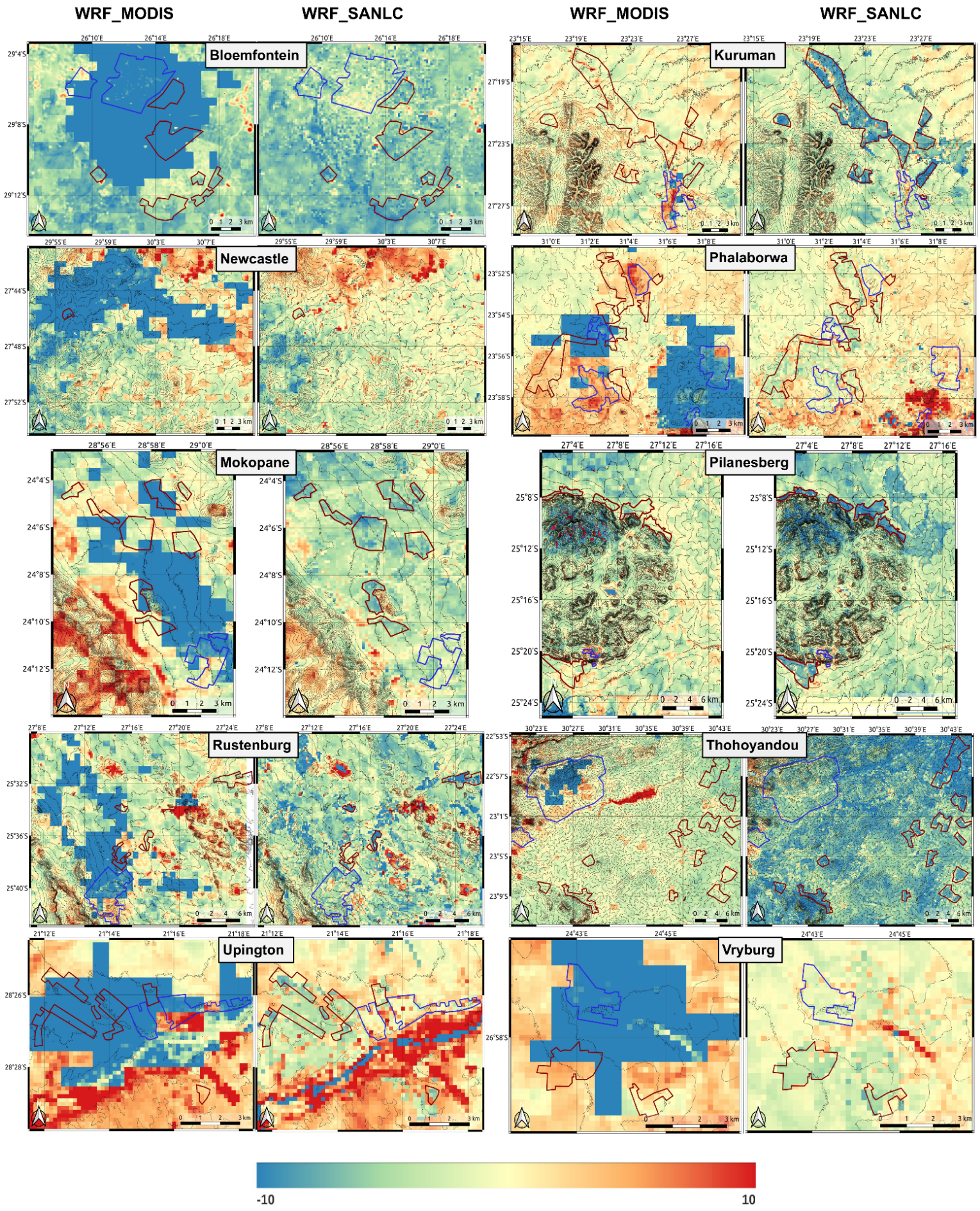

Figure 5.2 Biases (in °C) in the simulated LSTs from WRF_MODIS and WRF_SANLC.

Table 5.1 Statistics of the performance evaluation of simulated LST in WRF_MODIS and WRF_SANLC simulations. Cases where WRF_MODIS performs better than WRF_SANLC are indicated in red.

City	Absolute Error (ºC)		RMSE (ºC)		Correlation	
	WRF_MODIS	WRF_SANLC	WRF_MODIS	WRF_SANLC	WRF_MODIS	WRF_SANLC
Bloemfontein	-10.07	-5.53	11.92	6.78	0.31	0.23
Kuruman	-0.02	-2.57	2.37	3.96	0.23	0.22
Mokopane	-2.33	-2.49	7.12	4.05	-0.11	0.45
Newcastle	-4.50	-1.09	7.74	3.49	0.28	0.07
Phalaborwa	-1.88	0.36	6.11	2.81	0.27	0.28
Pilanesberg	-2.27	-3.61	3.61	4.63	0.29	0.32
Rustenburg	-2.94	-3.26	6.57	5.43	0.25	0.43
Thohoyandou	-1.99	-6.62	3.71	7.22	0.33	0.54
Upington	-4.04	1.62	10.61	6.78	0.23	0.42
Vryburg	-5.88	-0.86	9.96	2.51	0.33	0.44

In general, both WRF simulations show some skill in representing the observed LSTs. Large scale patterns of LST are fairly well identified. These include patterns such as warmer rural versus cooler urban; cooling with increased elevation and topographic shading; and cooling with increase in vegetation greenness. What this study is more interested in though, is how the updated landcover dataset impacts the skills of the simulations, particularly at a smaller scale and in the urban areas.

As was seen in the Landsat thermal imagery, the LST distributions (Fig 5.1) simulated by the WRF model are, for the most part, strongly related to the underlying land cover. This relationship is consistently observed across all the study areas, with changes in LST patterns closely mirroring those of the land cover changes (i.e., changes from WRF_MODIS to WRF_SANLC).

In the WRF_MODIS simulations this tends to result in the spatial patterns of temperature being very simplified, and in some cases very under or over-represented. Urban areas are good examples of this. In Phalaborwa, the simulated spatial extent of the urban temperatures to the east is more than 3 times their actual spatial extent, while in the settlements further west, the urban temperatures are very under-represented, with less than one-third of the area simulated as urban. While on average, the size of the total urban area is approximately correct, the distribution is very skewed and not representative when studying city-scale temperature. Most of the other study areas show similar urban simplification/skewing patterns to this. However, some of the more dispersed study areas show a different pattern, that of a very strong under-representation of urban areas. In Kuruman, Pilanesberg, and Thohoyandou, almost none of the urban areas are actually identified as such. These areas are instead treated as natural vegetation, and their temperatures reflect this. What the results have shown though, is that this is not necessarily a negative (as discussed later in this section).

Biases

Where urban areas are identified, the WRF_MODIS simulations consistently pick up the observed trend of cooler urban versus rural LST values, but also consistently overestimate these differences by large margins (i.e., show much cooler urban values than observed). For most of the cities this is by at least 10℃ in the cooler urban areas, and up to almost 20℃ in the warmer urban areas (Fig 5.2). In study domains where urban areas dominate, this can result in, or contribute to, a strong overall cool bias, evidenced by the fact that all 10 of the

study areas show negative Absolute Errors (Table 5.1). Of these, Bloemfontein (-10.07°C) and Vryburg (-5.88°C) show the strongest bias, with urban areas taking up much of their domains.

These cool biases also occur in the WRF_SANLC simulations, with 8 of the 10 study areas (not Phalaborwa and Upington) experiencing them. Again, these can be partly explained by underestimations of urban temperatures. This underestimation is most apparent in the more spread out and less established, and most importantly, warmer, urban areas. LST values range from 5°C to 10°C cooler than observed in the warmer urban parts of Kuruman, Thohoyandou, Pilanesberg and Rustenburg. While these underestimations are less severe than in the WRF_MODIS urban areas, the fact that more urban areas are actually identified in certain WRF_ SANLC study areas, means that this urban underestimation can contribute even more to overall cool biases (as seen in the absolute error values of Kuruman, Pilanesberg and Thohoyandou).

Outside of the urban areas, the simulations generated by both WRF_MODIS and WRF_SANLC become more similar to each other and to the observed values. In these areas, deviations between simulated and observed values typically lie below 3°C (Fig 5.2), with some exceptions rising up to and over 5°C. The most notable exception is in Thohoyandou, where the conversion of the SANLC2020 dataset has classified the dominant vegetation as forest, while it would likely be more accurately classified as savanna or woody savanna, as it is in the MODIS dataset. Combined with the cool bias that occurs from the underestimated urban temperatures, this leads to an overall 6.62°C cool bias across the Thohoyandou area. Less prominent examples of these differences in land cover classification are observed in Kuruman, Pilanesberg and Rustenburg, where WRF_MODIS has slightly lower cool bias, and in Vryburg, where WRF_SANLC has more comparable values to observed. In Bloemfontein, the cool bias is fairly consistent between the WRF_SANLC and WRF_MODIS simulations, indicating that either both land covers could be improved, or that the model/input data underestimate temperatures on the day..

Simulations of small-scale features

On a smaller scale, the WRF_MODIS and WRF_SANLC simulations show very different abilities in representing the thermal properties of features like rivers, dams, croplands and mining areas. The lower-resolution WRF_MODIS generally fails to identify any of these,

with notable examples being the large dams in Mokopane, Pilanesberg and Thohoyandou. The WRF_SANLC simulations show far greater skill in identifying these types of features, and in some cases do so with accurate values (e.g., most large dams), but can also skew the size of the features or assign values not representative of the features. The mining area in the SE corner of Phalaborwa (Fig 5.1) is a good example of this. Here the SANLC_converted dataset assigns most of the area as bare ground, leading to hot simulated temperatures, while in reality there is a complex mix of land cover, leading to patches of both very hot and very cold temperatures. Other complex features like crops, where irrigated parts emit very cold LSTs and non-irrigated, more bare parts, emit very hot LSTs, can also be mis-represented.

The smaller scale difference between the two simulation types is also evident in how they represent urban areas. WRF_MODIS generally assigns a single LST value across the whole urban landscape, missing the large variations which can occur. WRF_SANLC on the other hand does show some skill in identifying these differences. This is particularly evident in Bloemfontein, Phalaborwa and Upington (Fig 5.1), where the observed cooler and warmer urban sections are fairly well identified, although similar examples can be found in all the study areas. The differences the model does simulate are, however, not always spatially accurate, and also tend to be less substantial than in the observed LSTs. Modelled differences between cooler and warmer urban areas typically reach a maximum of 4-5℃, while observed values can often exceed 5℃ and even reach up to 10℃.

Performance comparison of WRF*_MODIS and* WRF*_SANLC simulations*

When analysing the domain wide statistics of the two simulation types (Table 5.1), it is found that WRF_SANLC generally demonstrates better results than the WRF_MODIS simulations, although not always to the extent expected considering its visual similarities to the observed LSTs.

RMSE values are better for WRF_SANLC simulations in 7 of the 10 study areas, and overall average 4.8ºC versus the 7ºC of WRF_MODIS. The study areas which show worse RMSE values are Kuruman, Pilanesberg, and most significantly, Thohoyandou. These exceptions can be partly explained by the WRF model's general underestimation of temperatures in warmer urban areas (which are generally the more spread out and open urban areas). The SANLC land cover identifies the spatial extent of these urban areas accurately, assigning them as urban and therefore underestimating temperatures. The MODIS land cover however,

whether by mistake or by design, does not identify the urban areas in these specific study areas, so treats them as natural, and therefore does not underestimate them. (i.e., treating the warm urban areas as natural vegetation results in more accurate simulations of these areas). In addition to this, in Thohoyandou the natural vegetation assigned by SANLC_converted is unrealistic, resulting in a strong cool bias and worse RMSE values.

While correlation values are fairly low across both WRF_MODIS and WRF_SANLC simulations, the WRF_SANLC simulations do generally show an improvement. These have average correlation values of 0.34 across the 10 study domains while WRF_MODIS averages 0.25. In terms of individual study areas, WRF_SANLC improves correlation values in 7 of the 10 study areas. Bloemfontein, Kuruman and Newcastle are the exceptions here. This is somewhat surprising in Bloemfontein given the visual similarities between the WRF_SANLC simulations and the observed, but could be attributed to slight differences in the spatial extent of features, but also to smaller scale variations like those seen in the irrigated cropland to the NE. In Kuruman, the decreased correlation is partly due to the strong underestimation of its urban areas' temperatures. Most of these areas are sparsely vegetated and therefore better simulated by WRF_MODIS (with its treatment of some urban areas as natural vegetation). In Newcastle, the urban areas do appear to be better simulated by WRF_SANLC, but the northern and western surroundings are strongly underestimated and overestimated respectively, leading to an overall poor correlation value.

Overall, the results show that the land cover datasets can vary in their skill depending on the study area and its characteristics. They also show the importance of using multiple methods to evaluate model skill. Visually, the WRF_SANLC simulations tend to appear far improved, which is testament to the increased resolution and improvements in representing features spatially, but the values simulated are not always better than what is seen in the WRF_MODIS simulations, as evidenced by some of the statistics.

What is very promising though, is that many of the errors that WRF_SANLC simulations do show, can be addressed. The differences that occur between these simulations and the observed are driven by the characteristics assigned to the urban land cover classes in the WRF setup and in the UCM. Because the SANLC_converted land cover dataset does identify the actual features well, it is possible to improve on the value discrepancies by adjusting the assigned characteristics (in contrast to MODIS land cover which does not actually identify

many of the features). This modification is, however, only worth making if the urban land cover classes themselves are reasonably assigned, which would require further work on improving the land cover dataset.

Although the WRF_SANLC simulations do still have significant room for refinement, the improvements they have already illustrated are enough to warrant using the SANLC_converted dataset over its MODIS equivalent. For this reason, the remaining parts of the study only use this dataset.

5.1.2 Air Temperature

The use of a climate model offers a significant advantage in that it allows for the study of a wide range of variables. Among these variables is air temperature. Air temperature is the most common measure used by people to quantify heat. It has also been the primary metric used when studying temperature-related illnesses and deaths (e.g., Bunker et al., 2016; Scovronick et al., 2018). Therefore, using air temperature in this study can improve the versatility of the research and its compatibility with similar studies. However, to effectively use the model outputs and trust its simulations, it is important to validate the model by comparing its outputs with observation (Fig 5.3).

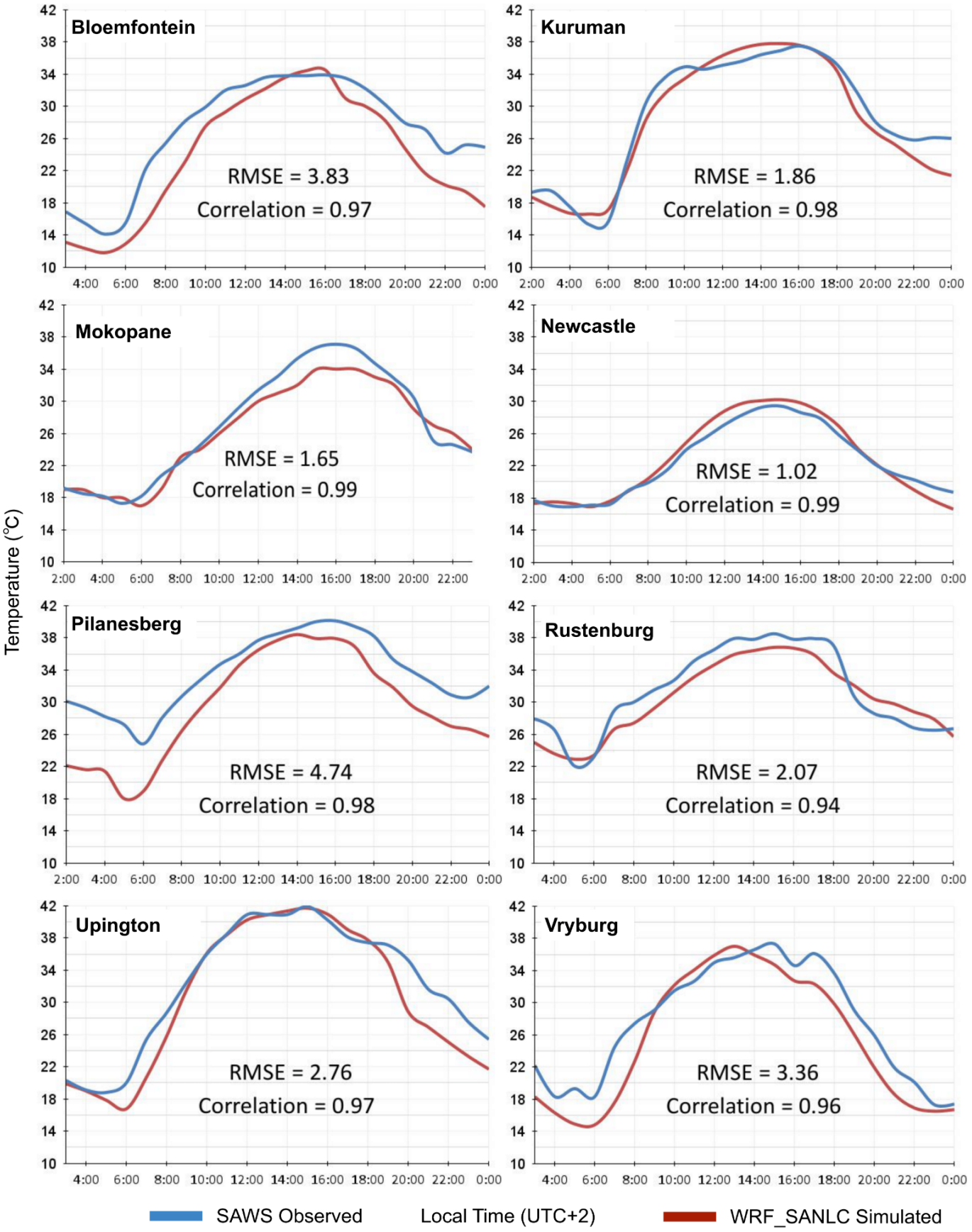

Figure 5.3 Plots comparing air temperatures of WRF_SANLC control simulations (red) with that of the available station observation air temperatures (blue) for the chosen days.

The comparisons between model-based air temperature and station recorded air temperature show that the diurnal variation of air temperature across the 8 cities is well simulated by the model, with correlation values all at 0.94 or above. This indicates that the model accurately identifies changes in temperature and produces a good overall representation of the "shape" of temperature in each location. Among the study areas, Mokopane and Newcastle have the highest correlation values (0.99) and exhibit almost identical observed and simulated temperature "shapes", while Rustenburg shows the lowest value (0.94) with slight underestimations of night-time temperatures and slight overestimations of day-time temperatures.

The actual values simulated by the model are also shown to be similar to the observed, with 7 of the 8 locations having RMSE values under 4℃, indicating that, on average, the simulated values differ from the observed values by less than 4℃. Pilanesberg has the largest RMSE (4.74℃), with it strongly underestimating the temperatures during the morning and late afternoon, but still performing well during the middle of the day. Newcastle (1.02℃), Mokopane (1.65℃), Kuruman (1.86℃), and Rustenburg (2.07℃) all provide very good estimations of air temperature across the day. What we are most interested in, however, is the prediction of the hot midday temperatures. Looking at the profiles, one can see that these too are well-simulated. 5 of the 8 locations show maximum temperatures within 1℃ of the observed values, while Pilanesberg (~2℃), Rustenburg (~2℃) and Mokopane (~3℃) show slight underestimations.

Knowing that WRF simulates the station recorded air temperatures well, we can have some confidence that the overall spatial patterns of air temperature are also well-simulated. Spatial maps for each study area are therefore produced (Fig 5.4) and their relationship with LST and the areas' underlying characteristics is analysed.

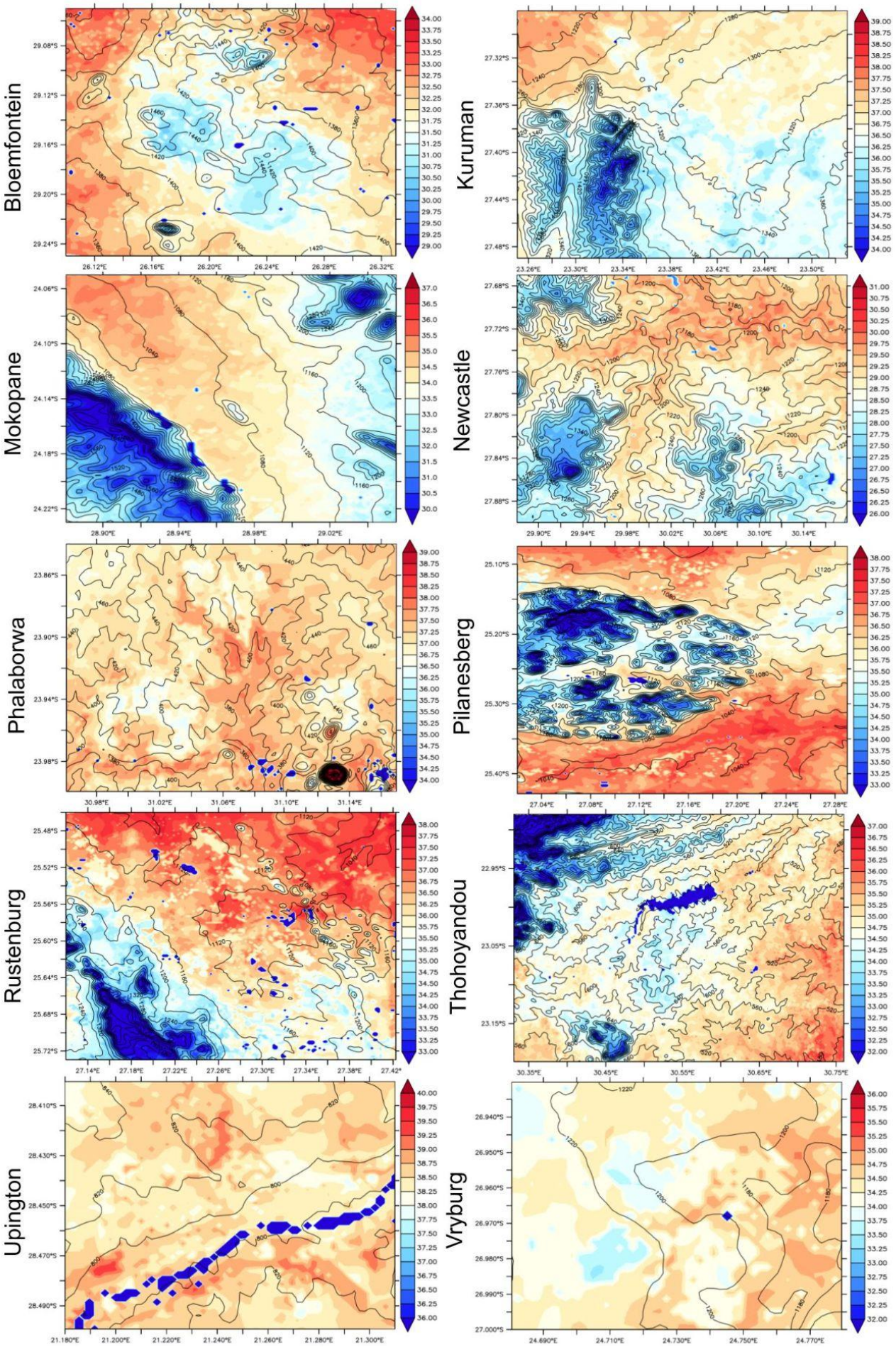

Figure 5.4 WRF_SANLC air temperature distribution (in °C) for each study area, averaged across the period 10 AM to 5 PM (UTC+2)

The air temperatures simulated by WRF_SANLC (Fig 5.4) show similar patterns to those seen in land cover and LST distributions (Fig 5.1), illustrating the dependency of air temperature on these variables. This is particularly prevalent in the flatter and denser locations, with these showing almost identical LST versus air temperature patterns (e.g., in Bloemfontein and Vryburg). In the other study areas there is still a very noticeable relationship between the temperature metrics, but other factors like topography (Mokopane) and water features (Upington) also seem to be impacting the distributions. Some of the biases simulated in the LSTs also appear to be present, with the cooler temperatures above Kuruman's northern urban areas likely to be a reflection of the underestimated LSTs, rather than actual cool temperatures. The same is true for Thohoyandou, where the cooler central temperatures are again likely to be a reflection of the cooler forest land cover assigned to this area, and not the actual conditions.

While it is difficult to properly validate air temperature distribution without an extensive observational study, the significant similarities observed between LST and air temperature in these results suggest that LST could serve as a valuable predictor of air temperature, consistent with previous research such as Oyler et al. (2014). This finding provides further support for using LST as a metric to quantify extreme heat and its impact on people.

5.1.3 Summary and potential improvements

In summary, the WRF_SANLC simulations show some good improvements in simulating city-scale LSTs compared to the WRF_MODIS equivalent, particularly in reproducing spatial patterns. This improvement can be primarily attributed to the higher resolution and better separation of classes. The separation of urban classes was particularly relevant, as it allowed the study to use the Urban Canopy Model to assign land cover class-specific characteristics.

Although the nationwide "one size fits all" conversion of the SANLC dataset has been shown to not work well in all situations, it has also proven to be a very good base to improve from. Ideally, the land cover of each study area should be specifically converted based on the area's local properties. For instance, in an area like Thohoyandou, the natural forest and low-density urban class could be easily converted into woody savanna and a more spread out urban class with less tree cover.

Similarly, the UCM characteristics can also be adjusted to suit each city's specific conditions. Characteristics such as building and road sizes, vegetation fraction, natural vegetation type, and albedos could all be chosen according to the observed values. This could significantly improve on this study's use of more generic characteristics. It would be especially important in differentiating between the low density urban classes of the more spread out and less vegetated areas (e.g., in Kuruman, Thohoyandou and Pilanesberg) and that of the denser, more vegetated equivalent (e.g., Bloemfontein, Vryburg and Upington). These changes could be guided by the results obtained in the WRF_MODIS simulations, where the urban areas that were not identified by the land cover dataset actually better predicted the LSTs of these more spread out, low vegetated areas.

Regarding air temperature, the validation of the WRF_SANLC simulations against the station data demonstrated very good results, especially in the simulation of the hottest parts of the day. However, this validation was restricted to the eight specific station "points" and may not accurately represent the entire study domain. Obtaining more ground-based measurements distributed throughout each study area would be useful in producing more realistic data or providing additional support for the current findings.

The WRF_SANLC's simulations have shown that they can identify changes in LSTs and air temperatures with relation to changed land cover. This allows the study to use these simulations as a control to test the impact of targeted land cover changes on both LST and air temperature. This is done by adjusting the land cover dataset to represent potential cooling scenarios.

5.2 Impacts of increased tree cover and roof reflectance on temperature

This section presents the results of the two land cover sensitivity experiments. This includes how the land cover changes impact both land surface temperature and air temperature, as well as the varying impact of the two scenarios.

5.2.1 Land surface temperature

The results show that the changes in both tree cover and roof reflectance have cooling effects across all the study areas, but these vary in effectiveness depending on the area and its land cover makeup (Fig 5.5).

The cooling as a result of increasing tree cover (WRF_TREE) is limited to the areas that were initially classified by the SANLC dataset as having few trees. These were the high-density urban and high-intensity commercial/industrial areas, both having been assigned initial values of 10% tree cover in the control scenarios. The low-density urban areas had initially been assigned values of 60% tree cover, so these did not change from control to experiment.

The cooling that does occur is about 3°C across these initially less vegetated areas. This is very prominent in the larger, denser cities of Bloemfontein and Newcastle. This is partly because these cities have large areas of previously low tree cover, and partly because of the size and density of the cities relative to other study areas (i.e., they produce a greater thermal signature). Apart from Thohoyandou, the other cities also all show significant cooling, but across less of the areas, or by lower amounts. Thohoyandou is the exception because of its initial dominance of low-density land cover. Most of the area already had the 60% tree cover in the control simulation and therefore would not have changed from control to experiment.

The cooling due to increased roof reflectance (WRF_ROOF) shows similar patterns to that of trees, with it also being related to the urban land cover type. This relationship is based on the roof surface area present in each urban class. The larger roofs of industrial areas, and the denser nature of the high-density class, means that both these have greater roof coverage than the more spread out, medium sized, roofs of the low-density class. The more roof area there is, the more the albedos in the areas change, the more light is reflected away from buildings, and the greater the observed cooling in the area. So even though the change in roof albedo values is the same for each urban class, the cooling experienced by them is still different. For most of the study areas, this results in an overall urban cooling averaging ~2°C, with slightly stronger cooling (~2-3°C) in higher density urban and industrial areas, and slightly less in the lower density areas (~1-2°C). The differences between the cooling of these classes is well visualised in the spatial maps of Mokopane and Phalaborwa.

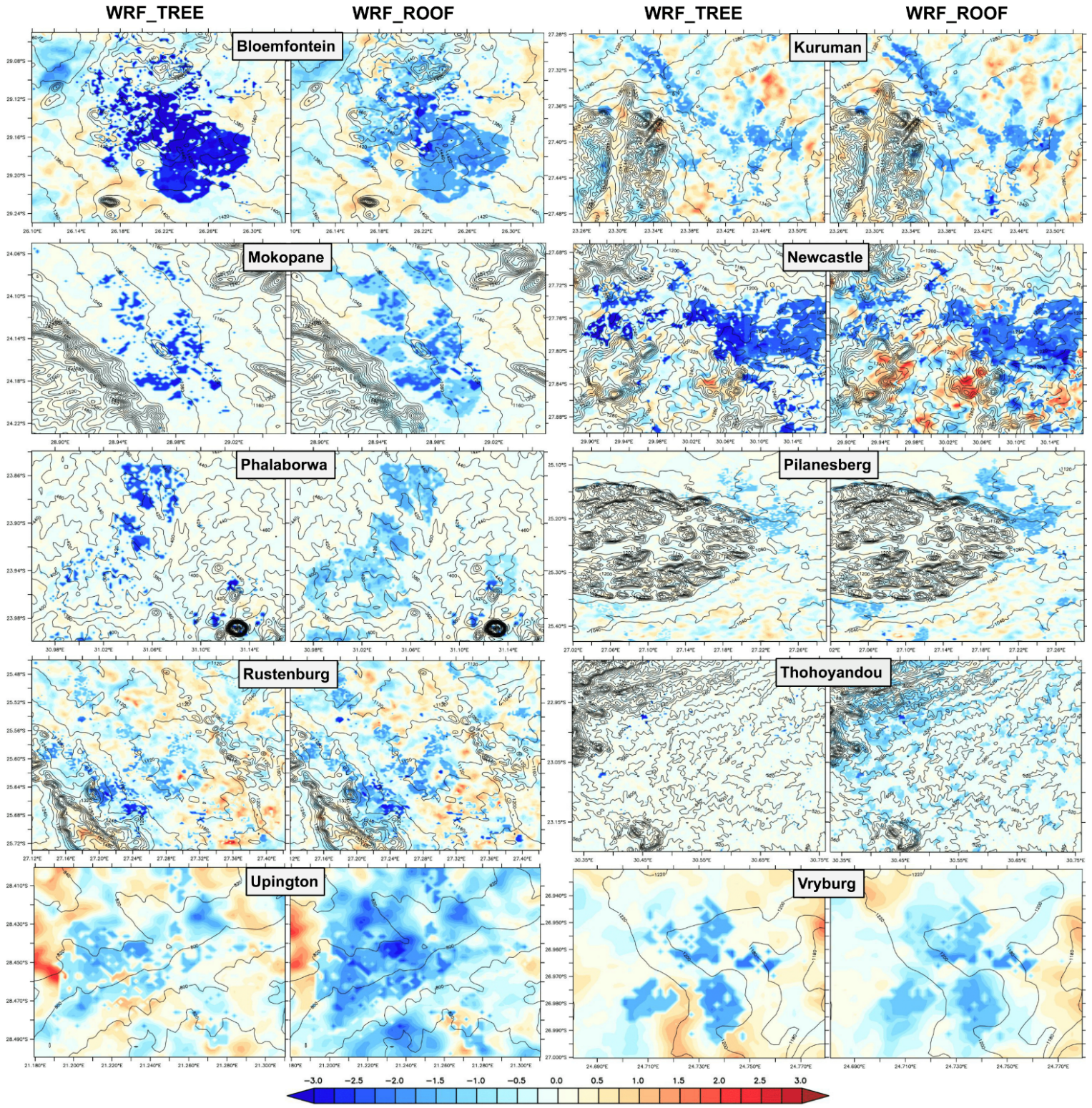

Figure 5.5 Difference in LST (in °C) between WRF experiments (WRF_TREE and WRF_ROOF) and the WRF_SANLC control for each study area. Differences are averaged across the period 10 AM to 5 PM.

The cooling effectiveness of WRF_TREE and WRF_ROOF also vary depending on time of day (Figs 5.6 and 5.7). The cooling by trees is generally present across the entire day (besides for Thohoyandou), but can fluctuate fairly significantly during this time. While these fluctuations in cooling differ from one study area to the next, there are a few general trends that occur. One of these is a sharp relative increase in WRF_TREE temperatures at around 6 AM (i.e as the sun rises), before another fairly sharp relative decrease soon after, as the evapotranspiration cooling impact starts to "kick in' and overtake the radiation warming from the sun. After these initial fluctuations, there is a general trend of increasing cooling through the rest of the daylight hours, with maximum cooling (of between 2°C and 5°C) often occurring in the late afternoon/early evening (where evapotranspiration is still high, but warming from radiation is lower). This sort of profile is consistent with studies like Meili et al. (2021), who analysed the diurnal profile of overall tree cooling, as well as the individual effects which contribute to this (e.g., radiation, evapotranspiration, roughness).

WRF_ROOF shows more consistent patterns of cooling, generally producing a strong U-shaped profile. This starts with early morning temperature differences close to zero (i.e very similar to the WRF_SANLC control). As the sun rises, the WRF_ROOF temperatures start to drop below that of the control, reaching maximum differences of ~2-3°C in the period between 11 AM and 3 PM. From here the differences shrink again, approaching the zero mark again when the sun sets. This clearly illustrates that this cooling scenario is directly dependent on the sun (as one would expect).

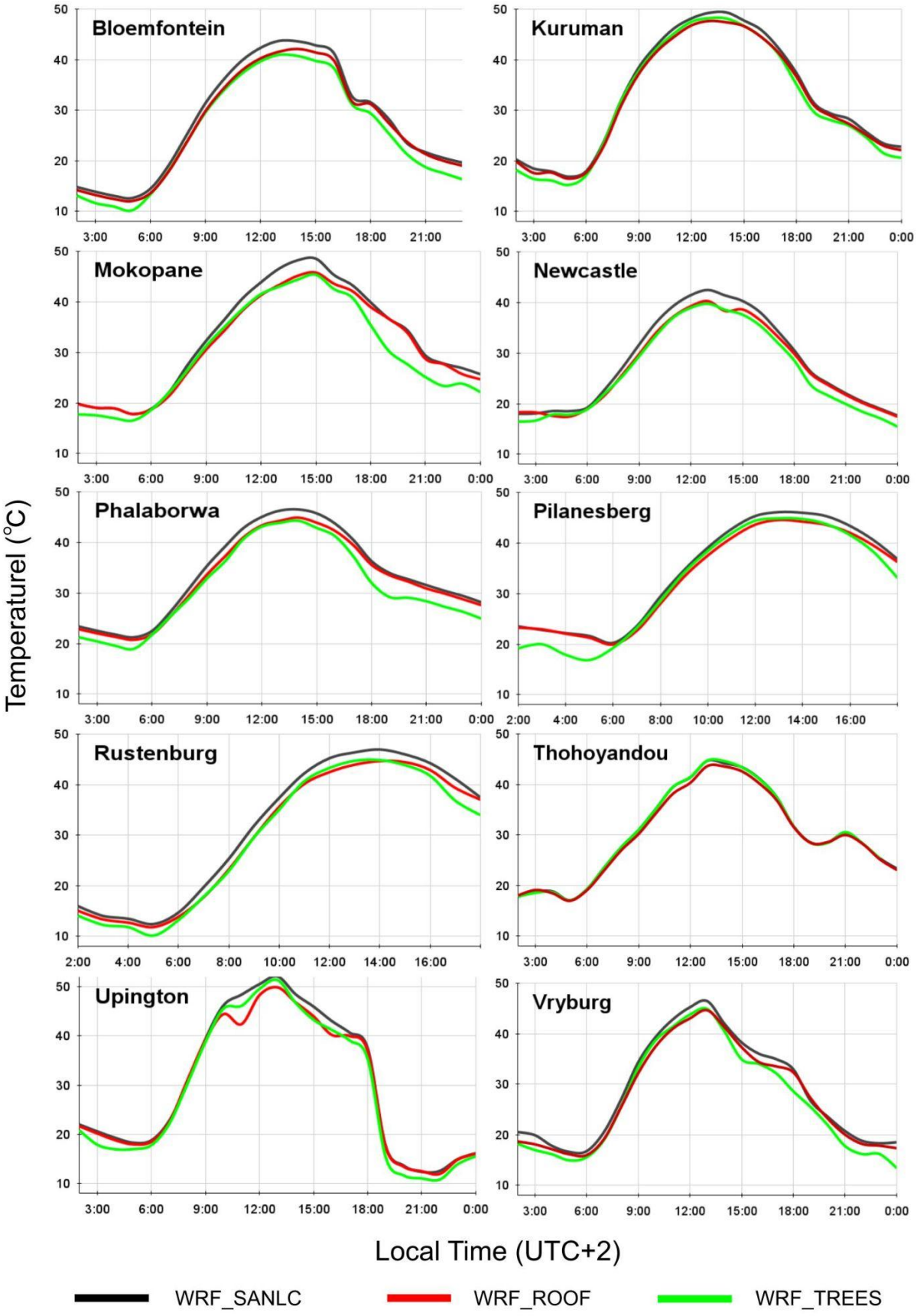

Figure 5.6 LST profiles for each study area over a section of high-density urban land cover. Black is the SANLC control simulation, green is the tree cover change scenario, and red is the whitening of roofs scenario.

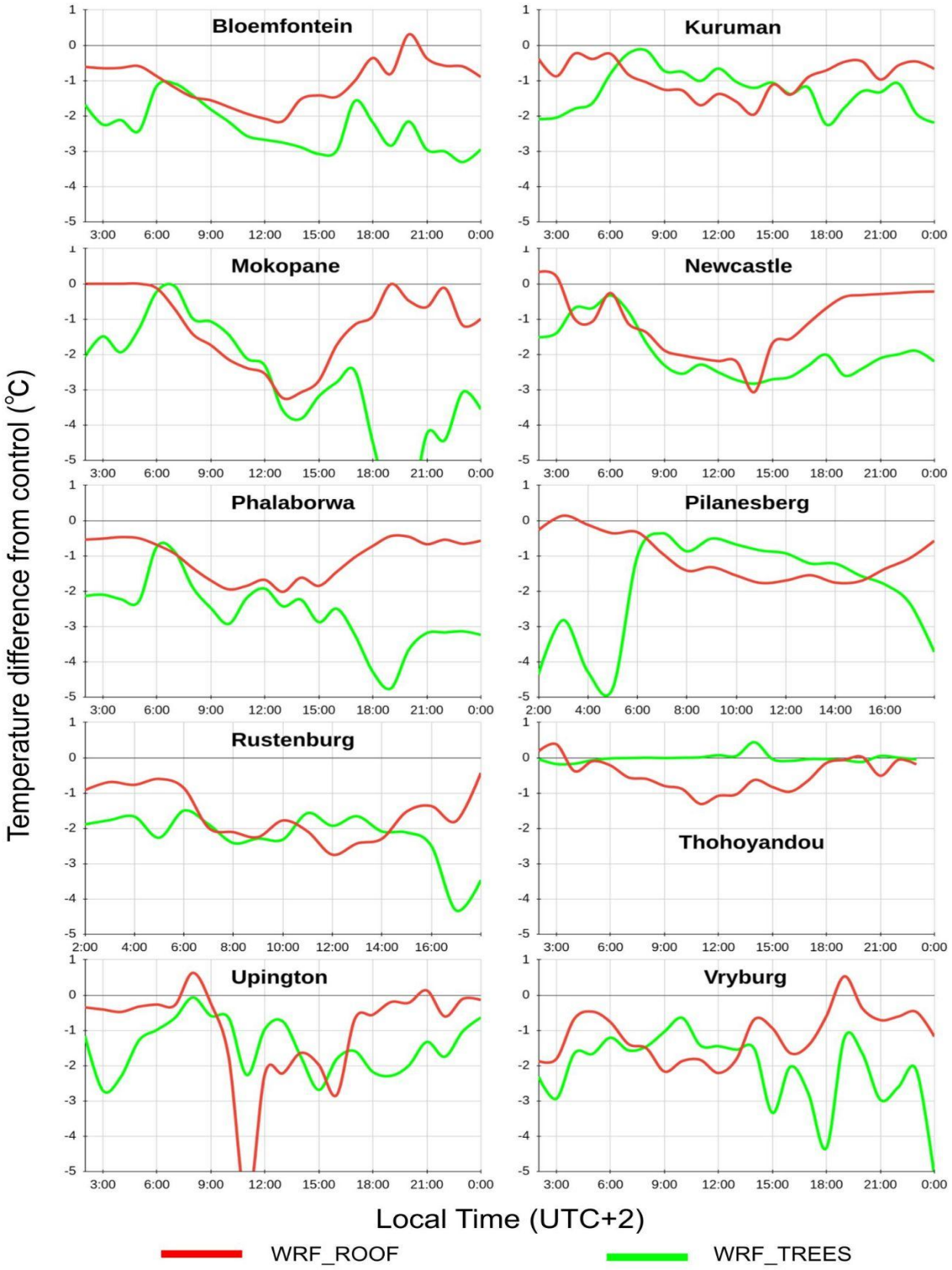

Figure 5.7 Differences between simulated and observed LSTs for each study area over a section of high-density urban land cover. Green indicates the tree cover change scenario, red indicates the whitening of roofs scenario.

5.2.2 Air temperature

Observing the impact of the land-cover change experiments on air temperature (Fig 5.8) adds extra versatility to the research and would allow for more direct comparisons with other studies, as well as the option of using the information in heat indexes such as thermal comfort and ambient temperature. The impact of these changes are summarised in Table 5.2.

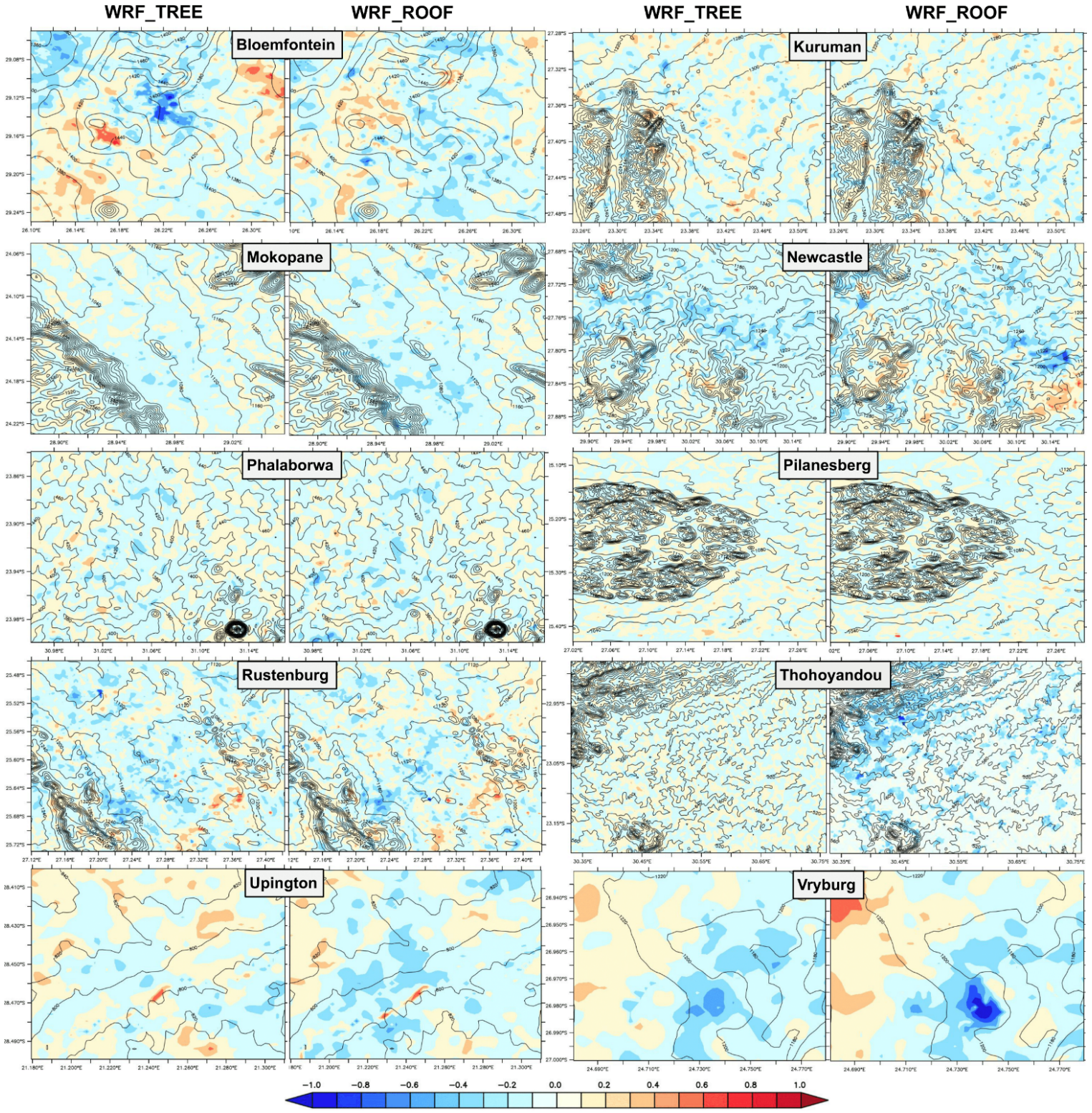

Figure 5.8 Difference in air temperature (in °C) between WRF experiments (WRF_TREE and WRF_ROOF) and the WRF_SANLC control for each study area. Differences are averaged across the period 10 AM to 5 PM.

Table 5.2 Impacts of land cover change experiments on air temperatures

Study Area	Tree cover change	Roof albedo change
Bloemfontein	• Temperatures in the commercial/industrial city centre show significant cooling (between 0.6°C and 1°C). • Two small patches show warming (~0.6°C).	• No areas of large temperature change • Consistent slight cooling in patches down the centre line of the area (~0.3°C). • Slight warming just west of this central line (~0.3°C).
Kuruman	• No consistent significant changes.	• No consistent significant changes.
Mokopane	• Very slight cooling across most of the urban areas (~0.1°C).	• Very slight cooling across most of the urban areas (~0.1°C). • Small patches of high density urban areas showing cooling up to 0.3°C.
Newcastle	• Slight cooling across most of the urban areas (~0.3-0.4°C).	• Very sight cooling across most of the urban areas (~0.2°C). • Small patches of high density urban areas showing greater cooling (up to ~0.6°C).
Phalaborwa	• Cooling of up to ~0.4°C in a few patches of high-density urban areas.	• Cooling up to ~0.4°C in a number of high-density urban areas .
Pilanesberg	• No consistent significant changes.	• No consistent significant changes.
Rustenburg	• Cooling of up to ~0.6°C in a number of high-density urban areas. • Line of warming (~0.5°C) in the SE.	• Cooling of up to ~0.6°C in a number of high-density areas. • Line of warming (~0.5°C) in the SE.
Thohoyandou	• No consistent significant changes.	• Slight cooling across most of the urban areas (~0.3°C). • Patches of urban areas in the NW cool by up to 0.5°C.
Upington	• No consistent significant changes.	• Slight cooling across the central and western urban areas (~0.4°C).
Vryburg	• Significant cooling in the SE settlement (~0.6°C). • Slight cooling in the industrial east (~0.4°C).	• Significant cooling in the SE settlement (~0.8-1°C). • Slight cooling in the industrial east (~0.5°C). • Warming in the NW (~0.6°C).

The cooling is, as expected, far less than that seen with surface temperatures, with the more fluid air temperatures not only dependent on land cover, but also heavily influenced by air movement and dissipation of energy to the atmosphere. The cooling is, however, still observed across all areas to some degree. In most locations, the impact of albedo change

versus that of tree cover change is similar in value, with larger cooling occurring for both scenarios in parts of Newcastle (~0.5 - 1℃), Rustenburg (~0.4 - 0.7℃), and Vryburg (~0.4 - 1℃).

What is also evident when comparing the distributions of air temperature cooling to that of the LST cooling, are the similarities in their patterns. These are particularly apparent in Newcastle and Rustenburg, but the other study areas, bar Kuruman, also show some similar patterns of change to those seen with LSTs. These are generally highlighted in the commercial/industrial and high density urban areas and show that in some cases the land cover, surface temperature, and air temperature can again be closely linked.

5.2.3 Trees and reflective roofs summary

Both the WRF_TREE and WRF_ROOF scenarios consistently produce cooling across the study areas, with both also tending to show similar values of LST cooling (~2-3°C) during the hot midday period we are most interested in. The cooling has been shown to be closely linked to the specified SANLC_converted urban classes, illustrating the direct impact the land cover characteristics have on the cooling (i.e., giving evidence that these land cover changes can be used to influence temperature).

Implementing these types of scenarios in real life would, however, depend on the specific study area's situation. Trees in real life take many years to be effective cooling mechanisms, and also come with a significant burden on water resources in hot, dry environments. Many of our study areas have also been shown to be vulnerable to cold related mortality during winter, and by adding trees this could actually negatively impact mortality. On the other hand, trees could also provide ecosystem services such as reducing carbon dioxide and soil erosion and producing fruit and firewood.

Increasing roof reflectance would be a comparatively simpler and more immediate strategy, with basic methods only requiring a good coat of reflective paint or a slight change in building material. It, though, does not have the added ecosystem and aesthetic benefits of trees.

5.3 Limitations

One major limitation of these experiments is that they rely on an LST control map that has been shown to underestimate temperatures in urban areas. To improve accuracy, the SANLC land cover map and the WRF-UCM model setup would need to be customised for each location to produce a more representative control map. Another limitation is that model-based changes in land cover are excellent in theory, but the implementation and scale of proposed changes can vary significantly on the ground, leading to differences in the actual impacts. Combining ground measurements and actual physical changes in land cover would be a valuable addition to test the model's effectiveness and provide better information for simulations.

Chapter 6: Discussion and Conclusion

This chapter discusses some of the key findings of the overall study (Section 6.1 and 6.2). It then looks at the potential applications of the research, with a focus on the South African context (Section 6.3). The chapter finishes off by presenting the conclusions of the study and the possibility for further research (Section 6.4).

6.1 Urban Heat and Cool Islands

The urban heat island (UHI) is a phenomenon seen where built-up areas experience warmer temperatures than their rural counterparts. This can be partly caused by changes in surface properties. Impervious surfaces such as roads, buildings and pavements tend to absorb, retain and release more energy than natural surfaces, and they do not store any water, which would otherwise cool the surroundings through evaporation. Other aspects are a reduction in green spaces and their shading and evapotranspiration properties, as well as the actual release of heat through transportation, and industrial and household activities. UHIs are generally associated with air temperature and tend to be most prominent at night and under stable high pressure synoptic conditions. Their presence can contribute negatively to the thermal comfort in cities, as well as to pollution levels, energy consumption and local weather patterns. Many studies have thus looked at ways of reducing UHIs.

What has been observed in this study though, is evidence of almost completely reversed UHIs, albeit most notably in the day-time temperatures. In all of the study areas, the ~10 AM urban LSTs are considerably cooler than the rural LSTs. Additionally, the simulated urban air temperatures are also shown to be slightly cooler than their surroundings for the entire 24 hours in all study areas. There is also a trend that the denser the settlement, the cooler the temperatures. These observations are contrary to what is found in most literature (e.g., Sithole & Odindi., 2015; Zhang & Sun., 2019), but similar findings have been observed in a few studies (mentioned below). This phenomena has been labelled an Urban Cool Island (UCI) when in reference to air temperatures, and a Surface Urban Cool Island (SUCI) when in reference to surface temperatures. Haashemi et al. (2016) observed summer daytime SUCIs of ~4°C in Tehran; Lazzarini et al. (2013) ~6°C in Abu Dhabi; and Shafieiyoun et al. (2022) up to 13.9°C in Isfahan, Iran. Shafieiyoun et al. (2022) also observed air temperatures in

conjunction with surface temperatures, finding that during most of the year the more traditional UHI was observed, but during summer, there was some evidence of slight UCIs forming.

These patterns of SUCI and UCI seem to be closely related to the climate and greening characteristics of the specific study area. Lazzarini et al. (2013) noted that cool islands tend to form in arid and semi-arid regions where the naturally occurring land cover consists of limited vegetation. In constructing cities, people bring in and cultivate tree growth and increase the amount of water available to the atmosphere through processes like irrigation. This leads to a form of oasis effect (Oke, 2002), with increased evaporative cooling in the cities causing cooler temperatures than what is experienced in the drier, more bare surroundings.

With reference to our study, the majority of our study areas are located in hot and relatively arid savanna, grassland and nama karoo biomes. The natural vegetation is generally low to the ground and spread out with no significant tree cover. A few areas (like Rustenburg) are also dominated by relatively dark, exposed soils with limited moisture retention. The urban areas in contrast tend to have far more tree cover, particularly in the more developed, denser neighbourhoods. The comparative reflectivity of some of the denser, more reflective housing can also be higher than that of the darker non-urban soils. Moisture in the urban areas is also likely to be higher due to irrigation of areas like gardens, parks and sports facilities. The combination of these factors appear to be the major contributor to the spatial patterns we have observed in the study.

What the study has shown is that in hotter, drier South African cities, where the natural vegetation is low or minimal, there is already evidence of how human-led land cover changes can actually reduce temperatures. This illustrates the great potential to create urban landscapes that not only mitigate urban heat, but actually improve it in comparison to the surrounding areas. While certain settlements in our study areas already demonstrate significant “cool spots”, this is definitely not universally observed across all communities.

6.2 Thermal inequality and apartheid legacy

The layout of the study areas and their underlying land-cover characteristics are themselves dependent on socio-economic and historical factors.

Thermal inequality

It is well known that wealthier populations tend to be better equipped to deal with hot temperatures. The type of housing plays a significant role with low-income communities tending to live in housing which is far less insulated and thermally efficient than what higher-income communities live in. In South Africa, Scovronick & Armstrong (2012) estimated that thermally inefficient housing was responsible for ~50% of heat related deaths. Aside from housing type, the reduced access to air-conditioning and medical care, as well as the need to live more physical lives (i.e., walking or public transport over driving, outdoor labourer over desk job, etc.) means poorer populations are at far greater risk of being exposed to hot temperatures, and are also less equipped to deal with the ill-effects. This relationship between temperature risk and socio-economic factors is known as thermal inequality. While the above contributors to thermal inequality are fairly well known, the relationship between wealth, land cover and hot temperatures has been less studied.

What we have found in this study is that higher-income areas are in most cases significantly cooler than their low-income counterparts during hot days. This appears to be closely linked to tree cover, and is most apparent in study areas where the climate does not naturally support extensive tree growth, but where trees and water are available at a cost (e.g., Upington and Kuruman). Similar results have been noted in other studies. Dialesandro et al. (2021) found that on average, the poorest 10% of neighbourhoods in southwestern U.S. cities had 2.2°C hotter LSTs than the wealthiest 10% during summer days. This difference rose to 3.7°C in certain cities. Barrera et al. (2019) also found that in Santiago, Chile, differences in LSTs between low and higher-income neighbourhoods were between 3.1°C and 3.3°C and had strong associations with differences in tree cover.

Diving deeper into this topic, Mitchell & Chakraborty (2018) studied 20 cities across the United States, finding very strong associations between lower-income communities and hot temperatures, but also finding strong thermal inequality between racial groups. Black and Asian populations had a 52% and 32% higher probability than white populations of living in conditions with greater land cover related heat risk. In South Africa, the direct relationship

between wealth, race and temperature does not appear to have been studied, but studies like that of Venter et al. (2020) have looked at the relationship between wealth, race and tree cover. Our study has already shown the close link between trees and temperature, making the comparison to wealth a reasonable one. The Venter et al. (2020) study used census data to show that white dominated districts have incomes 8.6, 6.8, and 2.9 times greater than those of Black African, Coloured and Indian dominated districts respectively. They also found that the coverage by trees increased 3.5% (private gardens) and 2.7% (public spaces) per 100% increase in income. (i.e., white dominated districts had on average 30% greater garden tree coverage and 23% greater public tree cover than black dominated districts). The contrasts in wealth and tree coverage and their link to racial groups can be well explained by South Africa's apartheid past.

Historical influence

During apartheid, the forced removal and relocation of people of colour to townships and homelands meant that white populations had their pick of the most desirable places to live, while other population groups were forced into areas that were not necessarily suitable or ideal for large settlements. On top of this, economic opportunities and government services were heavily skewed in favour of the minority white population (on the back of a cheap black and coloured labour force). This meant that most of the wealth and resources were accumulated in white communities. Greater wealth translated into resources being used to make these settlements more appealing. Part of this would have been the planting of trees and creation of green spaces.

When apartheid ended, the laws governing separation of racial groups were no longer there, but the distinction in wealth between groups very much was. White populations still had far greater access to opportunities and services because of their advantaged past and were still living in their more desirable cities. People of colour who did try to move to previously white-only areas, were limited by their financial ability, often being financially pressured into living in the less desirable outskirts. This contributed to the formation of unplanned informal settlements, where standards of living were (and are) extremely low and infrastructure and services very limited. Planting of trees was not an important consideration among people who had no discretionary income and governments did not have it high on their agenda either, given the unplanned nature of the settlements.

The impact of these historical policies can therefore still be seen in the current layout of many South African cities. Neighbourhoods are still very much separated by wealth (and therefore also race) and this strongly determines where they are located and what their land cover characteristics are. A number of our study areas illustrate this well. In Upington, its wealthier areas are situated right along the cooler river banks, with greater access to its water, while the poorer townships are further out and fully exposed to the harsher temperatures. This seems to have contributed to the amount of tree cover, with far greater coverage observed nearer the river. Rustenburg has similar geographical and vegetation separations, with wealthier suburbs situated on the cooler hillside more hospitable for tree growth, while poorer townships are located in the hotter, more degraded flats and mining areas where tree growth is more difficult.

Another worrying observation is that many newer government funded developments of low-cost housing projects (such as can be seen in the Vryburg study area) do not seem to be incorporating trees. Venter et al. (2020) also noted this, finding that these projects neglected a number of environmental justice, sustainability and quality of life aspects. The lack of government contribution to increasing green infrastructure in low-income communities has meant that the inequities of the past are not being resolved. Venter et al. (2020) in fact found that since apartheid, tree cover in black neighbourhoods has actually slightly decreased while cover has increased slightly in white (~4.3%), coloured (~2.4%) and Indian (0.6%) neighbourhoods.

The overall take from these findings is that while historical policies are no longer in place, their impacts on current settlement characteristics are still very much evident and little is being done to address them. This contributes to the situation where people who are the most exposed to hot temperatures are also those who are the least equipped to deal with them.

6.3 Applications and potential challenges in a South African context.

The results from this study show that there is significant potential to reduce city temperatures and thermal inequality by using reflective roofs and trees. Implementing these strategies successfully would, however, need to consider the specific context of the area and the associated challenges.

A first consideration would be to identify the areas that would actually benefit from the respective cooling strategies.

Trees. As studies like Manoli et al. (2019) and Cheng et al. (2022) found, climate influences the effectiveness of tree cooling, with arid regions showing far greater effectiveness than more humid areas. While all of our study areas were in relatively dry climates, other parts of the country (e.g., KwaZulu-Natal) are far more humid and would not necessarily be able to use trees as effectively. The area a tree cools is also limited. For maximum cooling, fairly continuous tree cover would be needed. This means that denser settlements would be far more practical to forest than more spread out areas because the tree to house ratio would be much higher, as individual trees could shade multiple houses. In relation to our study, the hot, denser housing seen in the many of the informal settlements would benefit far more from, for example, 500 large trees than an equivalent population spread out across a larger area (like in many hot Kuruman settlements).

For *reflective roofs*, how much cooling they provide is dependent on the insulation of the roof they are on, as well as its angle to the sun and the shading it receives. Less insulated roofs will show far greater variations in indoor temperatures with varying reflectivity (Kimemia et al., 2020), while flat roofs are generally more effective than angled roofs as they have more direct solar incident angles. They also do not reflect energy onto other buildings and they are easier to apply cool coatings onto (Akbari & Matthews, 2012). In the cities we looked at, most of the hot settlement areas tend to be lower-income housing, often dominated by informal, flat roofed buildings. These would be very good candidates for cool coatings, but some other settlements may be less suitable.

A second consideration when planning cooling strategies would be how to maximise their effectiveness.

For *trees*, the species type used would need to be suitable for the location it is to be planted in. In reference to its cooling ability, one would need to consider how fast the tree grows, the shade it produces, its transpirational ability and its hardiness (Rahman et al., 2014). In terms of other characteristics, one would need to consider how much water it uses; how much light it needs; what other benefits it provides, as well as its ecological impact and susceptibility to pathogens and predators (e.g., shot hole borer). Ideally, trees native to the area, fast growing and water-wise would be used, but in drier climates like our study areas, these often do not exist or are not as effective or feasible as some other species. It is thus necessary to find compromises that still suit the location, without having negative impacts .

For *roofs,* the effectiveness of the reflective surface is dependent on the material of the roof and the coating used. The simplest, most cost effective methods of increasing roof reflectivity involve merely adding a layer of white paint, but for greater effectiveness, specifically designed cool coatings and materials can be used. These all vary slightly with regards to their thermal emittance and the amount of solar radiation they reflect, but also differ in how long they last in different conditions, and how well they apply to different roof types (i.e., corrugated vs smooth, angled vs flat). The coating used therefore needs to be chosen accordingly.

The third consideration would be the challenges facing implementation.
One of the major challenges is financial capability. Most of the hot spots which have been identified consist of populations who are low-income and unable to spare money for non essentials. This means that either solutions would need to be:

1) Sponsored by government and other outside entities; or
2) Replace existing expenses which are already being incurred; or
3) Be free or very affordable.

On this first point, the South African government led cooling initiatives have in the past been very few. In general, these have been overlooked in favour of more pressing issues. (Goodness & Anderson, 2013; Gwedla & Shackleton, 2015; du Toit et al., 2018; Pasquini & Enqvist, 2019). More recently though, there has been an increased push to change this. Strategies like the “10 million trees programme” from the The Department of Forestry, Fisheries and the Environment (DFFE) and the “Cool Surfaces Project” from the South

African and American department of energy (RSA DOE and USA DOE) are significant steps in this process. Government only strategies will, however, not be fully successful or sustainable on their own. There needs to be buy-in from outside, both from business and individuals.

The “Million Cool Roof Challenge” run by the Clean Cooling Collaborative (2022) showed how this could work successfully. The programme scaled up the deployment of highly solar-reflective “cool” roofs in heat-stressed developing countries. The programme itself installed 1.1million cool roofs (equivalent to 250,000 small houses) across 10 countries, including South Africa, showing significant reductions in indoor temperatures (2-10°C). The temperature reductions were, however, not the only positive impacts. The effectiveness of the programme also helped to drive revisions in building code requirements in some of the countries, with passive cooling mechanisms now being legally required in new buildings in Kenya and Indonesia. A large part of the success of this programme was the community involvement. Cooling projects were run by local teams who were familiar with the context of the areas they worked in. The deployment of cool roofs also created jobs and training opportunities for low skilled workers and led to the creation of many cooling projects separate from the initial programme.

The success of projects like this will hopefully promote changes in South African building/urban planning requirements, with more emphasis on climate resilient houses and settlements. What they will also hopefully do though, is to change individuals and businesses mindsets on the usefulness of the strategies. Doing this could convince people to consider alternatives or support initiatives, especially if these do not have significant differences in cost. This could be in the construction of buildings where contractors or owners choose to use more heat resilient materials/methods; in the choice to plant and maintain trees for future benefits; or simply in the choice to add a layer of white paint to a roof.

This “buy-in” aspect of projects is a particularly important one in a South African context. Numerous previous projects, across many different spheres, have implemented changes, but without gaining community buy-in. This has led to cases of vandalism and destruction of resources, or simply a lack of maintenance.

6.4 Conclusion

The study has successfully identified areas within South African cities that are susceptible to hot temperatures. In doing so, it has clearly shown the link between land cover and temperature, and has emphasised the existence of significant thermal inequality in South African cities and its link to historical policies. Differences in land surface temperatures (LST's) of up to 10℃ between wealthier, well-forested houses and bare informal settlements have been observed, contributing to the increased exposure of communities who are already most vulnerable and least equipped to respond.

What the study has also shown, though, is the potential for these cities to become refuges from hot temperatures. Both LSTs and air temperatures have consistently illustrated significantly lower daytime values over the more vegetated and developed urban areas when compared with their rural surroundings. This is the combined result of the study areas' climatic and vegetation characteristics and the human influence of planting trees, adding moisture, and using more reflective surfaces.

By combining both thermal imagery and climate model simulations, the study provided information that is both spatially and temporally continuous and which can be manipulated to understand how climate variables in cities could change under different mitigation and adaptation scenarios. The addition of a converted SANLC land cover dataset was shown to have great potential in improving the simulations of temperature in the cities, and its use in simulating realistic increases in tree cover and albedo showed promising reductions (~2℃) in LSTs across whole cities.

There is, however, room to improve on the model-based study, with location-specific land cover maps expected to significantly improve the accuracy of simulations. If this were done, and validated with a greater network of ground-based measurements, it would also be useful to combine temperature with other heat-related variables (e.g., humidity and wind) into a thermal comfort index more representative of the heat people feel.

The overall take away from this research is that adaptation measures have already been proven to work across all of our study areas, and now by focusing on the identified

communities who are still at high risk to hot temperatures, it is possible to create cities that are liveable for all.

To do this, though, one needs to have solutions that are suitable for the specific location, have community backing, are practical to implement, and are also sustainable in the long term. The ideal way to do this would be by first implementing small-scale, on-the-ground, projects and testing the effectiveness of different strategies.

References

Abdulateef, M.F. and A. S. Al-Alwan, H. (2022) “The effectiveness of urban green infrastructure in reducing Surface Urban Heat Island,” Ain Shams Engineering Journal, 13(1), p. 101526. Available at: https://doi.org/10.1016/j.asej.2021.06.012.

Akbari, H., Damon Matthews, H. and Seto, D. (2012) “The long-term effect of increasing the albedo of urban areas,” Environmental Research Letters, 7(2), p. 024004. Available at: https://doi.org/10.1088/1748-9326/7/2/024004.

Akbari, H. and Matthews, H.D. (2012) “Global cooling updates: Reflective roofs and pavements,” Energy and Buildings, 55, pp. 2–6. Available at: https://doi.org/10.1016/j.enbuild.2012.02.055.

Alahmad, B. et al. (2020) “Spatial distribution of land surface temperatures in Kuwait: Urban heat and Cool Islands,” International Journal of Environmental Research and Public Health, 17(9), p. 2993. Available at: https://doi.org/10.3390/ijerph17092993.

Alchapar, N.L. and Correa, E.N. (2016) “The use of reflective materials as a strategy for urban cooling in an arid ‘oasis’ city,” Sustainable Cities and Society, 27, pp. 1–14. Available at: https://doi.org/10.1016/j.scs.2016.08.015.

Alizadeh, M.R. et al. (2022) “Increasing heat‐stress inequality in a warming climate,” Earth's Future, 10(2). Available at: https://doi.org/10.1029/2021ef002488.

Allen, M.A., Roberts, D.A. and McFadden, J.P. (2021) “Reduced urban green cover and daytime cooling capacity during the 2012–2016 California drought,” Urban Climate, 36, p. 100768. Available at: https://doi.org/10.1016/j.uclim.2020.100768.

Aram, F. et al. (2019) “Urban green space cooling effect in cities,” Heliyon, 5(4). Available at: https://doi.org/10.1016/j.heliyon.2019.e01339.

Armson, D., Stringer, P. and Ennos, A.R. (2012) “The effect of Tree Shade and grass on surface and globe temperatures in an urban area,” Urban Forestry & Urban Greening, 11(3), pp. 245–255. Available at: https://doi.org/10.1016/j.ufug.2012.05.002.

Artis, D.A. and Carnahan, W.H. (1982) “Survey of Emissivity Variability in Thermography of Urban Areas,” Remote Sensing of Environment, 12, 313-329. Available at: https://doi.org/10.1016/0034-4257(82)90043-8

Azhar, G.S. et al. (2014) “Heat-related mortality in India: Excess all-cause mortality associated with the 2010 Ahmedabad Heat Wave,” PLoS ONE, 9(3). Available at: https://doi.org/10.1371/journal.pone.0091831.

Bălă, G.-P. et al. (2021) “Air Pollution Exposure—the (in)visible risk factor for respiratory diseases,” Environmental Science and Pollution Research, 28(16), pp. 19615–19628. Available at: https://doi.org/10.1007/s11356-021-13208-x.

Barat, A. et al. (2021) “Surface urban heat island (suhi) over riverside cities along the Gangetic Plain of India,” Pure and Applied Geophysics, 178(4), pp. 1477–1497. Available at: https://doi.org/10.1007/s00024-021-02701-6.

Barrera, F.de et al. (2019) “Urban parks and social inequalities in the access to ecosystem services in Santiago, Chile,” IOP Conference Series: Materials Science and Engineering, 471, p. 102042. Available at: https://doi.org/10.1088/1757-899x/471/10/102042.

Barriopedro, D. et al. (2011) “The Hot Summer of 2010: Redrawing the temperature record map of Europe,” Science, 332(6026), pp. 220–224. Available at: https://doi.org/10.1126/science.1201224.

Benmarhnia, T. et al. (2015) “Review article,” Epidemiology, 26(6), pp. 781–793. Available at: https://doi.org/10.1097/ede.0000000000000375.

Berardi, U., Jandaghian, Z. and Graham, J. (2020) “Effects of greenery enhancements for the resilience to heat waves: A comparison of analysis performed through mesoscale (WRF) and microscale (Envi-Met) modeling,” Science of The Total Environment, 747, p. 141300. Available at: https://doi.org/10.1016/j.scitotenv.2020.141300.

Bhati, S. and Mohan, M. (2015) “WRF model evaluation for the urban heat island assessment under varying land use/land cover and reference site conditions,” Theoretical and Applied Climatology, 126(1-2), pp. 385–400. Available at: https://doi.org/10.1007/s00704-015-1589-5.

Bindajam, A.A. et al. (2020) “Impacts of vegetation and topography on land surface temperature variability over the semi-arid mountain cities of Saudi Arabia,” Atmosphere, 11(7), p. 762. Available at: https://doi.org/10.3390/atmos11070762.

Bobb, J.F. et al. (2014) “Heat-related mortality and adaptation to heat in the United States,” Environmental Health Perspectives, 122(8), pp. 811–816. Available at: https://doi.org/10.1289/ehp.1307392.

Bunker, A. et al. (2016) “Effects of air temperature on climate-sensitive mortality and morbidity outcomes in the elderly; a systematic review and meta-analysis of epidemiological evidence,” EBioMedicine, 6, pp. 258–268. Available at: https://doi.org/10.1016/j.ebiom.2016.02.034.

Burkart, K.G. et al. (2021) “Estimating the cause-specific relative risks of non-optimal temperature on daily mortality: A two-part modelling approach applied to the global burden of disease study,” The Lancet, 398(10301), pp. 685–697. Available at: https://doi.org/10.1016/s0140-6736(21)01700-1.

Carnahan, W.H. and Larson, R.C. (1990) “An analysis of an urban heat sink,” Remote Sensing of Environment, 33(1), pp. 65–71. Available at: https://doi.org/10.1016/0034-4257(90)90056-r.

CDO. Climate Data Interface, from the Max Planck Institute for Meteorologie

Jim, C. and Chen, W. (2009) “Value of Scenic Views: Hedonic Assessment of Private Housing in Hong Kong,” Landscape and Urban Planning, 91, 226-234. Available at: http://dx.doi.org/10.1016/j.landurbplan.2009.01.009

Cheng, H. et al. (2021) “Solar reflective coatings with luminescence and self-cleaning function,” Surfaces and Interfaces, 26, p. 101325. Available at: https://doi.org/10.1016/j.surfin.2021.101325.

Cheng, X. et al. (2022) “Non-linear effects of meteorological variables on cooling efficiency of African urban trees,” Environment International, 169, p. 107489. Available at: https://doi.org/10.1016/j.envint.2022.107489.

Coalition for Urban Transitions. (2021) “Seizing South Africa’s Urban Opportunity.” World Resources Institute (WRI) Ross Center for Sustainable Cities and C40 Cities Climate Leadership Group. London and Washington, DC. Available at: https://urbantransitions.global/en/publication/seizing-the-urban-opportunity/

Coates, L. et al. (2014) “Exploring 167 years of vulnerability: An examination of extreme heat events in Australia 1844–2010,” Environmental Science & Policy, 42, pp. 33–44. Available at: https://doi.org/10.1016/j.envsci.2014.05.003.

CSAG Climate information Platform (CIP). Available at: https://www.csag.uct.ac.za/climate-services/cip/.

de Munck, C. et al. (2012) “How much can air conditioning increase air temperatures for a city like Paris, France?,” International Journal of Climatology, 33(1), pp. 210–227. Available at: https://doi.org/10.1002/joc.3415.

Dialesandro, J. et al. (2021) “Dimensions of thermal inequity: Neighborhood Social Demographics and urban heat in the southwestern U.S.,” International Journal of Environmental Research and Public Health, 18(3), p. 941. Available at: https://doi.org/10.3390/ijerph18030941.

Diffenbaugh, N.S. and Burke, M. (2019) “Global warming has increased global economic inequality,” Proceedings of the National Academy of Sciences, 116(20), pp. 9808–9813. Available at: https://doi.org/10.1073/pnas.1816020116.

du Toit, M.J., Cilliers, S.S., Dallimer, M., Goddard, M., Guenat, S. and Cornelius, S.F. (2018). Urban green infrastructure and ecosystem services in sub-Saharan Africa. Landscape and Urban Planning

Ebi, K.L. et al. (2018) “Health risks of warming of 1.5 °C, 2 °C, and higher, above pre-industrial temperatures,” Environmental Research Letters, 13(6), p. 063007. Available at: https://doi.org/10.1088/1748-9326/aac4bd.

Ebi, K.L. et al. (2021) “Hot weather and heat extremes: Health risks,” The Lancet, 398(10301), pp. 698–708. Available at: https://doi.org/10.1016/s0140-6736(21)01208-3.

El-Samra, R., Bou-Zeid, E. and El-Fadel, M. (2018) “What model resolution is required in climatological downscaling over complex terrain?,” Atmospheric Research, 203, pp. 68–82. Available at: https://doi.org/10.1016/j.atmosres.2017.11.030.

Engelbrecht, F. 2019. Green Book – Detailed Projections of Future Climate Change over South Africa. Technical report, Pretoria: CSIR

Estoque, R.C., Murayama, Y. and Myint, S.W. (2017) “Effects of landscape composition and pattern on land surface temperature: An urban heat island study in the megacities of Southeast Asia,” Science of The Total Environment, 577, pp. 349–359. Available at: https://doi.org/10.1016/j.scitotenv.2016.10.195.

Giannaros, T.M. et al. (2013) “Numerical Study of the urban heat island over Athens (Greece) with the WRF model,” Atmospheric Environment, 73, pp. 103–111. Available at: https://doi.org/10.1016/j.atmosenv.2013.02.055.

GIZ. (2021) Deutsche Gesellschaft für Internationale Zusammenarbeit (GIZ)

Global Cool Cities Alliance (2012) https://c40--c.na81.content.force.com/servlet/servlet.ImageServer?id=0151Q000004VZeQ&oid=00D36000001Enhz&lastMod=1563832345000 (Accessed: 20 October 2022))

Goodness, J and Anderson, P. L. (2013) “Local assessment of Cape Town: navigating the management complexities of urbanization, biodiversity, and ecosystem services in the cape floristic region. In: urbanization, biodiversity and ecosystem services: challenges and opportunities, Springer Netherlands. 461-484. Available at: https://doi.org/10.1007/978-94-007-7088-1_24

Green, H. et al. (2019) “Impact of heat on mortality and morbidity in low and middle income countries: A review of the epidemiological evidence and considerations for future research,” Environmental Research, 171, pp. 80–91. Available at: https://doi.org/10.1016/j.envres.2019.01.010.

Gulati, M & Scholtz, L (2020) “The case for investment in green infrastructure in African Cities”. Cape Town, WWF South Africa.

Gubernot, D.M., Anderson, G.B. and Hunting, K.L. (2013) “The epidemiology of Occupational Heat Exposure in the United States: A review of the literature and assessment of research needs in a changing climate,” International Journal of Biometeorology, 58(8), pp. 1779–1788. Available at: https://doi.org/10.1007/s00484-013-0752-x.

Gwedla, N. and Shackleton, C.M. (2015) “The development visions and attitudes towards urban forestry of officials responsible for greening in South African towns,” Land Use Policy, 42, pp. 17–26. Available at: https://doi.org/10.1016/j.landusepol.2014.07.004.

Haashemi, S. et al. (2016) “Seasonal variations of the surface urban heat island in a semi-arid city,” Remote Sensing, 8(4), p. 352. Available at: https://doi.org/10.3390/rs8040352.

Hajat, S., O'Connor, M. and Kosatsky, T. (2010) “Health effects of hot weather: From awareness of risk factors to effective health protection,” The Lancet, 375(9717), pp. 856–863. Available at: https://doi.org/10.1016/s0140-6736(09)61711-6.

Hamann, C., T. Mkhize, and G. GÖtz. 2018. Backyard and informal dwellings (2001-2016). http://www.gcro.ac.za/outputs
map-of-the-month/detail/backyard-and-informal-dwellings-2001-2016/

He, C. et al. (2022) “The inequality labor loss risk from future urban warming and adaptation strategies,” Nature Communications, 13(1). Available at: https://doi.org/10.1038/s41467-022-31145-2.

Heisler, G. and Grant,R. (2000) “Ultraviolet radiation in urban ecosystems with consideration of effects on human health,” Urban Ecosystems, no. 4 (3), pp. 193-229, 2000. Available at: https://doi.org/10.2737/NE-GTR-268

Herold, N. et al. (2017) “Greater increases in temperature extremes in low versus high income countries,” Environmental Research Letters, 12(3), p. 034007. Available at: https://doi.org/10.1088/1748-9326/aa5c43.

Hsu, A. et al. (2021) “Disproportionate exposure to urban heat island intensity across major US cities,” Nature Communications, 12(1). Available at: https://doi.org/10.1038/s41467-021-22799-5.

Ioannou, L.G. et al. (2017) “Time-motion analysis as a novel approach for evaluating the impact of environmental heat exposure on labor loss in agriculture workers,” Temperature, 4(3), pp. 330–340. Available at: https://doi.org/10.1080/23328940.2017.1338210.

Jacobs, S.J. et al. (2018) “Use of cool roofs and vegetation to mitigate urban heat and improve human thermal stress in Melbourne, Australia,” Journal of Applied Meteorology and Climatology, 57(8), pp. 1747–1764. Available at: https://doi.org/10.1175/jamc-d-17-0243.1.

Jagarnath, M., Thambiran, T. and Gebreslasie, M. (2020) “Heat stress risk and vulnerability under climate change in Durban Metropolitan, South Africa—identifying urban planning priorities for adaptation,” Climatic Change, 163(2), pp. 807–829. Available at: https://doi.org/10.1007/s10584-020-02908-x.

Jiao, M. et al. (2017) “Patch size of trees affects its cooling effectiveness: A perspective from shading and transpiration processes,” Agricultural and Forest Meteorology, 247, pp. 293–299. Available at: https://doi.org/10.1016/j.agrformet.2017.08.013.

Jonsson, P. (2004) “Vegetation as an urban climate control in the subtropical city of Gaborone, Botswana,” International Journal of Climatology, 24(10), pp. 1307–1322. Available at: https://doi.org/10.1002/joc.1064.

Karlický, J. (2013). Regional Climate Simulations with WRF Model. Available at: https://www.mff.cuni.cz/veda/konference/wds/proc/pdf13/WDS13_314_f8_Karlicky.pdf

Keeratikasikorn, C. and Bonafoni, S. (2018) “Urban heat island analysis over the land use zoning plan of Bangkok by means of landsat 8 imagery,” Remote Sensing, 10(3), p. 440. Available at: https://doi.org/10.3390/rs10030440.

Kenny, G.P. and Jay, O. (2013) “Thermometry, calorimetry, and mean body temperature during heat stress,” Comprehensive Physiology, pp. 1689–1719. Available at: https://doi.org/10.1002/cphy.c130011.

Keramitsoglou, I. et al. (2011) “Identification and analysis of urban surface temperature patterns in Greater Athens, Greece, using MODIS imagery,” Remote Sensing of Environment, 115(12), pp. 3080–3090. Available at: https://doi.org/10.1016/j.rse.2011.06.014.

Kimemia, D. et al. (2020) “Passive cooling for thermal comfort in informal housing,” Journal of Energy in Southern Africa, 31(1), pp. 28–39. Available at: https://doi.org/10.17159/2413-3051/2020/v31i1a7689.

Kloog, I. et al. (2016) “Modelling spatio-temporally resolved air temperature across the complex geo-climate area of France using satellite-derived land surface temperature data,” International Journal of Climatology, 37(1), pp. 296–304. Available at: https://doi.org/10.1002/joc.4705.

Krayenhoff, E.S. and Voogt, J.A. (2010) “Impacts of urban albedo increase on local air temperature at daily–annual time scales: Model results and synthesis of previous work,” Journal of Applied Meteorology and Climatology, 49(8), pp. 1634–1648. Available at: https://doi.org/10.1175/2010jamc2356.1.

Krayenhoff, E.S. et al. (2021) “Cooling hot cities: A systematic and critical review of the Numerical Modelling Literature,” Environmental Research Letters, 16(5), p. 053007. Available at: https://doi.org/10.1088/1748-9326/abdcf1.

Kusaka, Hiroyuki & KIMURA, Fujio. (2004) “Coupling a Single-Layer Urban Canopy Model with a Simple Atmospheric Model: Impact on Urban Heat Island Simulation for an Idealized Case,” Journal of the Meteorological Society of Japan. 82. 67-80. Available at: http://dx.doi.org/10.2151/jmsj.82.67

Lazzarini, M., Marpu, P.R. and Ghedira, H. (2013) “Temperature-land cover interactions: The inversion of urban heat island phenomenon in desert city areas,” Remote Sensing of Environment, 130, pp. 136–152. Available at: https://doi.org/10.1016/j.rse.2012.11.007.

Laue, F., Adegun, O.B. and Ley, A. (2022) “Heat stress adaptation within informal, low-income urban settlements in Africa,” Sustainability, 14(13), p. 8182. Available at: https://doi.org/10.3390/su14138182.

Li, M. et al. (2014) “Improving mesoscale modeling using satellite-derived land surface parameters in the Pearl River Delta region, China,” Journal of Geophysical Research: Atmospheres, 119(11), pp. 6325–6346. Available at: https://doi.org/10.1002/2014jd021871.

Li, H. et al. (2017) “Impact of land cover data on the simulation of urban heat island for Berlin using WRF coupled with bulk approach of Noah-LSM,” Theoretical and Applied Climatology, 134(1-2), pp. 67–81. Available at: https://doi.org/10.1007/s00704-017-2253-z.

Li, T., R.M. Horton, D.A. Bader, F. Liu, Q. Sun, and P.L. Kinney. (2018) “Long-term projections of temperature-related mortality risks for ischemic stroke, hemorrhagic stroke, and acute ischemic heart disease under changing climate in Beijing, China,” Environ. Int., 112, 1-9, Available at: doi:10.1016/j.envint.2017.12.006.

Li, H. et al. (2022) “Improving the WRF/urban modeling system in China by developing a National Urban Dataset,” Geoscience Frontiers, 13(4), p. 101385. Available at: https://doi.org/10.1016/j.gsf.2022.101385.

Lynch, P. (2008) “The origins of Computer Weather Prediction and climate modeling,” Journal of Computational Physics, 227(7), pp. 3431–3444. Available at: https://doi.org/10.1016/j.jcp.2007.02.034.

Madanian, M. et al. (2018) “The study of thermal pattern changes using landsat-derived land surface temperature in the central part of Isfahan Province,” Sustainable Cities and Society, 39, pp. 650–661. Available at: https://doi.org/10.1016/j.scs.2018.03.018.

Magidi, J. and Ahmed, F. (2022) “Spatio-temporal variations of land surface temperature using landsat and modis: Case study of the City of Tshwane, South Africa,” South African Journal of Geomatics, 9(2), pp. 379–396. Available at: https://doi.org/10.4314/sajg.v9i2.25.

Manisalidis, I. et al. (2020) “Environmental and health impacts of Air Pollution: A Review,” Frontiers in Public Health, 8. Available at: https://doi.org/10.3389/fpubh.2020.00014.

Manoli, G. et al. (2019) “Magnitude of urban heat islands largely explained by climate and population,” Nature, 573(7772), pp. 55–60. Available at: https://doi.org/10.1038/s41586-019-1512-9.

Manyuchi, A.E. et al. (2022) “Extreme heat events, high ambient temperatures and human morbidity and mortality in Africa: A systematic review,” South African Journal of Science, 118(11/12). Available at: https://doi.org/10.17159/sajs.2022/12047.

Masson, V. et al. (2020) “City-descriptive input data for urban climate models: Model requirements, data sources and challenges,” Urban Climate, 31, p. 100536. Available at: https://doi.org/10.1016/j.uclim.2019.100536.

McGeehin, M.A. and Mirabelli, M. (2001) “The potential impacts of climate variability and change on temperature-related morbidity and mortality in the United States.,” Environmental Health Perspectives, 109(suppl 2), pp. 185–189. Available at: https://doi.org/10.1289/ehp.109-1240665.

Mehrotra, S., Bardhan, R. and Ramamritham, K. (2018) “Urban informal housing and surface urban heat island intensity,” Environment and Urbanization ASIA, 9(2), pp. 158–177. Available at: https://doi.org/10.1177/0975425318783548.

Meili, N. et al. (2021) “Tree effects on urban microclimate: Diurnal, seasonal, and climatic temperature differences explained by separating radiation, evapotranspiration, and roughness effects,” Urban Forestry & Urban Greening, 58, p. 126970. Available at: https://doi.org/10.1016/j.ufug.2020.126970.

Mentaschi, L. et al. (2022) “Global long-term mapping of surface temperature shows intensified intra-city urban heat island extremes,” Global Environmental Change, 72, p. 102441. Available at: https://doi.org/10.1016/j.gloenvcha.2021.102441.

Million cool roofs challenge: Local champions for a global movement (2022) Clean Cooling Collaborative. Available at: https://www.cleancoolingcollaborative.org/ blog/million-cool-roofs-challenge-local-champi ons-for -a-g lobal-movement/ (Accessed: January 10, 2023).

Mirzaei, M. et al. (2020) “Urban Heat Island Monitoring and impacts on Citizen’s general health status in Isfahan Metropolis: A remote sensing and field survey approach,” Remote Sensing, 12(8), p. 1350. Available at: https://doi.org/10.3390/rs12081350.

Mitchell, B.C. and Chakraborty, J. (2018) “Exploring the relationship between residential segregation and thermal inequity in 20 U.S. cities,” Local Environment, 23(8), pp. 796–813. Available at: https://doi.org/10.1080/13549839.2018.1474861.

Mlilwana, T.P. and Kearsley, E.P. (2022) “Light-coloured concrete surfacing for urban heat-island mitigation in Southern Africa,” Journal of the South African Institution of Civil Engineering, 64(2), pp. 1–11. Available at: https://doi.org/10.17159/2309-8775/2022/v64no2a1.

Montaner-Fernández, D. et al. (2020) “Spatio-temporal variation of the urban heat island in Santiago, Chile during Summers 2005–2017,” Remote Sensing, 12(20), p. 3345. Available at: https://doi.org/10.3390/rs12203345.

Mohammed, A., Khan, A. and Santamouris, M. (2021) “On the mitigation potential and climatic impact of modified urban albedo on a subtropical Desert City,” Building and Environment, 206, p. 108276. Available at: https://doi.org/10.1016/j.buildenv.2021.108276.

Mohegh, A. et al. (2018) “Observational evidence of neighborhood scale reductions in air temperature associated with increases in roof albedo,” Climate, 6(4), p. 98. Available at: https://doi.org/10.3390/cli6040098.

Morini, E. et al. (2016) “The impact of albedo increase to mitigate the urban heat island in Terni (Italy) using the WRF model,” Sustainability, 8(10), p. 999. Available at: https://doi.org/10.3390/su8100999.

Mughal, M.O., Li, X.-X. and Norford, L.K. (2020) “Urban heat island mitigation in Singapore: Evaluation using WRF/multilayer urban canopy model and local climate zones,” Urban Climate, 34, p. 100714. Available at: https://doi.org/10.1016/j.uclim.2020.100714.

Ng, E. et al. (2012) “A study on the cooling effects of greening in a high-density city: An experience from Hong Kong,” Building and Environment, 47, pp. 256–271. Available at: https://doi.org/10.1016/j.buildenv.2011.07.014.

Nurwanda, A. and Honjo, T. (2018) “Analysis of land use change and expansion of surface urban heat island in Bogor City by Remote Sensing,” ISPRS International Journal of Geo-Information, 7(5), p. 165. Available at: https://doi.org/10.3390/ijgi7050165.

Pasquini, L.; Enqvist, J.P. Green infrastructure in South African cities. In Report for Cities Support Programme; African Centre forCities: Cape Town, South Africa, 2019.

Pelta, R., Chudnovsky, A.A. and Schwartz, J. (2016) “Spatio-temporal behavior of brightness temperature in Tel-Aviv and its application to air temperature monitoring,” Environmental Pollution, 208, pp. 153–160. Available at: https://doi.org/10.1016/j.envpol.2015.09.007.

Naicker, N. et al. (2017) “Indoor temperatures in low cost housing in Johannesburg, South Africa,” International Journal of Environmental Research and Public Health, 14(11), p. 1410. Available at: https://doi.org/10.3390/ijerph14111410.

NASA Shuttle Radar Topography Mission (SRTM)(2013). Shuttle Radar Topography Mission (SRTM) Global. Distributed by OpenTopography. https://doi.org/10.5069/G9445JDF. Accessed: 2023-02-10

NWS (National Weather Service). 2013. National Weather Service 73-Year List of Severe Weather Fatalities. Available: http://www.nws.noaa.gov/om/hazstats/resources/weather_fatalities.pdf [accessed 24 May 2013

Observatoire géodes (2020) Géodes - Santé publique France. Available at: https://geodes.santepubliquefrance.fr/#c=home. (Accessed: September 22, 2022).

Oke, T.R. (2002) “Boundary layer climates.” Available at: https://doi.org/10.4324/9780203407219.

Oleson, K.W., Bonan, G.B. and Feddema, J. (2010) “Effects of white roofs on urban temperature in a global climate model,” Geophysical Research Letters, 37(3). Available at: https://doi.org/10.1029/2009gl042194.

Petkova, E.P., Gasparrini, A. and Kinney, P.L. (2014) “Heat and mortality in New York City since the beginning of the 20th century,” Epidemiology, 25(4), pp. 554–560. Available at: https://doi.org/10.1097/ede.0000000000000123.

Potchter, O. et al. (2008) “The oasis effect in an extremely hot and arid climate: The case of southern israel,” Journal of Arid Environments, 72(9), pp. 1721–1733. Available at: https://doi.org/10.1016/j.jaridenv.2008.03.004.

Rahman, M.A. et al. (2011) “Effect of rooting conditions on the growth and cooling ability of Pyrus calleryana,” Urban Forestry & Urban Greening, 10(3), pp. 185–192. Available at: https://doi.org/10.1016/j.ufug.2011.05.003.

Rahman, M.A., Armson, D. and Ennos, A.R. (2014) “A comparison of the growth and cooling effectiveness of five commonly planted urban tree species,” Urban Ecosystems, 18(2), pp. 371–389. Available at: https://doi.org/10.1007/s11252-014-0407-7.

Rahman, M.A. et al. (2017) “Within canopy temperature differences and cooling ability of tilia cordata trees grown in urban conditions,” Building and Environment, 114, pp. 118–128. Available at: https://doi.org/10.1016/j.buildenv.2016.12.013.

Rasul, A., Balzter, H. and Smith, C. (2015) “Spatial variation of the daytime surface Urban Cool Island during the dry season in Erbil, Iraqi kurdistan, from Landsat 8,” Urban Climate, 14, pp. 176–186. Available at: https://doi.org/10.1016/j.uclim.2015.09.001.

Robine, J.-M. et al. (2008) “Death toll exceeded 70,000 in Europe during the summer of 2003,” Comptes Rendus Biologies, 331(2), pp. 171–178. Available at: https://doi.org/10.1016/j.crvi.2007.12.001.

Rohat, G. et al. (2019) “Projections of human exposure to dangerous heat in African cities under multiple socioeconomic and climate scenarios,” Earth's Future, 7(5), pp. 528–546. Available at: https://doi.org/10.1029/2018ef001020.

Rosenfeld, A. et al. (2017) “Estimating daily minimum, maximum, and mean near surface air temperature using hybrid satellite models across Israel,” Environmental Research, 159, pp. 297–312. Available at: https://doi.org/10.1016/j.envres.2017.08.017.

SA National Land-cover datasets (2021) SA National Land-Cover Datasets | Environmental Geographical Information Systems (E-GIS). Department of Forestry, Fisheries and the Environment. Available at: https://egis.environment.gov.za/sa_national_land_cover_datasets (Accessed: January 30, 2022).

Sanedi (2019], Kheis Cool Coating Project. Private communications

Santamouris, M. (2014) “Cooling the cities – a review of reflective and green roof mitigation technologies to fight Heat Island and improve comfort in urban environments,” Solar Energy, 103, pp. 682–703. Available at: https://doi.org/10.1016/j.solener.2012.07.003.

Santamouris, M. et al. (2017) “Passive and active cooling for the outdoor built environment – analysis and assessment of the cooling potential of mitigation technologies using performance data from 220 large scale projects,” Solar Energy, 154, pp. 14–33. Available at: https://doi.org/10.1016/j.solener.2016.12.006.

Santamouris, M. and Fiorito, F. (2021) “On the impact of modified urban albedo on ambient temperature and heat related mortality,” Solar Energy, 216, pp. 493–507. Available at: https://doi.org/10.1016/j.solener.2021.01.031.

Schilling, J. et al. (2020) “Climate change vulnerability, water resources and social implications in North Africa,” Regional Environmental Change, 20(1). Available at: https://doi.org/10.1007/s10113-020-01597-7.

Schwaab, J. et al. (2021) “The role of urban trees in reducing land surface temperatures in European cities,” Nature Communications, 12(1). Available at: https://doi.org/10.1038/s41467-021-26768-w.

Scovronick, N. and Armstrong, B. (2012) “The impact of housing type on temperature-related mortality in South Africa, 1996–2015,” Environmental Research, 113, pp. 46–51. Available at: https://doi.org/10.1016/j.envres.2012.01.004.

Scovronick, N. et al. (2018) ‘The association between ambient temperature and mortality in South Africa: A Time-series analysis’, Environmental Research, 161, pp. 229–235. doi:10.1016/j.envres.2017.11.001.

Shackleton, C.M. et al. (2014) “Low-cost housing developments in South Africa miss the opportunities for household level urban greening,” Land Use Policy, 36, pp. 500–509. Available at: https://doi.org/10.1016/j.landusepol.2013.10.002.

Shi, Y., Xiang, Y. and Zhang, Y. (2019) “Urban design factors influencing surface urban heat island in the high-density city of Guangzhou based on the local climate zone,” Sensors, 19(16), p. 3459. Available at: https://doi.org/10.3390/s19163459.

Simpson, J.R. and McPherson, E.G. (1997) “The effects of roof albedo modification on cooling loads of scale model residences in Tucson, Arizona,” Energy and Buildings, 25(2), pp. 127–137. Available at: https://doi.org/10.1016/s0378-7788(96)01002-x.

Sithole, K. and Odindi, J.O. (2015) “Determination of urban thermal characteristics on an urban/rural land cover gradient using remotely sensed data,” South African Journal of Geomatics, 4(4), p. 384. Available at: https://doi.org/10.4314/sajg.v4i4.3.

Skamarock, W.C., Klemp, J.B., Dudhia, J., Gill, D.O., Liu, Z., Berner, J., Wang, W., Powers, J.G., Duda, M.G., Barker, D.M. and Huang, X.Y., 2019. A description of the advanced research WRF model version 4. National Center for Atmospheric Research: Boulder, CO, USA, 145(145), p.550.

Son, J.-Y., Liu, J.C. and Bell, M.L. (2019) “Temperature-related mortality: A systematic review and investigation of effect modifiers,” Environmental Research Letters, 14(7), p. 073004. Available at: https://doi.org/10.1088/1748-9326/ab1cdb.

Souverijns, N. et al. (2022) “Urban heat in Johannesburg and Ekurhuleni, South Africa: A meter-scale assessment and vulnerability analysis,” Urban Climate, 46, p. 101331. Available at: https://doi.org/10.1016/j.uclim.2022.101331.

Stathopoulou, M. and Cartalis, C. (2007) “Daytime urban heat islands from landsat ETM+ and corine land cover data: An application to major cities in Greece,” Solar Energy, 81(3), pp. 358–368. Available at: https://doi.org/10.1016/j.solener.2006.06.014.

Statistics South Africa (2022), "Mid-year population estimates", Statistical Release P0302, Statistics South Africa, Pretoria.

Sun, S. et al. (2016) “The influence of pre-existing health conditions on short-term mortality risks of temperature: Evidence from a prospective Chinese elderly cohort in Hong Kong,” Environmental Research, 148, pp. 7–14. Available at: https://doi.org/10.1016/j.envres.2016.03.012.

Sun, Y. et al. (2019) “Quantifying the effects of urban form on land surface temperature in subtropical high-density urban areas using machine learning,” Remote Sensing, 11(8), p. 959. Available at: https://doi.org/10.3390/rs11080959.

Synnefa, A., Santamouris, M. and Livada, I. (2006) “A study of the thermal performance of reflective coatings for the urban environment,” Solar Energy, 80(8), pp. 968–981. Available at: https://doi.org/10.1016/j.solener.2005.08.005.

Tewari, M., Chen, F., Wang, W., Dudhia, J., Lemone, M. A., Mitchell, K. E. (2004) “Implementation and verification of the unified Noah land-surface model in the WRF model” In 20th Conference on Weather Analysis and Forecasting/16th Conference on Numerical Weather Prediction. American Meteorological Society: Seattle, WA, US.

Turner‐Skoff, J.B. and Cavender, N. (2019) “The benefits of trees for livable and sustainable communities,” PLANTS, PEOPLE, PLANET, 1(4), pp. 323–335. Available at: https://doi.org/10.1002/ppp3.39.

Vahmani, P. and Ban-Weiss, G.A. (2016) “Impact of remotely sensed albedo and vegetation fraction on simulation of urban climate in WRF-Urban Canopy Model: A case study of the urban heat island in Los Angeles,” Journal of Geophysical Research: Atmospheres, 121(4), pp. 1511–1531. Available at: https://doi.org/10.1002/2015jd023718.

Vaidyanathan, A. et al. (2020) “Heat-related deaths — United States, 2004–2018,” MMWR. Morbidity and Mortality Weekly Report, 69(24), pp. 729–734. Available at: https://doi.org/10.15585/mmwr.mm6924a1.

Venter, Z.S. et al. (2020) “Green apartheid: Urban green infrastructure remains unequally distributed across income and race geographies in South Africa,” Landscape and Urban Planning, 203, p. 103889. Available at: https://doi.org/10.1016/j.landurbplan.2020.103889.

Vicedo-Cabrera, A.M. et al. (2021) “The burden of heat-related mortality attributable to recent human-induced climate change,” Nature Climate Change, 11(6), pp. 492–500. Available at: https://doi.org/10.1038/s41558-021-01058-x.

Voogt, J.A. and Oke, T.R. (2003) “Thermal remote sensing of urban climates,” Remote Sensing of Environment, 86(3), pp. 370–384. Available at: https://doi.org/10.1016/s0034-4257(03)00079-8.

Weng, Q. Lu, D. Schubring, J. (2004) “Estimation of land surface temperature–vegetation abundance relationship for urban heat island studies,” Remote Sens. Environ. 2004,89, 467–483. Available at: https://doi.org/10.1016/j.rse.2003.11.005

Wickham J, Homer C, Vogelmann J, McKerrow A, Mueller R, Herold N, Coulston J. (2014) “The Multi-Resolution Land Characteristics (MRLC) Consortium — 20 Years of Development and Integration of USA National Land Cover Data,” Remote Sensing. 6(8):7424-7441. Available at: https://doi.org/10.3390/rs6087424

Wichmann, J. (2017) “Heat effects of ambient apparent temperature on all-cause mortality in Cape Town, Durban and Johannesburg, South Africa: 2006–2010,” Science of The Total Environment, 587-588, pp. 266–272. Available at: https://doi.org/10.1016/j.scitotenv.2017.02.135.

Wozniac, S. and Brauer, M. (2021) Hot, cold, and deadly: Think global health, Council on Foreign Relations. Available at: https://www.thinkglobalhealth.org/article/hot-cold-and-deadly (Accessed: September 20, 2022).

Wright, C.Y. et al. (2014) “Human health impacts in a changing South African climate,” South African Medical Journal, 104(8), p. 579. Available at: https://doi.org/10.7196/samj.8603.

Yang, J. et al. (2021) “Projecting heat-related excess mortality under climate change scenarios in China,” Nature Communications, 12(1). Available at: https://doi.org/10.1038/s41467-021-21305-1.

Zhang, J., Gou, Z. and Shutter, L. (2019) “Effects of internal and external planning factors on park cooling intensity: Field measurement of urban parks in Gold Coast, Australia,” AIMS Environmental Science, 6(6), pp. 417–434. Available at: https://doi.org/10.3934/environsci.2019.6.417.

Zhang, Y. and Sun, L. (2019) “Spatial-temporal impacts of urban land use land cover on land surface temperature: Case studies of two Canadian urban areas,” International Journal of Applied Earth Observation and Geoinformation, 75, pp. 171–181. Available at: https://doi.org/10.1016/j.jag.2018.10.005.

Zhou, B. et al. (2019) “‘surface,’ ‘satellite’ or ‘Simulation’: Mapping intra‐urban microclimate variability in a Desert City,” International Journal of Climatology, 40(6), pp. 3099–3117. Available at: https://doi.org/10.1002/joc.6385.

Zografos, C., Anguelovski, I. and Grigorova, M. (2016) “When exposure to climate change is not enough: Exploring heatwave adaptive capacity of a multi-ethnic, low-income urban community in Australia,” Urban Climate, 17, pp. 248–265. Available at: https://doi.org/10.1016/j.uclim.2016.06.003.

Appendix

Table A.1 Summary of LST differences between WRF_MODIS and WRF_SANLC simulations, differentiating between the results for both urban and non-urban areas.

City	WRF_MODIS	WRF_SANLC
Bloemfontein	**Non-urban** - Non-built-up areas show ~5℃ cool bias compared to observed. Without the cold bias, simulated patterns are fairly well identified. **Urban** - Most of the urban expanse is identified, but is estimated to be ~15-20℃ cooler than observed. It also shows a slightly cooler south vs north where observed shows the opposite.	**Non-urban** - There is again an approximate 5℃ cold bias across the whole study area. Without this bias LSTs are consistently within 3℃ of the observed. **Urban** - The spatial extent and variations within the urban area are very well identified. The observed cooler north vs south is well simulated by the model, but underestimated in value (~4℃ vs observed differences up to 7℃).
Kuruman	**Non-urban** - The majority of the study area is identified as natural vegetation. Simulations show very similar values to observed across these areas (the errors are within 3°C). **Urban** - Only 4 small squares are identified as urban with these 10-15℃ cooler than observed. The cool southern settlement is not well represented and temperatures are generally overestimated here (up to 8℃).	**Non-urban** -. Outside of urban areas, values are generally well predicted (mostly within 4℃). Some NE LSTs are slightly overestimated and some southern values are underestimated. These seem to be related to temporary land cover changes like controlled burning. **Urban** - The model significantly underestimates the warmer northern urban area LSTs (5-10℃ cooler than observed), but identifies the vegetated southern areas well (deviations within 3℃). Simulations show slight differences between LSTs of different urban classes, but this is not spatially accurate.
Mokopane	**Non-urban** - Non-built-up areas in the valley are generally well simulated (within ~4℃), but water features and more mountainous areas in the SW are not well represented. **Urban** - Most urban areas are roughly identified, showing 10-15℃ lower LSTs than observed. Those which are treated as natural show far more similar values to the observed .	**Non-urban** - In the valley the non-built-up areas LSTs are generally slightly underestimated (up to ~4℃), but the variation between classes is fairly well identified. The SW mountain LSTs are overestimated. **Urban** - The cooler southern settlements are well simulated (within 3°C), but the less vegetated and warmer urban areas are underestimated by 5℃+. Differences between cooler and warmer settlements are mostly identified, but underestimated.
Newcastle	**Non-urban** - Outside of urban areas the model shows mixed results. The central areas are reasonably well simulated, but there is a strong cool bias to the west (5℃+) and warm bias to the east (~3℃) **Urban** - The urban expanse is roughly identified, but skewed to the north of its actual location. LSTs here are 10-15°C lower than observed .	**Non-urban** - Non-urban areas are for the most part underestimated, most notably in the western section (~5℃). The northern area is however overestimated (also ~5℃). **Urban** - Urban areas consistently show very similar LSTs to observed (within 3℃). The slightly cooler urban areas to the north of the centre are also noted, but the hotter commercial centre is not.

Phalaborwa	**Non-urban**. Outside of the settlements the LSTs are generally well simulated (within 3℃). The cool SW section is an exception, being overestimated by 5℃+.	**Non-urban** - Outside of the settlements is again well simulated (within 3℃), apart from the small sections in the cooler SW (slightly overestimated) and the SE mining area (strongly overestimated, ~10°C).
	Urban - The extent of the urban area to the east is significantly overrepresented and the areas to the west significantly underrepresented. In the areas that are identified, there is ~10℃ underestimation of LSTs. Cool areas not identified as urban are strongly overestimated (~7℃), while hotter areas are fairly similar to observed (within 3℃)	**Urban** - Urban LSTs are well represented (within 3℃ of observed for the most part). The cooler areas are particularly well identified while the warmer are slightly underestimated. The differences within urban areas are identified, though again slightly underestimated and not always spatially accurate.
Pilanesberg	**Non-urban** - Simulated non-urban values are generally similar to the observed, but the strong contrasts in LSTs between the east and north and east and south are not well identified .	**Non-urban** - As with MODIS, simulations of non-urban areas are similar to observed. The contrasts between east and north, and east and south are better represented, but still underestimated. Small scale features like dams are identified.
	Urban - No urban areas are identified by the land cover, so urban areas are treated as natural. This shows LSTs across most areas to be very similar to the observed (within 3℃). The exceptions to this are the warmer NW temps (underestimated by ~5℃) and the cooler Sun City (overestimated by ~5℃).	**Urban** - Urban LSTs are significantly underestimated (5-10℃), apart from the cooler Sun city which is similar to observed (within 3℃). Differences within urban classes are identified, but not accurately.
Rustenburg	**Non-urban** -. The non=urban LSTs are fairly well simulated with a very slight ~2℃ underestimation. The cooler LSTs of the hilly sections in the east are, however, not identified.	**Non-urban**- The model picks up the spatial patterns of non-urban LSTs very well, but the values are generally underestimated slightly again (2-3℃).
	Urban - The majority of the urban expanse is roughly identified. LSTs are 10-15℃ cooler than observed here.	**Urban** - Spatial patterns in the urban areas are well identified and there is some evidence of the model picking up the observed differences between cooler and warmer urban areas. In general though, the hotter urban areas are again strongly underestimated (5-10°C) while cooler areas are well-represented.
Thohoyandou	**Non-urban** - The main trend of cooler NW areas and warmer south and east areas is identified, but values are underestimated. Eastern LSTs are ~4-5°C cooler, and NW values ~2-3°C warmer than observed.	**Non-urban** - The patterns of NW to SE temperature gradient, and most of the very hot eastern areas, are well identified. There is, however, a strong underestimation of LST values across the study area. This averages ~5℃ and comes about because of SANLC treating the natural vegetation here as forest, where in this area, another class would've been more appropriate. Taking out the 5℃ cool bias shows values similar to observed, apart from the still underestimated hot NE.
	Urban - Only a small area in the NW is identified as urban. This has LSTs of 10-15℃ lower than observed. The other urban areas are treated as natural vegetation and for most of them this makes their LSTs similar values to observed (within 3℃). The hot NE is an exception, with LSTs being underestimated by ~5°C.	**Urban** - The urban areas are also affected by the cool bias, but even with this gone, the majority of the southern and eastern settlements still show underestimations of temperatures (~5°C , but up to almost 10°C in the NE). The two cooler NW settlements are well represented with the removal of the cool bias.

Upington	**Non-urban** - The non-urban areas away from the river are similar to observed (within ~3℃) , while the river areas and those adjacent to it are less representative of the observed (up to 10℃ difference in parts). **Urban** - The urban areas are roughly identified, apart from the southern settlement which is not recognized. Where they are identified, they are underestimated by between 8℃ (cool settlements) and 18℃ (warm settlements) and where not, they are ~5℃ lower than observed.	**Non-urban** - Away from the river, non-urban areas are very similar to observed (~3℃ difference), but irrigated land near the river is under-represented, leading to much hotter simulation LSTs here than is observed (10℃+). **Urban** - Settlement patterns are well identified, differentiating between cooler and hotter parts quite accurately. The values themselves are very similar to those observed in the cooler parts, but are still underestimated in the warmer parts (~4-5℃).
Vryburg	**Non-urban** - Non-urban LSTs are consistently overestimated (~4℃), with little variation across these. **Urban** - Simulations roughly identify the urban extent, but are slightly skewed to the north. Within this extent, they underestimate urban LSTs by 10-15℃. The hot settlements not identified as urban, show similar values to observed.	**Non-urban** - Non-urban LSTs are within 3℃ of observed and also identify some of the smaller variations within these areas. **Urban** - The spatial patterns of LSTs are well identified and there is some evidence of a differentiation between the cooler NW sector and the others, but this is still a lot smaller than observed. This cooler NW shows almost identical values to observed, while the warmer urban parts are underestimated by ~3-4℃.